APRIL-JUNE 2023 VOL. 15 № 2 (57)

ISSN 2075-8251

ActaNaturae

Connectivity of the Brain in the Light of Chemogenetic Modulation of Neuronal Activity

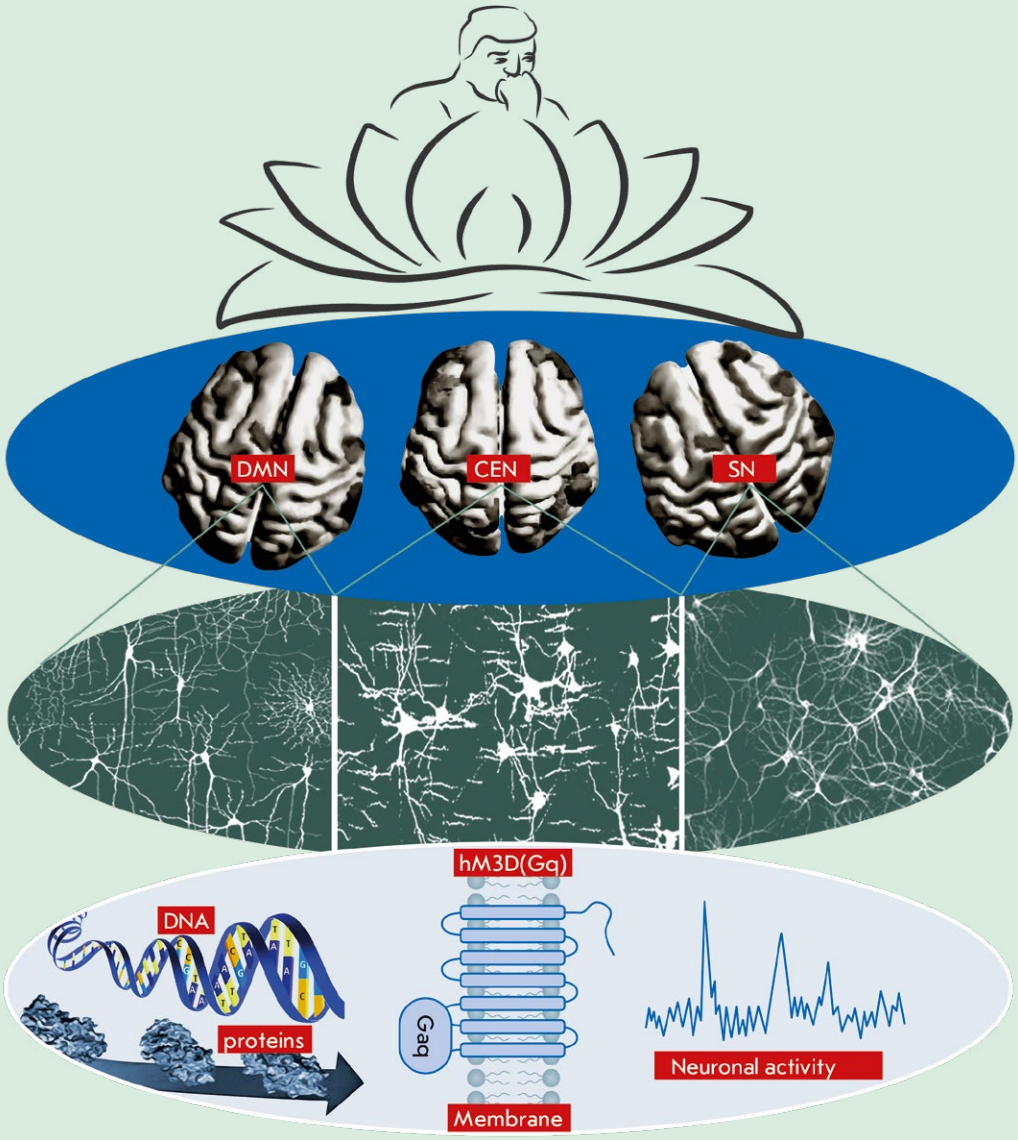

The Unique Genome of the Virus and Alternative Strategies for its Realization

O. P. Zhirnov

The genome of some RNA-containing viruses comprises ambipolar genes that are arranged in stacks (one above the other) encoding proteins in opposite directions. Ambipolar genes provide a new approach for developing viral diversity when virions possessing an identical genome may differ in its expression scheme (strategy) and have distinct types of progeny virions varying in the genomic RNA polarity and the composition of proteins expressed by positive- or negative-sense genes, the so-called ambipolar virions. So far, this pathway of viral genome expression remains hypothetical and hidden from us, like the dark side of the Moon, and deserves a detailed study.

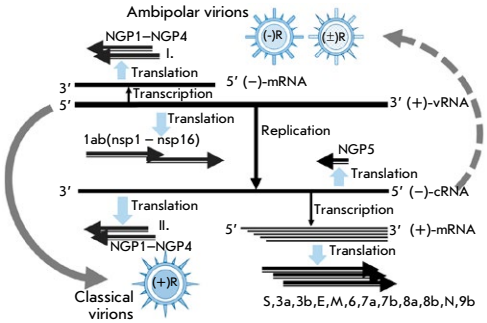

Scheme of gene coding in the RNA genome of coronavirus in the SARS-CoV2 model

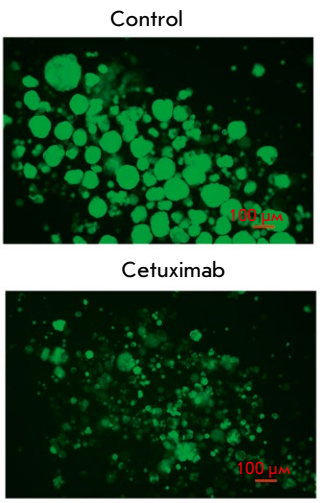

Analysis of the cetuximab effect on the structure of the MCF7-EGFR spheroids

EGFR Suppression Inhibits the Sphere Formation of MCF7 Cells Overexpressing EGFR

D. D. Novak, O. S. Troitskaya, A. A. Nushtaeva, M. V. Zhilnikova, V. A. Richter, M. I. Meschaninova, O. A. Koval

The epidermal growth factor receptor (EGFR) is an oncogenic tyrosine kinase that is involved in tumor initiation and progression. EGFR transgene expression in the human breast adenocarcinoma cell line MCF7 (MCF7-EGFR) stimulates the 3D spheroid-like growth. The primary focus of the present work was to investigate whether EGFR inhibition could affect the assembly of spheroids or lead to the destruction of pre-existing spheroids. The suppression of EGFR mRNA with siRNA was found to reduce the sphere formation, whereas treating the pre-existing spheroids had no such effect. Authors have demonstrated that N-cadherin is involved in the EGFR-dependent formation of MCF7-EGFR spheroids. Accordingly, MCF7-EGFR spheroids can be considered a suitable model for studying aggressive hormone-positive breast tumors.

Search for Inhibitors of *Mycobacterium tuberculosis* Transketolase in a Series of Sulfo-Substituted Compounds

I. V. Gushchina, D. K. Nilov, T. A. Shcherbakova, S. M. Baldin, V. K. Švedas

As a result of the computer screening of a library of sulfo-substituted compounds, molecules capable of binding to the active site of transketolase from *Mycobacterium tuberculosis* were identified. An experimental verification of the inhibitory activity of the most promising compound, STK045765, against a highly purified recombinant enzyme preparation was carried out. It was shown that the STK045765 molecule competes for the binding site of the pyrophosphate group of the thiamine diphosphate cofactor and, at micromolar concentrations, is able to suppress the activity of mycobacterial transketolase. The discovered furansulfonate scaffold may serve as the basis for the creation of anti-tuberculosis drugs.

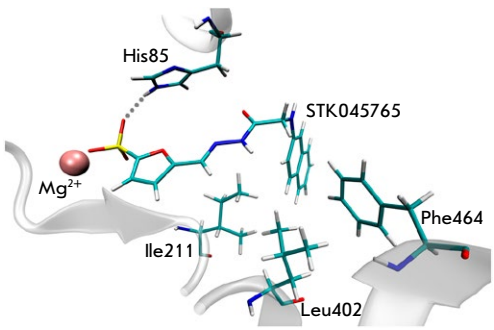

Model of the enzyme-inhibitor complex of mbTK and STK045765

ActaNaturae
APRIL–JUNE 2023 VOL. 15 № 2 (57)
since april 2009, 4 times a year

Founders
Acta Naturae, Ltd,
National Research University
Higher School of Economics

Adress: 101000, Moscow, Myasnitskaya Ulitsa, 13, str. 4
Phone/Fax: +7 (495) 727 38 60
E-mail: actanaturae@gmail.com

Номер подписан в печать 30 июня 2023 г.
Тираж 15 экз. Цена свободная.
Отпечатано в типографии: НИУ ВШЭ,
г. Москва, Измайловское шоссе, 44, стр. 2

Founder and Chairman
of the Editorial Board (from 2009 to 2023)
of the journal Acta Naturae
Academician Grigoriev Anatoly Ivanovich

Indexed in PubMed, Web of Science, Scopus, and RISC

Impact Factor: 2.0 (WOS); 3.5 (Scopus)

CONTENTS

REVIEWS

RESEARCH ARTICLES

SHORT REPORTS

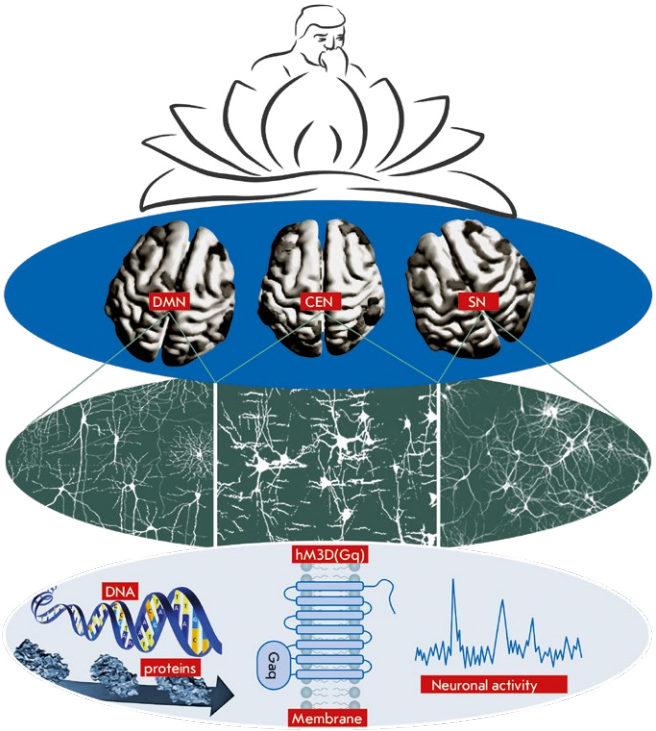

IMAGE ON THE COVER PAGE
(see the article by Dygalo)

Connectivity of the Brain in the Light of Chemogenetic Modulation of Neuronal Activity

N. N. Dygalo
Institute of Cytology and Genetics, Siberian Branch of Russian Academy of Sciences (IC&G SB RAS), Novosibirsk, 630090 Russian Federation
E-mail: dygalo@bionet.nsc.ru
Received: December 24, 2022; in final form, May 10, 2023
DOI: 10.32607/actanaturae.11895

ABSTRACT **Connectivity is the coordinated activity of the neuronal networks responsible for brain functions; it is detected based on functional magnetic resonance imaging signals that depend on the oxygen level in the blood (blood oxygen level-dependent (BOLD) signals) supplying the brain. The BOLD signal is only indirectly related to the underlying neuronal activity; therefore, it remains an open question whether connectivity and changes in it are only manifestations of normal and pathological states of the brain or they are, to some extent, the causes of these states. The creation of chemogenetic receptors activated by synthetic drugs (designer receptors exclusively activated by designer drugs, DREADDs), which, depending on the receptor type, either facilitate or, on the contrary, inhibit the neuronal response to received physiological stimuli, makes it possible to assess brain connectivity in the light of controlled neuronal activity. Evidence suggests that connectivity is based on neuronal activity and is a manifestation of connections between brain regions that integrate sensory, cognitive, and motor functions. Chemogenetic modulation of the activity of various groups and types of neurons changes the connectivity of the brain and its complex functions. Chemogenetics can be useful in reconfiguring the pathological mechanisms of nervous and mental diseases. The initiated integration, based on the whole-brain connectome from molecular-cellular, neuronal, and synaptic processes to higher nervous activity and behavior, has the potential to significantly increase the fundamental and applied value of this branch of neuroscience.**
KEYWORDS **brain connectivity, functional magnetic resonance imaging, chemogenetics, neuronal activity, behavior.**
ABBREVIATIONS **BOLD – blood oxygen level-dependent fMRI signal; CaMKII – calcium–calmodulin-dependent protein kinase II; CEN – central executive network; CNO – clozapine N-oxide; DREADD – designer receptors exclusively activated by designer drugs; DMN – default mode network; GABA – gamma-aminobutyric acid; Gq – activating guanine nucleotide-binding protein; fMRI – functional magnetic resonance imaging; rs-fMRI – functional magnetic resonance imaging at rest; hM3D(Gq) – activating chemogenetic receptor; hM4D(Gi) – inhibitory chemogenetic receptor; hSyn – human synapsin promoter; KORD – inhibitory chemogenetic receptor; LC – locus coeruleus; mCherry – red fluorescent protein; NE – norepinephrine; PFC – prefrontal cortex; rAVV – recombinant adeno-associated virus; SN – salience network.**

INTRODUCTION

One of the main goals in neurobiology is to establish the relationship between the brain neuronal activity and the higher nervous system functions, including normal and pathological cognitive and psycho-emotional states. Recent experimental and clinical data demonstrate a significant contribution of not only neurotransmitter, neuroendocrine, neurotrophic, immunologic, molecular and genetic regulators [1–8], but also interaction between brain structures (connectivity [9–15]), which is the coordinated activity of the neuronal networks responsible for one of the brain functions, to the mechanisms underlying brain functions. For instance, this is evidenced by the observed relations between the activity of neuronal networks and attention [16, 15], memory [11, 17], as well as oth-

er many behavioral and psychological manifestations. [18–20]. A direct or indirect effect a group of neurons has on another group is called effective activity.

The increased interest in brain connectivity is due to the promise of intravital non-invasive registration of its manifestations using functional magnetic resonance imaging (fMRI). This tool makes it possible to receive blood oxygen level-dependent (BOLD) signals from the blood supplying the brain. The local blood oxygenation level and, thus, the intensity of the BOLD signal, are believed to correspond to the general neuronal activity in the structure. The correlation between low-frequency fluctuations in BOLD signals from distant brain regions at rest, as well as upon brain activation by either sensory stimulation or pharmacological load is considered a measure of the connectivity between the structures [12].

Despite an increase in the number of studies in this field of neuroscience, the question of whether connectivity and its disorders are either one of the manifestations of normal or pathological states of the brain, or the causes of these states, remains open. In order to answer this question, one should distinguish the causal relationships between these states and connectivity from random correlations between them. Experimental effects triggering a functional brain response (behavioral, vegetative, and other responses) and changes in the connectivity accompanying them are not sufficient to establish a causal relationship between them. Both induced responses and changes in connectivity can be independent manifestations of the state resulting from the exposure. Specific physiological interventions changing neuronal activity and, presumably, connectivity, which is based on this activity, are required. The majority of these effects are not applicable to humans. For this reason, experiments are conducted on animals [21].

Chemogenetic methods, which have only recently come to the fore [22], have significantly improved our ability to study brain functions. These methods make it possible to control the activity of specific neurons using synthetic receptors; e.g., receptors to guanine nucleotide-binding proteins (G) and ligand-gated ion channels. Among these, designer receptors exclusively activated by designer drugs (DREADD) seem promising. Leveraging these receptors either facilitates or, on the contrary, inhibits the neuronal response to the natural physiological stimuli received, depending on the receptor type. At the same time, they do not impose the activity of the effect external to the brain and neuron. Therefore, they make it possible to take the most objective look at the neuronal network organization of brain functions in the light of neuronal activity modulation. The description and systematization of the available data on this issue are the goal of this study.

DESIGNER RECEPTORS EXCLUSIVELY ACTIVATED BY DESIGNER DRUGS

DREADD is the most popular chemogenetic approach used to study the regulation of various aspects of brain activity by neuronal networks in experimental animals [22–28]. In addition to solving fundamental science tasks, chemogenetics can potentially become useful for restructuring the pathological mechanisms of nervous and mental diseases and regulate them using designer drugs [29]. DREADDs interact with exogenous synthetic ligands, which are inert to natural body receptors. The activity of neurons expressing these synthetic receptors can either be enhanced or inhibited, depending on the type of the receptor used. DREADD variants and the features of their expression by the viral vectors and transgenes used in experiments for assessing their chemogenetic effects on brain connectivity are presented below.

Two DREADD variants based on the human muscarinic acetylcholine receptors (hM3D(Gq) and hM4D(Gi)) are widely used. To create DREADD-hM3D(Gq), which enhances the neuronal response to physiological stimuli upon interaction with the synthetic ligand clozapine N-oxide (CNO), a metabotropic type 3 acetylcholine receptor, coupled with the activating guanine nucleotide-binding protein Gq, was used. The functional effect of these receptors is considered to be due to an increase in neuronal sensitivity to the stimulation resulting from neuron membrane depolarization. DREADD-hM4D(Gi) inhibiting activation of a cell with these receptors upon interaction with CNO was developed using a modified type 4 metabotropic acetylcholine receptor, coupled to the inhibitory guanine nucleotide-binding protein (Gi). Receptor hM4D(Gi) is considered to decrease neuronal excitation though cell hyperpolarization. In addition to acetylcholine receptors, the kappa-opioid receptor, coupled with the inhibitory guanine nucleotide-binding Gi (KORD), which inhibits cell activity upon interaction with its pharmacologically inert ligand salvinorin b, was used [30]. Chemogenetic inhibition/inactivation in experimental neurobehavioral neuroscience is often referred to as chemogenetic silencing. DREADDs enter the brain either as part of a transgene, whose expression in the structure of interest is achieved by crossing specific mouse lines [31], or as part of a vector, which is usually based on an adeno-associated virus [24–28]. Stereotaxic administration of the viral vector provides its localization in the brain structure of interest, while the promoter governing the

expression ensures the presence of the DREADD in the desired type (or types) of cells.

DREADDs are well expressed in the central nervous system cells as part of viral vectors or transgenes and can be used for reversible activation and inhibition of target cells upon systemic administration of the ligands to these receptors or direct injection of these ligands into the brain. High expression level in the brain is provided by promoters nonselective to the neuron type, such as cytomegalovirus [32] and human synapsin (hSyn) promoters [31–36]. The use of promoters that are active only in certain neurons, such as CaMKII, which is active in glutamatergic pyramidal neurons [31, 37], promoters specific to GABAergic interneurons synthesizing parvalbumin and expressing prodynorphin or proenkephalin [31], as well as serotonergic- [38], noradrenergic-specific, and dopamine-responding neurons [39–41], makes it possible to study the effect of a change in the activity of a certain neuron type and subtype on brain connectivity.

CONNECTIVITY

Functional connectivity is determined based on the correlation between BOLD signals measured in different brain regions by functional magnetic resonance imaging (fMRI). The signal registered in the absence of external stimuli is considered resting-state fMRI (rs-fMRI). BOLD signals associated with task performance are called responses; e.g., in tactile fMRI used in limb stimulation [42]. Spatial maps showing the intrinsic functional network organization of the brain are obtained based on these signals [43].

Each network consists of groups of neurons that are located in different structures of the brain but respond in a coordinated way, with changes in their activity depending on the external and/or internal stimuli. For instance, the default mode network (DMN) is responsible for cogitation and self-reflection, which are independent of external stimuli in a healthy brain. Inhibition of its activity improves the performance of tasks requiring attention [9]. The DMN core includes the posterior medial and the parietal brain cortices, as well as separate zones of the temporal and frontal lobes [44]. The salience network (SN) fosters attention to important events; it perceives and responds to signals related to homeostasis [45]. The main SN structures are anterior insula, the anterior cingulate cortex, and ventral striatum. The central executive network (CEN) operates with working memory information; it is responsible for making decisions in goal-informed behavior. Its centers are the dorsolateral prefrontal and the posterior lateral parietal cortices. These and other large-scale networks that were first identified in humans [46] demonstrate pronounced homology with similar networks in monkeys and rodents [47, 48].

The activity of the functional connectivity networks assessed by rs-fMRI correlates well with cognitive abilities and behavior [49], as well as changes in the brain excitation level [10, 50]. It is of practical importance that rs-fMRI signals in patients with mental [13, 20, 51, 52] and neurodegenerative [53] diseases clearly differ in functional connectivity from those of a healthy human brain. Despite the fact that they make it possible to use rs-fMRI for disease diagnosis [54], the results related to these differences are usually difficult to interpret, since the BOLD signal is only weakly and indirectly related to the underlying neuronal activity.

For this reason, the right approaches to identifying any possible relation between regional functional connectivity and direct indicators of neuron activation, neurotransmitter release, and metabolism in brain cells are currently being sought. In order to do this, it is necessary to induce changes in neuronal activity and register either the rs-fMRI or positron-emission tomography (PET) signals. The latter method is attempted much less frequently than rs-fMRI, since it requires the use of positron-emitting radioisotopes, such as 18F-fluorodeoxyglucose (18-FDG) [55]. Transcranial magnetic stimulation used in humans indeed affects DMN connectivity [56]. However, changes in the activity of neurons beyond the scope of its normal patterns affect network structure and function. In this regard, only modulation within the natural range can be used to assess the effect of neuronal activity on the connectivity [57]. The chemogenetic approach is the most suitable among the others (pharmacological, electrophysiological, magnetic field exposure-based, and optogenetic methods) when seeking to alter neuronal activity. This approach mainly facilitates or, on the contrary, inhibits the neuronal response to natural physiological stimuli. Some variants of these methods were given specific names by the authors. For instance, the method including the DREADD approach and 18F-fluorodeoxyglucose imaging by PET is called DREADD-assisted metabolic mapping [55]. The combination of DREADD and rs-fMRI to study changes in spontaneous neuronal activity is called chemo-fMRI [38].

It should be noted that activation of nodal neurons affects even distant regions of the brain. For instance, chemogenetic stimulation of neurons expressing the D1 dopamine receptor in the dorsal striatum of only one hemisphere activates electrophysiological responses in the medial thalamus, nucleus accumbens, and both hemisphere cortices in mice [41]. Inhibition of neuronal activity in nodal regions can also elicit a

spiking nature of propagation that goes beyond the connections with the node and affects other neuronal networks [35].

The bulk of the experimental data available to date, which are to be discussed below, indicate a change in the connectivity upon chemogenetic modulation of the activity of different groups and types of brain neurons.

MODULATION OF NEURONAL ACTIVITY NON-SPECIFIC TO NEURONAL TYPE

Currently, a number of laboratories use chemogenetic modulation of neuronal activity non-selective to the neuron type, in combination with fMRI [34–39, 58], to study the responses of the neuronal network connectivity in laboratory animals.

The mammalian brain is a complex system, and a change in neuronal activity even in one region can lead to large-scale effects on its many functions. For instance, chemogenetic inactivation of all types of neurons expressed under the hSyn DREADD–hM4D promoter, which inhibits the activity of the neurons in the amygdala, a subcortical region with broad connections in the cortex, disrupted the amygdalocortical fMRI connectivity and the distribution of corticocortical connections between functional brain networks in rhesus macaques [33]. A higher number of DREADD-transfected cells in the amygdala was associated with a more pronounced disruption of the functional connectivity between this structure and monosynaptically connected, as well as non-directly connected, brain regions. The combination of communication contacts through the monosynaptic and polysynaptic pathways explains to a large extent the correlational structure of endogenous brain activity and many of the changes in it resulting from a decrease in amygdala activity. These results indicate a structural basis for neuronal activity and a possible relation between neuropathology and neurophysiological changes in regions distant from the presumptive focus [33].

The DMN is the main network in the mammalian brain. However, the functional role of the nodes in this network and the mechanisms underlying the connection between its structure and the behavior it regulates remain unclear. To gather information on these issues, chemogenetic inactivation of the key DMN node, namely the dorsal anterior cingulate cortex, was used, in combination with rs-fMRI and behavioral testing in awake rats [34]. The authors called this method the hemo-rsfMRI-behavior approach. Inhibition of the activity of the dorsal anterior cingulate cortex using DREADD-hM4Di, expressed under the hSyn promoter, significantly deactivated the neurons in the prelimbic and dorsal cortices of the middle cingulate gyrus and induced multidirectional changes in connectivity between DMN nodes. The changes in the connectivity correlated with the animal's behavior: anxiety and motor activity in the home cage were noted. The results indicate that DMN activity in both rodents and humans is aligned with behavior [34].

Chemogenetic activation of the mesolimbic and mesocortical pathways, which are projections of the ventral tegmental area to the nucleus accumbens and medial prefrontal cortex (PFC), respectively, induced BOLD responses not only in DREADD-expressing regions, but also in neuronal networks distant from the sites of the chemogenetic vector injections not expressing DREADD [36]. The neurochemical nature of these pathways is apparently heterogeneous. This conclusion is based on the fact that the hSyn promoter, which is nonselective to the neuron type, was used for DREADD-hM3D(Gq) expression, while projections from the ventral tegmental region to the nucleus accumbens release dopamine, glutamate, GABA, the brain-derived neurotrophic factor, and other signaling molecules [59]. The duration of the brain activity corresponded to the onset of the behavioral response: motor hyperactivity in animals with chemogenetically induced mesolimbic pathway. This activation specifically increased neuronal activity, while functional connectivity measured by rs-FMRI remained stable. Positive and negative BOLD signals clearly showed simultaneous activation of the ventral pallidum and deactivation of the pars reticulata of the substantia nigra, respectively, by demonstrating coordinated reversely directed changes in the activity of different areas of the neuronal network after the stimulation of specific midbrain projection neurons [36]. It should be noted that, in contrast to Roelofs et al. [36], who noted the stability of the functional connectivity in chemogenetic activation of subcortical pathways, other authors mentioned in the present review observed changes in functional connectivity upon chemogenetic modulation of the activity of different neurons in various brain structures.

Acute chemogenetic inhibition of PFC neurons by DREADD-hM4D(Gi) under the nonselective hSyn promoter enhanced fMRI connectivity between this region and its direct thalamocortical targets. PFC inhibition increased the power of low-frequency oscillations by reducing the discharge activity of neurons, which was unrelated in phase to slow the rhythms. This led to an increase in coherence between the slow and δ-bands of the electroencephalogram rhythms between the regions demonstrating fMRI overconnectivity. Apparently, cortex inactivation can increase fMRI connectivity through the enhancement of slow oscillatory processes [31].

Simultaneous chemogenetic reactivation of a set of many of the neuron ensembles involved in the formation of the memory engrams responsible for threat processing and associated with increased expression of the early response gene *c-fos* in these conditions, which are functionally associated, in particular, with hippocampus and amygdala neurons, yielded a more effective behavioral engram, compared to the reactivation of only one ensemble, and reproduced the fear factor caused by the threatening situation more fully. These results show that connectivity of distant structures is a natural occurrence in the implementation of complex brain functions [60].

Chemogenetic inhibition of connectivity as relates to the orbitofrontal cortex and the rostromedial caudate nucleus in rhesus macaques through a contralateral expression of the inhibitory DREADD hM4Di in these brain structures disrupted the capacity to adequately capture the food reward value [32]. In these experiments, DREADD expression was enabled by the cytomegalovirus promoter and the disrupted connectivity could not have been due to a decrease in the activity of any particular type of neurons or glial cells [61]. Nevertheless, it is clear that connectivity in the orbitofrontal cortex and rostromedial caudate nucleus is likely crucial in the formation of motivated behavior based on the integration of external stimuli with the internal drive of monkeys [32].

In addition to nonselective modulation of neuronal activity, changes in the activity of any particular type of neurons also affected connectivity and, apparently, the manifestation of the higher brain functions controled by it.

MODULATION OF NEURONAL ACTIVITY IN MONOAMINERGIC NEUROTRANSMISSION

Chemogenetic-induced tonic activation of noradrenergic norepinephrine (NE) neurons in the locus coeruleus (LC) in the pontine region of the mouse brain led to a reduction in its blood supply and glucose uptake because of these neurons. What is more, it also increased the synchronous low-frequency fMRI activity in the frontal cortex of the DMN, which is significantly distant from the LC. LC-NE activation induced NE release, enhanced neuronal calcium signals, and decreased blood supply into the anterior cingulate cortex. LC-NE stimulation also enhanced functional connectivity in the frontal DMN and, apparently, boosted the behavior associated with this brain network [40]. LC activation in humans is associated with a shift in connectivity amongst the brain networks in favor of processing of the most relevant information [62]. A possible causal relationship within this association was analyzed in mice by using chemogenetic activation of LC coupled with rs-fMRI [39]. This approach is called chemo-connectomics. LC activation was found to rapidly interrupt current behavior and significantly increase brain-wide connectivity, with the most pronounced effects being noted in the salience and amygdala networks. Changes in functional connectivity correlated with the levels of the alpha-1- and beta-1-adrenergic receptor transcripts in the brain, while functional network connectivity correlated with NE metabolism within the brain structures. It is likely that these changes in large-scale network connectivity affect the optimization of neuronal information processing, which is significant in increasing vigilance and detecting threats [39].

Chemogenetic activation of neurons expressing dopamine D1 receptors in the mouse left dorsal striatum increased the fractional amplitude of low-frequency fluctuations (fALFF) in the medial thalamus, nucleus accumbens, and the cortexes of both hemispheres. In addition, gamma-band local field potentials were increased in the stimulated striatum and the cortices of both hemispheres [41].

Serotonin-producing neurons abundantly innervate brain regions through their extended projections [63]. The use of chemo-fMRI to identify any possible effect of serotonergic neurotransmission on regional and global functional activity showed that endogenous stimulation of serotonin-producing neurons did not affect global brain activity but caused regional activation of a series of primary target regions encompassing the cortico-hippocampal and ventral striatal areas. At the same time, the pharmacological increase in serotonin levels led to widespread fMRI deactivation in the brain, which probably is an indication of a combined contribution of central and perivascular constrictive effects. These results identify the main functional targets of endogenous serotonergic stimulation and suggest a possible causal relationship between serotonergic neuron activation and regional fMRI signals [38].

MODULATION OF THE ACTIVITY OF PYRAMIDAL NEURONS AND INTERNEURONS

Chemogenetic stimulation of the bed nucleus of the stria terminalis expressing the vesicular γ-aminobutyric acid (GABA) transporter using DREADD-hM3Dq prompted anxiety-like behavior and resulted in long-term depression in glutamatergic neurotransmission, indicating changes in synaptic plasticity. Metabolic mapping of whole-brain activity after such exposure revealed enhanced activity within the ventral midbrain structures, including the ventral tegmental area, and hindbrain structures such as the

LC and the parabrachial nucleus. The activity of these brain nuclei is associated with anxiety-like behavior. The use of microfluidics profiling of the receptor system of individual neurons in the bed nucleus of the stria terminalis expressing the vesicular GABA transporter showed that stimulation of the Gq-coupled type 2c serotonin receptor is responsible for anxiety-like behavior [64].

DREADD modulation combined with 18F-FDG-PET imaging called DREADD-assisted metabolic mapping (DREAMM) made it possible to create whole-brain metabolic maps of animals under conditions of free behavior [65]. This method was used to demonstrate the association of various corticolimbic networks with specific manifestations during inhibition of the activity of prodynorphin- and proenkephalin-expressing inhibitory GABAergic medium spiny neurons in the nucleus accumbens shell [65], which are associated with neuropsychiatric disorders.

Decreased activity of glutamatergic neurons in the right anterior cingulate cortex in mice due to the effect of the inhibitory kappa-opioid receptor DREADD (KORD) expressed under the CaMKII promoter resulted in a reduced fMRI BOLD signal in this brain region and increased the fMRI BOLD signal in the brain regions of both hemispheres associated with the anterior cingulate cortex. Changes in neuronal activity were observed in functional networks, including connections with the sensory cortex, thalamus, basolateral amygdala, and globus pallidus (s. pallidum). These regions are responsible for attention, working memory, fear, and reward, respectively. This modulation of neuronal activity was accompanied by a decrease in intra- and interhemispheric functional connectivity [58].

Chemogenetic excitation of the main glutamatergic pyramidal neurons expressing activating DREADD-hM3D(Gq) under the CaMKII promoter and inhibition of parvalbumin-expressing GABAergic interneurons in the PFC weakened the connection between the latter and DMN cortical projections. Both types of exposure increased the local excitation rate and shifted the local field potential (LFP) power towards higher frequencies, while effectively reversing the electrophysiological effects of the inhibitory DREADD-hM4D(Gi) expressed in the cortex under the nonselective hSyn promoter. Stimulation of pyramidal neurons suppressed slow- and delta-band LFP activity more effectively than interneuron inhibition. The functional overconnectivity observed in these experiments is assumed to be due to both an increased excitation-to-inhibition ratio in the PFC and a nonspecific functional decrease in the activity of GABAergic neurons [31].

Chemogenetic activation of the glutamatergic neurons of the paraventricular hypothalamic nucleus expressing the rAVV-CaMKIIα-hM3Dq-mCherry vector increased BOLD signals measured by chemo-fMRI and functional connectivity between paraventricular and olfactory nuclei, the cingulate cortex, the paraventricular thalamic nucleus, the periaqueductal gray nucleus, and the hippocampus after CNO administration to rats [66].

NEURONAL ACTIVITY MODULATES BEHAVIOR THROUGH CONNECTIVITY

The results of recent experiments similar to the ones described above allow one to consider specific chemogenetically induced changes in connectivity not only as concomitant signs of higher nervous activity dysfunction, but also as a likely cause of the disorder. For instance, an association between corticolimbic networks and specific behavior manifestations was found upon inhibition of the activity of inhibitory GABAergic medium spiny neurons. Levorotatory behavior was increased in prodynorphin-expressing neurons, and dextrorotatory behavior was enhanced in proenkephalin-expressing neurons. Inhibition of neuronal activity in awake state and under anesthesia changed the activity of different neuronal networks [65]. Chemogenetic inactivation of the interaction between the orbitofrontal and rhinal cortices using hM4Di-DREADD reduced the ability of monkeys to discriminate among expected rewards in a behavioral experiment [67]. Chemogenetic impairment in the connectivity of the orbitofrontal cortex and the rostromedial region of the caudate nucleus changed the formation of motivated behavior due to a combination of external stimuli with the internal drive of monkeys [32]. Inhibition of activity in the dorsal anterior cingulate cortex using DREADD-hM4D(Gi) expressed under hSyn significantly decreased the activity of the neurons in the prelimbic and dorsal cortices of the middle cingulate gyrus and induced multidirectional changes in the connectivity between DMN nodes. These changes correlated with animal behavior: anxiety and motor activity in the home cage were noted. It is apparent that DMN activity in both rodents and humans is coordinated with behavior manifestations [34]. Chemogenetic activation of LC-NE induced NE release, enhanced neuronal calcium signals, and decreased blood supply to the anterior cingulate cortex. LC-NE activation also enhanced functional connectivity in the frontal DMN and, as a consequence, promoted a behavior response associated with this brain network [40].

Both contralateral and bilateral, but not ipsilateral, chemogenetic inactivation of predominantly gluta-

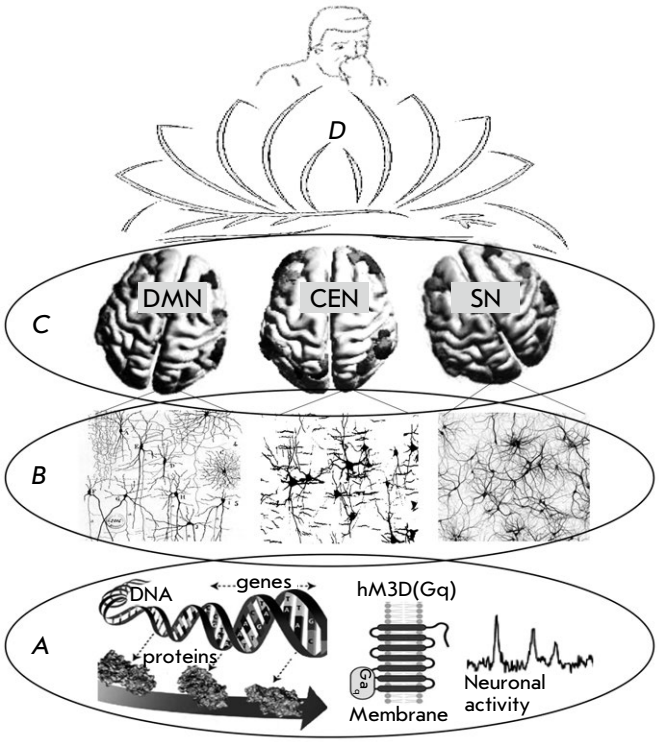

Fig. 1. Schematic presentation of the multilevel organization of brain functions in mammals. (*A*) – molecular and cellular processes, genes, proteins, cell membrane with proteins (as an example, the chemogenetic activating hM3D (Gq) receptor is presented schematically), and electrophysiological activity of the neuron. (*B*) – neuronal network ensembles of neurons interconnected through contacts, which form the basis of the structural and functional organization of the brain. (*C*) – large-scale brain networks, each of which emerged during evolution based on neuronal ensembles, which are presented schematically in (*B*), for predominant performance of certain adaptive functions by each of them. Pictures of the apical surface of the human brain show three large-scale networks: the default mode network (DMN), the central executive network (CEN), and the salience network (SN). The most important sections of each of the networks are shaded. Apparently, the interactions of DMN, CEN, SN, as well as a number of other large-scale brain networks, ensure cognitive and behavioral manifestations in an individual (*D*)

matergic neurons in two structures (dorsal hippocampus and PFC) impaired learning in rats in the W-maze. These results indicate that the connectivity of the dorsal hippocampus and PFC plays a key role in spatial learning and memory [68]. The combined use of chemogenetic inactivation of the activity of the primary somatosensory cortex using tactile fMRI revealed a link between neuronal activity, connectivity, and behavior in macaques. Focal chemogenetic silencing of the functionally identified hand region in the somatosensory cortex impaired grasping. The same inhibition also attenuated the fMRI signal induced by hand stimulation both at the local silencing site and anatomically and/or functionally connected downstream network underlying the induced grasping behavior disorder. In addition, inhibition of the hand region unexpectedly disinhibited foot representation, with concomitant behavioral hypersensitization [42].

CONCLUSION

Connectivity is the manifestation of natural connections between brain regions that selectively integrate sensory, cognitive, and motor activation. These connections are rooted in brain evolution [69], and their individual features take shape during ontogeny [70]. The genetic component substantially contributes to the formation of individual connectome features. The majority of the 19 various neuropsychiatric and idiopathic conditions studied in more

than 30,000 individuals had specific connectome profiles that correlated with the genomic and transcriptomic features of these conditions [71]. Genes play an important role in the formation of functionally important and metabolically costly interactions between the nodal regions of the connectomes. These regions share transcriptional activity patterns owing to the similarity of their metabolic and cytoarchitectonic features. The genes involved in the formation and maintenance of synapses and axons are important for establishing connections between different brain regions; in particular, the transcriptome features of the nodal centers of neural networks are determined by the metabolic needs of these centers [72, 73]. It should be noted that DREADD activation alters gene expression. For instance, chemogenetic activation of the glutamatergic neurons of the superior colliculus significantly changed the transcriptome of this structure towards the predominance of neurotrophic processes [74]. Thirteen defects in nervous system development, neurological and mental disorders, whose predictors are molecular genetic and biochemical disorders, were found to be associated with the structural and anatomical patterns of cortical anomalies affecting the main brain network architecture; this indicates a likely mutual enhancement of the negative contributions of local molecular and global connectome mechanisms to the pathology [75].

Many studies and reviews have discussed the variability of gene expression patterns in the brain in one psycho-emotional state, up to almost complete discrepancy between different mouse lines [76]. Therefore, one of the ways to clarify the structure and function of the mechanisms underlying these conditions may be to analyze the brain parameters that are more closely related to psycho-emotional regulation, such as connectivity, which is also regulated by gene expression [8]. The results available to date, including the ones discussed in the current review, provide sufficient evidence of this.

In addition, identification of the biological meaning of the connectome requires not only its analysis data, but also the results of studies in related science fields such as anatomy, physiology, molecular genetics, and behavior analysis. Information regarding intracellular and cell properties, synapse plasticity, and the effects of neuromodulators on cells and synapses is of the utmost importance. Such data will make it easier to map out the entire pathway of connnectivity, from molecular and cellular, neuronal and synaptic processes to higher nervous activity and behavior based on the connectome (*Fig. 1*). ●

This work was supported by the Russian Foundation for Basic Research (project No. 20-015-00129) and FWNR-2022-0023.

REFERENCES

1. McEwen B.S. // Physiol. Rev. 2007. V. 87. № 3. P. 873–904.
2. McEwen B.S., Bowles N.P., Gray J.D., Hill M.N., Hunter R.G., Karatsoreos I.N., Nasca C. // Nat. Neurosci. 2015. V. 18. № 10. P. 1353–1363.
3. Dygalo N.N., Shishkina G.T., Kalinina T.S., Yudina A.M., Ovchinnikova E.S. // Pharmacol Biochem. Behav. 2006. № 85. № 1. P. 220–227.
4. Shishkina G.T., Kalinina T.S., Sournina N.Y., Dygalo N.N. // J. Neurosci. 2001. V. 21. № 2. P. 726–731.
5. Shishkina G.T., Kalinina T.S., Dygalo N.N. // Neuroscience. 2004. V. 129. № 3. P. 521–528.
6. Shishkina G.T., Kalinina T.S., Berezova I.V., Bulygina V.V., Dygalo N.N. // Behav. Brain. Res. 2010. V. 213. № 2. P. 218–224.
7. Shishkina G.T., Dygalo N.N. // Zh. Vyssh. Nerv. Deiat. im. I.P. Pavlova. 2010. V. 60. № 2. P. 138–152.
8. Dygalo N.N., Kalinina T.S., Shishkina G.T. // Stress. 2020. V. 23. № 6. P. 700–707.
9. Whitfield-Gabrieli S., Ford J.M. // Annu. Rev. Clin. Psychol. 2012. V. 8. P. 49–76.
10. Allen E.A., Damaraju E., Plis S.M., Erhardt E.B., Eichele T., Calhoun V.D. // Cereb. Cortex. 2014. V. 24. № 3. P. 663–676.
11. Avery E.W., Yoo K., Rosenberg M.D., Greene A.S., Gao S., Na D.L., Scheinost D., Constable T.R., Chun M.M. // J. Cogn. Neurosci. 2020. V. 32. № 2. P. 241–255.
12. Friston K.J. // Brain Connect. 2011. V. 1. № 1. P. 13–36.
13. Duman R.S., Sanacora G., Krystal J.H. // Neuron. 2019. V. 102. № 1. P. 75–90.
14. Dygalo N.N., Shishkina G.T. // Zh. Vyssh. Nerv. Deiat. im. I.P. Pavlova. 2020. V. 70. № 1. P. 3–11.
15. Rosenberg M.D., Scheinost D., Greene A.S., Avery E.W., Kwon Y.H., Finn E.S., Ramani R., Qiu M., Constable R.T., Chun M.M. // Proc. Natl. Acad. Sci. USA. 2020. V. 117. № 7. P. 3797–3807.
16. Kucyi A., Daitch A., Raccah O., Zhao B., Zhang C., Esterman M., Zeineh M., Halpern C.H., Zhang K., Zhang J., Parvizi J. // Nat. Commun. 2020. V. 11. № 11. P. 325.
17. Yamashita M., Yoshihara Y., Hashimoto R., Yahata N., Ichikawa N., Sakai Y., Yamada T., Matsukawa N., Okada G., Tanaka S.C., et al. // Elife. 2018. V. 10. № 7. P. e38844.
18. Woodward N.D., Cascio C.J. // JAMA Psychiatry. 2015. V. 72. № 8. P. 743–744.
19. Yan C.G., Chen X., Li L., Castellanos F.X., Bai T.J., Bo Q.J., Cao J., Chen G.M., Chen N.X., Chen W., Cheng C.,

et al. // Proc. Natl. Acad. Sci. USA. 2019. V. 116. № 18. P. 9078–9083.
20. Li S., Hu N., Zhang W., Tao B., Dai J., Gong Y., Tan Y., Cai D., Lui S. // Front. Psychiatry. 2019. № 10. P. 482.
21. Pais-Roldán P., Mateo C., Pan W.J., Acland B., Kleinfeld D., Snyder L.H., Yu X., Keilholz S. // Neuroimage. 2021. № 245. P. 118630.
22. Armbruster B.N., Li X., Pausch M.H., Herlitze S., Roth B.L. // Proc. Natl. Acad. Sci. USA. 2007. V. 104. № 12. P. 5163–5168.
23. Atasoy D., Sternson S.M. // Physiol. Rev. 2018. V. 98. № 1. P. 391–418.
24. Roth B.L. // Neuron. 2016. V. 89. № 4. P. 683–694.
25. Dygalo N.N. // Neurosci. Behav. Physiol. 2020. V. 50. № 8. P. 1051–1056.
26. Dygalo N.N., Lanshakov D.A., Komysheva N.P., Drozd U.S., Shaburova E.V., Sukhareva E.V., Shishkina G.T. // Dokl. Biochem. Biophys. 2020. V. 490. № 1. P. 16–18.
27. Kolesov D.V., Sokolinskaya E.L., Lukyanov K.A., Bogdanov A.M. // Acta Naturae. 2021. V. 13. № 4. P. 17–32.
28. Swanson J.L., Chin P.S., Romero J.M., Srivastava S., Ortiz-Guzman J., Hunt P.J., Arenkiel B.R. // Front. Neural Circuits. 2022. V. 16. P. 886302.
29. Ozawa A., Arakawa H. // Behav. Brain Res. 2021. V. 406. P. 113234.
30. Vardy E., Robinson J.E., Li C., Olsen R.H.J., DiBerto J.F., Giguere P.M., Sassano F.M., Huang X.P., Zhu H., Urban D.J., et al. // Neuron. 2015. V. 86. № 1. P. 936–946.
31. Rocchi F., Canella C., Noei S., Gutierrez-Barragan D., Coletta L., Galbusera A., Stuefer A., Vassanelli S., Pasqualetti M., Iurilli G., et al. // Nat. Commun. 2022. V. 13. № 1. P. 1056.
32. Oyama K., Hori Y., Mimura K., Nagai Y., Eldridge M.A.G., Saunders R.C., Miyakawa N., Hirabayashi T., Hori Y., Inoue K.I., et al. // J. Neurosci. 2022. V. 42. № 32. P. 6267–6275.
33. Grayson D.S., Bliss-Moreau E., Machado C.J., Bennett J., Shen K., Grant K.A., Fair D.A., Amaral D.G. // Neuron. 2016. V. 91. № 2. P. 453–466.
34. Tu W., Ma Z., Ma Y., Dopfel D., Zhang N. // Cereb. Cortex. 2021. V. 31. № 1. P. 312–323.
35. Tu W., Ma Z., Zhang N. // Neuroimage. 2021. V. 237. P. 118219.
36. Roelofs T.J.M., Verharen J.P.H., van Tilborg G.A.F., Boekhoudt L., van der Toorn A., de Jong J.W., Luijendijk M.C.M., Otte W.M., Adan R.A.H., Dijkhuizen RM. // Neuroimage. 2017. V. 156. P. 109–118.
37. Peeters L.M., van den Berg M., Hinz R., Majumdar G., Pintelon I., Keliris G.A. // Science. 2020. V. 9. P. 101455.
38. Giorgi A., Migliarini S., Galbusera A., Maddaloni G., Mereu M., Margiani G., Gritti M., Landi S., Trovato F., Bertozzi S.M., Armirotti A., et al. // Cell Rep. 2017. V. 21. № 4. P. 910–918.
39. Zerbi V., Floriou-Servou A., Markicevic M., Vermeiren Y., Sturman O., Privitera M., von Ziegler L., Ferrari K.D., Weber B., De Deyn P.P., et al. // Neuron. 2019. V. 103. № 4. P. 702–718.
40. Oyarzabal E.A., Hsu L.M., Das M., Chao T.H., Zhou J., Song S., Zhang W., Smith K.G., Sciolino N.R., Evsyukova I.Y., et al. // Sci. Adv. 2022. V. 8. № 17. P. eabm9898.
41. Nakamura Y., Nakamura Y., Pelosi A., Djemai B., Debacker C., Hervé D., Girault J.A., Tsurugizawa T. // Neuroimage. 2020. V. 220. P. 117079.
42. Hirabayashi T., Nagai Y., Hori Y., Inoue K.I., Aoki I., Takada M., Suhara T., Higuchi M., Minamimoto T. // Neuron. 2021. V. 109. № 20. P. 3312–3322.
43. Biswal B., Zerrin Yetkin F., Haughton V.M., Hyde J.S. // Magn. Reson. Med. 1995. V. 34. P. 537–541.
44. Raichle M.E. // Annu. Rev. Neurosci. 2015. V. 8. № 38. P. 433–447.
45. Seeley W.W.J. // Neurosci. 2019. V. 39. № 50. P. 878–882.
46. Power J.D., Cohen A.L., Nelson S.M., Wig G.S, Barnes K.A., Church J.A., Vogel A.C., Laumann T.O., Miezin F.M., Schlaggar B.L., et al. // Neuron. 2011. V. 72. № 4. P. 665–678.
47. Grandjean J., Canella C., Anckaerts C., Ayrancı G., Bougacha S., Bienert T., Buehlmann D., Coletta L., Gallino D., Gass N., et al. // Neuroimage. 2020. V. 205. P. 116278.
48. Xu N., LaGrow T.J., Anumba N., Lee A., Zhang X., Yousefi B., Bassil Y., Clavijo G.P., Khalilzad Sharghi V., et al. // Front. Neurosci. 2022. V. 16. P. 816331.
49. Smith S.M., Nichols T.E., Vidaurre D., Winkler A.M., Behrens T.E., Glasser M.F., Ugurbil K., Barch D.M., van Essen D.C., Miller K.L. // Nat. Neurosci. 2015. V. 18. № 11. P. 1565–1567.
50. Tagliazucchi E., Laufs H. // Neuron. 2014. V. 82. № 3. P. 695–708.
51. Zhang L., Wu H., Xu J., Shang J. // Front. Neurosci. 2018. V. 12. P. 692.
52. Yang H., Zhang H., Meng C., Wohlschläger A., Brandl F., Di X., Wang S., Tian L., Biswal B. // Hum. Brain Map. 2022. V. 43. № 12. P. 3792–3808.
53. Sorg C., Riedl V., Mühlau M., Calhoun V.D., Eichele T., Läer L., Drzezga A., Förstl H., Kurz A., Zimmer C., et al. // Proc. Natl. Acad. Sci. USA. 2007. V. 104. № 47. P. 18760–18765.
54. Lee M.H., Smyser C.D., Shimony J.S. // AJNR Am. J. Neuroradiol. 2013. V. 34. № 10. P. 1866–1872.
55. Michaelides M., Hurd Y.L. // Neuropsychopharmacology. 2015. V. 40. № 1. P. 239–240.
56. Liston C., Chen A.C., Zebley B.D., Drysdale A.T., Gordon R., Leuchter B., Voss H.U., Casey B.J., Etkin A., Dubin M.J. // Biol. Psychiatry. 2014. V. 76. № 7. P. 517–526.
57. Jazayeri M., Afraz A. // Neuron. 2017. V. 93. № 5. P. 1003–1014.
58. Peeters L.M., Hinz R., Detrez J.R., Missault S., De Vos W.H., Verhoye M., van der Linden A., Keliris G.A. // Neuroimage. 2020. V. 220. P. 117088.
59. Morales M., Margolis E.B. // Nat. Rev. Neurosci. 2017. V. 18. P. 73–85.
60. Roy D.S., Park Y.G., Kim M.E., Zhang Y., Ogawa S.K., DiNapoli N., Gu X., Cho J.H., Choi H., Kamentsky L., et al. // Nat. Commun. 2022. V. 13. P. 1799.
61. Betley J.N., Sternson S.M. // Hum. Gene. Ther. 2011. V. 22. № 6. P. 669–677.
62. Hermans E.J., Henckens M.J., Joëls M., Fernández G. // Trends Neurosci. 2014. V. 37. № 6. P. 304–314.
63. Awasthi J.R., Tamada K., Overton E.T.N., Takumi T. // J. Comp. Neurol. 2021. V. 529. № 7. P. 1391–1429.
64. Mazzone C.M., Pati D., Michaelides M., DiBerto J., Fox J.H., Tipton G., Anderson C., Duffy K., McKlveen J.M., Hardaway J.A., et al. // Mol. Psychiatry. 2018. V. 23. № 1. P. 143–153.
65. Michaelides M., Anderson S.A., Ananth M., Smirnov D., Thanos P.K., Neumaier J.F., Wang G.J., Volkow N.D., Hurd Y.L. // J. Clin. Invest. 2013. V. 123. № 12. P. 5342–5350.
66. Liu Y., Rao B., Li S., Zheng N., Wang J., Bi L, Xu H. // Front. Pharmacol. 2022. V. 13. P. 814623.
67. Eldridge M.A., Lerchner W., Saunders R.C., Kaneko H., Krausz K.W., Gonzalez F.J., Ji B., Higuchi M., Minami-

moto T., Richmond B.J. // Nat. Neurosci. 2016. V. 19. № 1. P. 37–39.
68. Maharjan D.M., Dai Y.Y., Glantz E.H., Jadhav S.P. // Neurobiol. Learn. Mem. 2018. V. 155. P. 351–360.
69. Thiebaut de Schotten M., Forkel S.J. // Science. 2022. V. 378. № 6619. P. 505–510.
70. Bragg-Gonzalo L., De León Reyes N.S., Nieto M. // Semin. Cell. Dev. Biol. 2021. V. 118. P. 24–34.
71. Moreau C.A., Kumar K., Harvey A., Huguet G., Urchs S., Schultz L.M., Sharmarke H., Jizi K., Martin C.O., Younis N., et al. // Brain. 2022. awac315.
72. Arnatkevičiūtė A., Fulcher B.D., Fornito A. // Front. Neural Circuits. 2019. V. 13. P. 47.
73. Arnatkeviciute A., Fulcher B.D., Oldham S., Tiego J., Paquola C., Gerring Z., Aquino K., Hawi Z., Johnson B., Ball G., et al. // Nat. Commun. 2021. V. 12. P. 4237.
74. Claes M., Geeraerts E., Plaisance S., Mentens S., Van den Haute C., De Groef L., Arckens L., Moons L. // Cells. 2022. V. 11. № 11. P. 1784.
75. Hansen J.Y., Shafiei G., Vogel J.W., Smart K., Bearden C.E., Hoogman M., Franke B., van Rooij D., Buitelaar J., McDonald C.R., et al. // Nat. Commun. 2022. V. 13. № 1. P. 4682.
76. Mozhui K., Karlsson R.M, Kash T.L., Ihne J., Norcross M., Patel S., Farrell M.R., Hill E.E., Graybeal C., Martin K.P., et al. // J. Neurosci. 2010. V. 30. № 15. P. 5357–5367.

The Unique Genome of the Virus and Alternative Strategies for its Realization

O. P. Zhirnov[1,2]
[1]The N.F.Gamaleya Research Center of epidemiology and microbiology, The D.I. Ivanovsky Institute of Virology, Moscow, 123098 Russian Federation
[2]The Russian-German Academy of medico-social and biotechnological sciences; The Innovation Center of Skolkovo, Moscow, 121205 Russian Federation
E-mail: zhirnov@inbox.ru
Recieved December 31, 2022; in final form May 11, 2023
DOI: 10.32607/actanaturae.11904

Dedicated to the 130th anniversary of Dmitry Ivanovsky's discovery of the virus kingdom as a new form of biological life.

ABSTRACT **The genome of some RNA-containing viruses comprises ambipolar genes that are arranged in stacks (one above the other) encoding proteins in opposite directions. Ambipolar genes provide a new approach for developing viral diversity when virions possessing an identical genome may differ in its expression scheme (strategy) and have distinct types of progeny virions varying in the genomic RNA polarity and the composition of proteins expressed by positive- or negative-sense genes, the so-called ambipolar virions. So far, this pathway of viral genome expression remains hypothetical and hidden from us, like the dark side of the Moon, and deserves a detailed study.**
KEYWORDS **virus diversity, genome strategy, ambisense genes, virus classification.**

130 years ago, the outstanding Russian scientist D.I. Ivanovsky reported having discovered a new form of biological life, the so-called *"contagium vivum fixum"* [1, 2], which was later classified into a separate kingdom of viruses [3, 4]. According to the current International Committee on the Taxonomy of Viruses (ICTV) Release (https://ictv.global/taxonomy), the virus domain comprises six superkingdoms (realms), 65 orders, 233 families, 2,606 genera, and more than 10,000 viral variants (strains) [5].

According to the well-known classification by D. Baltimore [6], which is based on the characteristics of the genomic nucleic acid (NA) and the strategy for its expression in an infected cell, viruses are divided into seven genetic classes: I. Double-stranded DNA viruses; II. Single-stranded (+)-sense DNA viruses; III. Double-stranded RNA viruses; IV. Single-stranded (+)-sense RNA viruses; V. Single-stranded (–)-sense RNA viruses; VI. Single-stranded (+)-sense RNA viruses with a DNA intermediate in their life cycle; and VII. Double-stranded DNA viruses with an RNA intermediate. This classification is based on the concept of positive-sense viral mRNAs; i.e., RNA molecules translated by cellular ribosomes to form viral proteins [7, 8]. Contrarywise, negative-sense RNAs encode and translate proteins through the intermediate synthesis of a complementary (positive-sense) mRNA strand. In genomic viral DNAs, a strand identical to the translated (+)-mRNA molecule is designated as a positive-sense strand, whereas a strand complementary to mRNA is designated as a negative-sense strand.

Differences in the viral genome structure and variations in the patterns of its expression in an infected cell (i.e., strategies for viral genome expression) underlie virus diversity, pantropic adaptation of viruses to various organisms such as bacteria, fungi, plants, fish, and animals, in particular humans, and ensure the global spread of viruses on Earth, and possibly in space and other planets [6].

The genetic diversity of viruses, which underlies the Baltimore classification, was considered as follows: one unique viral genome develops one genome strategy; i.e., one genome has one replication scheme and directs the formation of one structural and functional class of virions (i.e., one type of virus reproduction). This implies a uniform and unified process for the synthesis of viral particles (virions) within one

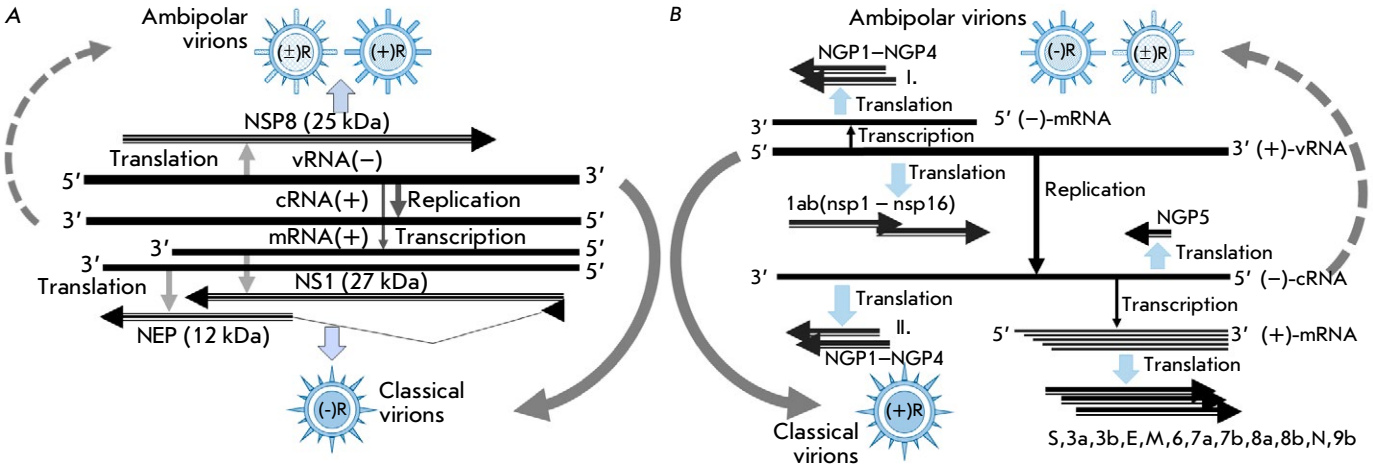

Fig. 1. Localization of ambipolar genes in the RNA genome of the influenza A virus and coronavirus and the formation of ambipolar virions. (*A*) Scheme of gene coding in the influenza virus genome segment *NS* in the A/Aichi/2/68 (H3N2) model. The influenza virus has a negative-sense genome that encodes three proteins: negative-sense NS1 and NEP and the positive-sense stacking protein NSP8. The canonical pathway strategy for segment 8 (*NS*) is shown. This pathway is realized through synthesis of the NS1 and NEP proteins, formation of classical enveloped virions containing the PB1, PB2, PA, HA, NP, NA, M1, and M2 proteins, and a possible alternative pathway with the formation of the non-canonical (ambipolar) NSP8 protein and similar ambipolar proteins of positive-sense genes, found in the PB1, PB2, PA, NP, M, and NS segments (NSP1–NSP8 proteins, respectively, according to the numbering of RNA segments in the viral genome). Non-canonical ambipolar virions decorated with NSP1–NSP8 proteins have not yet been found and remain hypothetical in nature (dotted arrow). (*B*) Scheme of gene coding in the RNA genome of coronavirus in the SARS-CoV2 model. Coronavirus has a positive-sense genome encoding five major structural (S1/S2, N, E, M) and 16 (nsp 1–16) accessory non-structural polypeptides. The classical pathway of positive-sense strategy leads to the formation of classical enveloped virions containing the S1/S2, N, E, and M proteins (solid arrow). The negative genome direction (3′ → 5′) encodes extended open reading frames in complimentary positive polarity (5′ → 3′) RNA molecules possessing all essential elements, such as the initiator AUG, Kozak element, IRES, and stop codons. These translational frames (genes) are designated as negative gene proteins (NGPs), and the most extended NGPs, NGP1–NGP5, have a molecular weight in the range of 7–20 kDa [17]. The dash arrow shows an alternative pathway of genome strategy with the formation of non-canonical (ambipolar) virions. The double arrow shows proteins and the direction of their coding in the genome. Ambipolar NGP1–NGP5 polypeptides are synthetized through the formation of a subgenomic (−)-mRNA and its translation (pathway I), and also through translation of a full-length complementary genomic (−)-cRNA (pathway II)

viral genus (or family) [7, 8]. However, our discovery of unique genes in the genome of RNA viruses which are arranged according to the stacking principle (the so-called gene stacking) and encode proteins in opposite (ambipolar) directions, indicates the possibility of several alternative strategies for genome implementation in one virus, which leads to different structural classes of viral particles.

In 2007, we analyzed the negative-sense genome of influenza A viruses (orthomyxovirus family) and found extended open reading frames (ORFs) that, unlike the canonical influenza virus genes (*PB1*, *PB2*, *PA*, *HA*, *NP*, *NA*, *M*, *NS*) with negative coding polarity in the genomic RNA in the 3' → 5' direction, had additional positive coding polarity (in the 5' → 3' direction of the genomic molecule) (*Fig. 1A*). The peculiarity of these ambipolar genes was their localization in genome regions overlapping the corresponding classical negative-sense genes; the so-called stacking arrangement [9–14]. Later, in 2019, we identified extended open reading frames with a negative encoding direction (3' → 5') in the positive-sense RNA genome of coronaviruses [15–18] (*Fig. 1B*). The ambipolar genes identified in the genomes of orthomyxo- and coronaviruses were found to be characterized by the presence of all the functional elements necessary for expression of these genetic frameworks as translational genes [19, 20]: ATG start codons (or an alternative CUG codon), translational stop codons [21], canonical initiation Kozak sequences in the initiation codon site (Kozak element [22]), and the presence of internal ribosome entry sites (IRESs) [23] possessing a typical

secondary structure in the ambipolar gene start site. Computer analysis of algorithms of the viral genome primary structure revealed various structural and functional domains in the predicted protein products of ambipolar genes, in particular transmembrane elements of ion channel proteins, structural domains of ubiquitin dehydrogenase, and several domains typical of the proteins involved in immunity and inflammation regulation [9, 14, 18].

Today, the genome of one virus species (genus) is believed to have one strategy that determines the formation of viral particles of a certain (canonical) structure and a characteristic range of hosts. The discovery of ambipolar stacking genes in the genomes of RNA viruses suggests the existence of alternative strategies in the genome of one virus species (genus) whose expression pathways may (1) provide the synthesis of several structural and functional classes of virions that differ in both their protein composition and the structural form (polarity) of genomic RNA and/or (2) develop several different strategies for virus replication and its pathogenesis in an infected macroorganism. The presence of several strategies in one viral genome provides a reserve of viral adaptive properties, which may be considered as a pathway (or modification) of genetic bet-hedging (i.e., genetic rescue of viruses).

The multiple strategies of the genome in one virus species (genus) and the expression schemes of its classical and alternative strategies are shown in *Fig. 2* for the influenza virus and coronavirus models. The influenza virus comprising genomic (–)-RNA is characterized by the possibility of both a classical pathway of genome implementation (pathway I; central arrow in *Fig. 2A*) and alternative strategies (*Fig. 2*, II–V). Implementation of alternative genome strategies may lead to the formation of ambipolar virions that may contain both classical proteins (PB1, PA, PB2, HA, NA, NP, M1, M2) and additional proteins—products of the ambipolar genes *NSP1–NSP8* (*NSP* – Negative Strand Protein) of appropriate genomic RNA segments (*Fig. 2A*). Expression of the classic coronavirus strategy also leads to the formation of virions containing the canonical (+)-RNA genome and classical structural proteins: N (nucleocapsid protein), S (surface glycoprotein), E (membrane protein), and M (internal matrix protein) and a number of auxiliary non-structural regulatory proteins (nsp1-nsp16) that support viral replication in target cells and suppression of the host's immune response. However, the products of the main ambipolar genes *NGP1–NGP5* (negative gene proteins [17]), which may form a new structural class of virions (the so-called ambipolar virions; *Fig. 2B*, dotted arrow), escape the attention of researchers. So far,

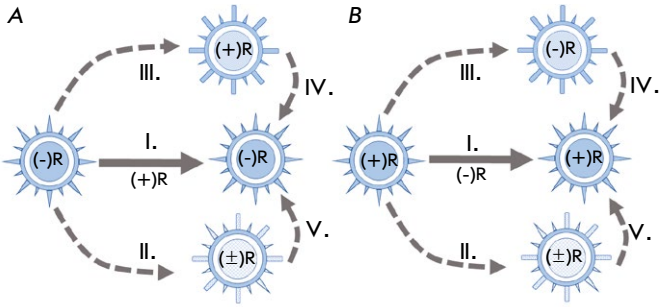

Fig. 2. Alternative strategies of the influenza virus negative-sense genome and the formation of ambipolar virions. The diagram illustrates the alternative strategies of the viral genome using the influenza virus (*A*) and coronavirus (*B*) genome models and is applicable to other viruses (pneumo-, paramyxo-, rhabdo-, filoviruses, etc.) possessing a negative-sense RNA genome (–R). Genome strategy is outlined as a viral genome replication pathway leading to the formation of canonical viral particles of a given structure and composition, both in terms of viral genome polarity and protein composition of the viral envelope. Three alternative strategies possible for one unique viral genome are shown. Currently, pathway 1 is considered as canonical, while four other strategies remain hypothetical. Probably, in a given biochemical context of infected cells, strategies II–V may be implemented, when full-length genomic RNA chains ((+)R and (±)R) are packaged by proteins of distinct compositions (denoted by different symbols (▯,▮,◭,△), including proteins of ambipolar genes. In this case, different virion types may have different envelope structures with/without cellular lipids, the so-called enveloped and non-enveloped virions. Genetic realization of viral genome replication is performed by RNA-dependent polymerase that can be included in the virion and provide the beginning of viral replication in the target cell. (+)R, (–)R, and (±)R are three possible variants of a progeny virion genomic RNA with a single-stranded positive/negative sense and double-stranded structure, respectively. Possible pathways to alter the genome expression strategy in one species of virus are shown by dotted arrows and labels (II–V); the classical pathway of the negative-sense strategy for the influenza virus is shown by the main arrow (I), respectively. A targeted search for the virions of the indicated non-canonical structural classes II–V is required to pinpoint strategies II–V

these proteins encoded by open ambipolar genes have not been found in infected cells. A possible reason lies in either the minor level of their synthesis or their strictly selective expression only in specialized body cells containing the unique factors necessary for the expression of these viral stacking genes under certain conditions of the intracellular and/or surrounding extracellular environment. At the same time, there are

indirect approaches to observe ambipolar gene expression in an infected macroorganism. Animals infected with the influenza A virus were found to develop clones of cytotoxic lymphocytes that recognize specific peptide domains of the influenza virus ambipolar proteins, in particular the NSP8 protein encoded by the ambipolar *NSP8* gene of the influenza A virus *NS* segment [24–26].

We may posit that these non-canonical proteins are able to decorate the viral genome from a new class of viral particles performing unique regulatory functions, and altering the virus behavior in an infected organism; e.g., switching from productive virus infection to a latent persistent (low reproductive) viral infection process. Furthermore, there may be an alternative when a genome molecule becomes an RNA chain complementary (ambipolar replica) to the canonical virus genome: the coronavirus (–)RNA or influenza virus (+)RNA (*Fig. 2*). Thus, ambipolar viral particles may contain both ambipolar proteins and ambipolar genomic RNA replicas, providing an alternative pathway for the viral genome strategy. As a result, one unique viral genome may be implemented in several, alternative strategies – with or without involvement of ambipolar genes – and viruses may possess several possible life pathways, depending on the context of the surrounding cellular processes. This idea is illustrated in *Fig. 2*. This multivariant mechanism of a unique viral genome strategy may be considered as a way of bet-hedging by viruses, which promotes the establishment of alternative ways of virus replication and the creation of reserve adaptive potentials for viruses of various families. In this aspect, RNA viruses may be similar to DNA viruses and RNA-containing retroviral (virus-like) transposons that have a dual-track lifestyle: as a DNA provirus and a mature virus, respectively, which determines the vertical (a viral genome DNA copy integrated into the cell genome) and horizontal (mature virions) ways of their existence in the host, depending on the propagation environment and the range of hosts [27–29].

The ambipolar genes of viruses are endowed with high evolution stability. In particular, in the natural population of highly variable influenza viruses, these genes have been observed in the genome with all the necessary regulatory elements for more than 100 years, despite a noticeable population variability in both canonical and identified ambipolar genes with a characteristic high dN/dS coefficient that indicates pronounced immunological pressure from the host macroorganism in nature [14]. The evolutionary stability of ambipolar genes in the natural population of viruses emphasizes the vital role of these genes for the virus and, therefore, resistance to natural restrictive selection. The presence of ambipolar genes in the genome of RNA-containing viruses provides a new pathway for the formation of viral diversity, when virions possessing an identical genome may vary in the expression scheme (strategy) of the genome and have different replication pathways that provide variations both in the composition of the proteins expressed by "positive" or "negative" genes (the so-called ambipolar virions) and in genome polarity [17]. Alternative genome strategies and a change in the profile of synthesized proteins and the viral envelope give the virus additional opportunities to adapt to a new host and extend a host's range of viruses. In this case, a virus can not only use different strategies to express its genome, but also change these strategies depending on the host, which is illustrated in *Fig. 2* (dotted arrows). So far, these pathways of multiple expression strategy of the viral genome remain as hypothetical and enigmatic as the "dark side of the Moon." Experimental verification of this crystal-ball reading exercise will enable us to evaluate the possible existence of ambipolar classes of stealth virions hidden from the eye of researchers. To date, mature protein products encoded by identified ambipolar viral genes in an infected organism have not yet been detected. But this does not mean that expression of these viral stacking genes is not implemented in nature. Identification of the expression of these genes requires a targeted search using original approaches and highly sensitive methods for identifying proteins in various organs and the specific cells of an infected host macroorganism. It is possible that the unraveling of alternative strategies of viral genomes may be important for understanding virus evolution and the pathogenesis of viral infections, as was the case in covid-2019 when long-term and severe complications of the viral infection could develop due to the formation of ambipolar virions hidden from the attention of researchers and medical practitioners.

Obviously, the ambipolar stacking of genes found in RNA viruses provides the virus with, first, an enhanced information capacity of the genome. Second, it underlies the linked (reciprocal) evolution of viral genes when mutations in one gene generate changes in a stacking gene and, thus, represent a kind of genetic synteny. Third, the protein products of stacked genes may be functionally linked and have a predetermined structural correspondence to each other, which remains a hypothetical and requires experimental evidence [14, 17]. The gene-stacking trait distinguishes these viruses from the known four genera of ambipolar viruses (tospo-, phlebo-, arena-, and bunyaviruses), in which ambipolar genes are located sepa-

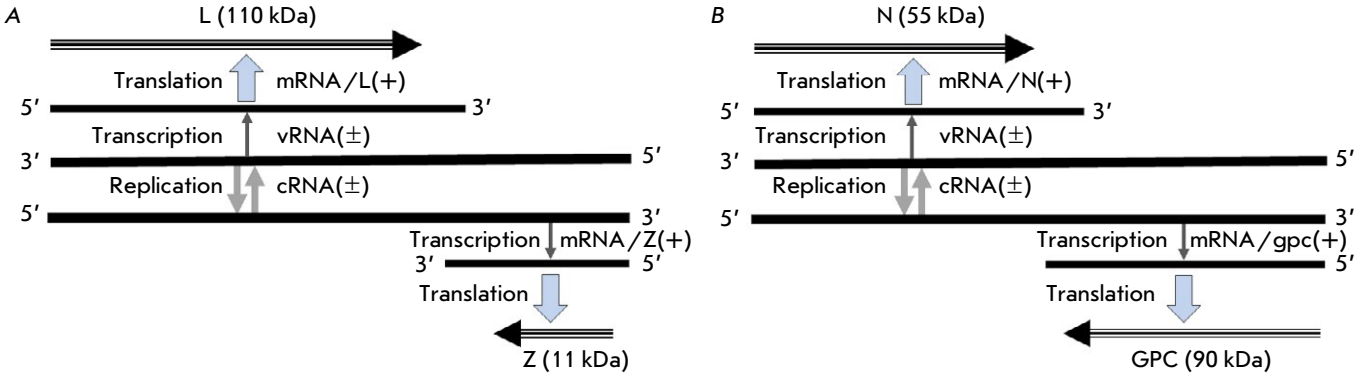

Fig. 3. Schematic diagram of the bipolar (ambisense) strategy of the arenavirus genome (Arenaviridae family; Mammarenavirus genus). The arenavirus genome (lymphocytic choriomeningitis virus (LCMV); ac.n. AY847350; AY847351) is used. The family combines pathogens of severe human hemorrhagic fevers (Lassa, Lujo, Machupo, Junin, Chapare, Guanarito, Sabia, etc.). The arenavirus genome contains four genes that encode: (*A*) polymerase protein (L, 110 kDa) and non-structural multifunctional protein (Z, 11 kDa); (*B*) nucleocapsid protein (N, 55 kDa) and surface glycoprotein (GPC; 90 kDa) [31]. Coding of the *L* and *N* genes has negative polarity, and that of the *GPC* and *Z* genes has opposite (positive) polarity. All four genes are uncoupled in the arenavirus genome and do not overlap, and expression of each of the genes in infected cells requires the synthesis of individual 5′-capped mRNAs

rately in the genome, without overlapping with other genes, and function as the main genes that drive the synthesis of the major structural and regulatory viral proteins [30]. This strategy of the viral genome with separated ambisense genes devoid of stacking localization is shown in *Fig. 3* using an arenavirus model (Arenaviridae family, Mammalovirus genus). In this regard, the difference in stacking allows us to consider two major groups of ambipolar viruses. To date, the following division seems logical: in the first group of viruses (influenza viruses, coronaviruses) with gene stacking in the viral genome, pathways of ambipolar genome strategies may have an alternative (optional) character, while in viruses lacking gene stacking (tospo-, phlebo-, arena-, and bunyaviruses), the implementation of the ambisense genome strategy should be considered as an obligatory (mandatory) reality for virus replication. Further targeted search for the expression pathways of alternative genome strategies in one viral species and identification of a hypothetical class of ambipolar virions will answer the question of the existence of this type of viral life diversity and its role in the evolution of viruses of various genera. This knowledge will come handy in the development of new vaccines and antiviral drugs and add to our understanding of the molecular basis of viral disease pathogenesis. ●

The author is grateful to A.I. Chernyshova for assistance in preparing this article.

REFERENCES

1. Ivanovsky D.I. // Agriculture and Forestry. 1892. № 2. P. 108–121.
2. Ivanowsky D. Concerning the mosaic disease of the tobacco plant. 1892. In: Johnson J, editor. Phytopathological classics № 7. St. Paul, MN: American Phytopathological Society; 1942. p. 27–30.
3. Zhirnov O.P., Georgiev G.P. // Annals of the Russian Academy of Medical Sciences. 2017. V. 72. № 1. P. 84–86.
4. Lvov D.K., Alkhovsky S.V., Zhirnov O.P. // Probl. Virol. 2022. V. 67. № 5. P. 357–384. doi: 10.36233/0507-4088-140.
5. Walker P.J., Siddell S.G., Lefkowitz E.J., Mushegian A.R., Adriaenssens E.M., Alfenas-Zerbini P., Dempsey D.M., Dutilh B.E., García M.L., Curtis Hendrickson R., et al. // Arch. Virol. 2022. V. 167. № 11. P. 2429–2440. doi: 10.1007/s00705-022-05516-5.
6. Baltimore D. // Bacteriol. Rev. 1971. V. 35. № 3. P. 235–241. doi: 10.1128/br.35.3.235-241.1971.
7. Koonin E.V., Krupovic M., Agol V.I. // Microbiol. Mol. Biol. Rev. 2021. V. 85(3). P. e0005321. doi: 10.1128/MMBR.00053-21.
8. Agol V.I. // Biosystems. 1974. V. 6. № 2. P. 113–132. doi: 10.1016/0303-2647(74)90003-3.
9. Zhirnov O.P., Poyarkov S.V., Vorob'eva I.V., Safonova O.A., Malyshev N.A., Klenk H.D. // Dokl. Biochem. Biophys. 2007. V. 414. P. 127–133. doi: 10.1134/s1607672907030106.
10. Gong Y.N., Chen G.W., Chen C.J., Kuo R.L., Shih S.R. // PLoS One. 2014. V. 9. № 12. P. e115016. doi: 10.1371/journal.pone.011501625506939.
11. Clifford M., Twigg J., Upton C. // Virol. J. 2009. V. 6. P. 198. doi: 10.1186/1743-422X-6-198.
12. Yang C.W., Chen M.F. // PLoS One. 2016. V. 11. № 1.

P. e0146936. doi: 10.1371/journal.pone.0146936.
13. Sabath N., Morris J.S., Graur D. // J. Mol. Evol. 2011. V. 73. № 5–6. P. 305–315. doi: 10.1007/s00239-011-9477-9.
14. Zhirnov O.P. // Biochemistry (Moscow). 2020. V. 85. № 3. P. 387–392. doi: 10.1134/ S0006297920030141325647 43.
15. Zhirnov O.P., Poyarkov S.V. Unknown negative genes in the positive RNA genomes of coronaviruses. Authorea 2020. doi: 10.22541/au.160614900.06870227/v2.
16. Zhirnov O.P., Poyarkov S.V. // Dokl. Biochem. Biophys. 2021. V. 496. № 1. P. 27–31. doi: 10.1134/S1607672921010130.
17. Zhirnov O. // World J. Virol. 2021. V. 10. № 5. P. 256–263. doi: 10.5501/wjv.v10.i5.256.
18. Bartas M., Volná A., Beaudoin C.A., Poulsen E.T., Červeň J., Brázda V., Špunda V., Blundell T.L., Pečinka P. // Brief Bioinform. 2022. V. 23. № 3. P. bbac045. doi: 10.1093/bib/bbac045.
19. Zhirnov O.P., Klenk H.D. // Vopr. Virusol. (Rus.) 2010. V. 55. № 2. P. 4–8.
20. Zhirnov O.P., Akulich K.A., Lipatova A.V., Usachev E.V. // Dokl. Biochem. Biophys. 2017. V. 473. № 1. P. 122–127. doi: 10.1134/ S1607672917020090285101 27.
21. Kearse M.G., Wilusz J.E. // Genes Dev. 2017. V. 31. P. 1717–1731. doi: 10.1101/gad.305250.117.
22. Acevedo J.M., Hoermann B., Schlimbach T., Teleman A.A. // Sci. Rep. 2018. V. 8. № 1. P. 4018. doi: 10.1038/s41598-018-22330-9.
23. Kolekar P., Pataskar A., Kulkarni-Kale U., Pal J., Kulkarni A. // Sci. Rep. 2016. № 6. P. 27436. doi: 10.1038/srep27436.
24. Zhong W., Reche P.A., Lai C.C., Reinhold B., Reinherz E.L. // J. Biol. Chem. 2003. V. 278. P. 45135-45144. doi: 10.1074/jbc.M307417200.
25. Hickman H.D., Mays J.W., Gibbs J., Kosik I., Magadán J.G., Takeda K., Das S., Reynoso G.V., Ngudiankama B.F., Wei J. // J. Immunol. 2018. V. 201. P. 2187. doi: 10.4049/jimmunol.1801100.
26. Zhirnov O.P., Konakova T.E., Anhlan D., Ludwig S., Isaeva E.I. // MIR J. 2019. № 6. P. 28–36. doi: 10.18527/2500-2236-2019-6-1-28-36.
27. Krupovic M., Blomberg J., Coffin J.M., Dasgupta I., Fan H., Geering A.D., Gifford R., Harrach B., Hull R., Johnson W., et al. // J. Virol. 2018. № 92. P. e00515-18. doi: 10.1128/JVI.00515-18.
28. Avlund M., Dodd I.B., Semsey S., Sneppen K., Krishna S. // J. Virol. 2009. V. 83. № 22. P. 11416–11420. doi: 10.1128/JVI.01057-09.
29. Maslov S., Sneppen K. // Sci. Rep. 2015. V. 5. P. 10523. doi: 10.1038/srep10523.
30. Nguyen M., Haenni A.L. // Virus Res. 2003. V. 93. P. 141–150. doi: 10.1016/s0168-1702(03)00094-7.
31. Grande-Pérez A., Martin V., Moreno H., de la Torre J.C. // Curr. Top. Microbiol. Immunol. 2016. V. 392. P. 231–276. doi: 10.1007/82_2015_468.

Gene Therapy for Cystic Fibrosis: Recent Advances and Future Prospects

M. A. Lomunova*, P. M. Gershovich
JSC BIOCAD, Saint-Petersburg, 198515 Russian Federation
*E-mail: lomunova@biocad.ru
Received: March 22, 2023; in final form, May 22, 2023
DOI: 10.32607/actanaturae.11708

ABSTRACT **Gene replacement therapies are novel therapeutic approaches that seek to tackle hereditary diseases caused by a congenital deficiency in a particular gene, when a functional copy of a gene can be delivered to the cells and tissues using various delivery systems. To do this, viral particles carrying a functional copy of the gene of interest and various nonviral gene delivery systems, including liposomes, nanoparticles, etc., can be used. In this review, we discuss the state of current knowledge regarding the molecular mechanisms and types of genetic mutations that lead to cystic fibrosis and highlight recent developments in gene therapy that can be leveraged to correct these mutations and to restore the physiological function of the carrier protein transporting sodium and chlorine ions in the airway epithelial cells. Restoration of carrier protein expression could lead to the normalization of ion and water transport across the membrane and induce a decrease in the viscosity of airway surface fluid, which is one of the pathological manifestations of this disease. This review also summarizes recently published preclinical and clinical data for various gene therapies to allow one to make some conclusions about future prospects for gene therapy in cystic fibrosis treatment.**
KEYWORDS **gene therapy, cystic fibrosis, CFTR, viral vector, nanoparticles.**
ABBREVIATIONS ***CFTR*** **– cystic fibrosis transmembrane conductance regulator; NBD – nucleotide-binding domain; TM – transmembrane; MCC – mucociliary clearance; CT – clinical trials; Ad – Adenovirus; AAV – Adeno-Associated Virus; LV – Lentivirus; LNP – Liposomal NanoParticles; FDA – Food and Drug Administration.**

INTRODUCTION

Mucoviscidosis or cystic fibrosis (CF) is a rather common monogenic disease. CF is a congenital systemic disease caused by the mutated gene coding for the CF transmembrane conductance regulator protein (*CFTR*) [1]. The molecular pathogenetic mechanism of the disease is based on the dysfunction or total absence of the *CFTR*-encoded carrier protein that transports sodium and chlorine ions. This ion channel ensures normal functioning of epithelial cells in the lungs, intestines, pancreas, and some other organs. *CFTR* regulates sodium and chlorine ion transport across the membrane, as well as water exchange in secretory the epithelial cells in the respiratory, gastrointestinal, hepatobiliary, and reproductive systems [2, 3]. Impairment of the protein's function causes a severe progressive pathology that clinically manifests itself in pulmonary (respiratory failure), pancreatic, and hepatic lesions (sometimes as severe as cirrhosis), as well as increased electrolyte content in the perspiratory secretion.

There are several forms of CF: 75–80% of cases are accounted for by a mixed pulmonary/intestinal form of CF; pulmonary CF is diagnosed in 15–20% of cases; and intestinal CF, in 5% of cases. Mixed CF is considered the most severe form of the disease, because it combines clinical signs of both the pulmonary and intestinal forms. In addition, one could argue for recognition of relatively rare forms, such as meconium ileus (15–20% of cases), anemic edematous CF, cirrhotic CF, and others. However, these classifications are mostly made for the sake of discussion, since a major respiratory tract lesion is often accompanied by digestive disorders. The same is true for the intestinal form of CF; i.e., intestinal lesions are often accompanied by bronchopulmonary lesions. The main complications associated with CF include pulmonary and gastric hemorrhages, intestinal ob-

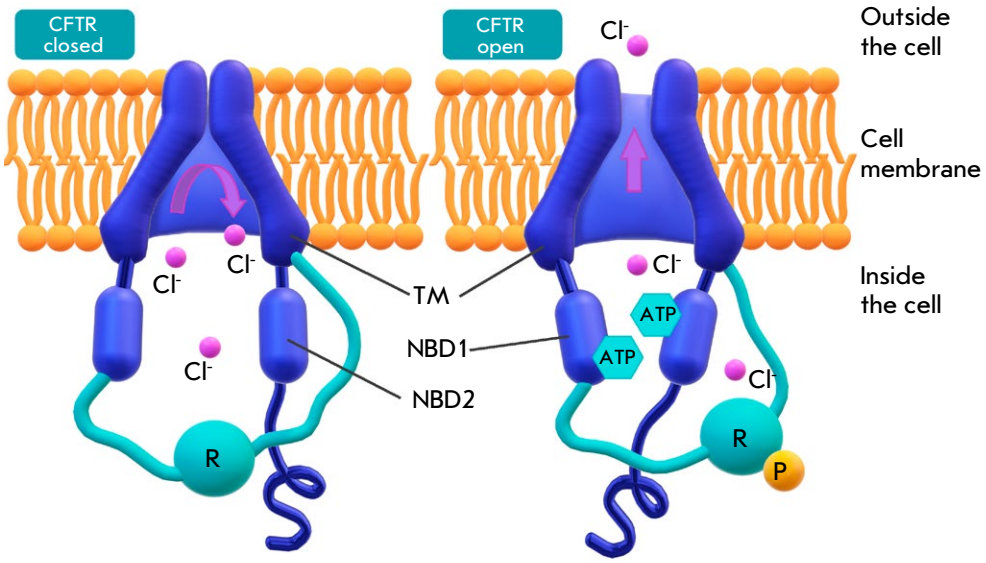

Fig. 1. Schematic representation of a *CFTR* protein in the closed (left) and open (right) positions. TM – the transmembrane domains that form a channel for chloride ions transport. NSD1 and NSD2 – intracellular nucleotide-binding domains 1 and 2. R – the regulatory domain that contains phosphorylation sites (P). Channel activation requires the presence of a phosphoric acid residue on the regulatory domain. NSD1 and NSD2 bind and hydrolyze ATP, resulting in the opening of the channel through interaction with transmembrane domains [7]

struction, bronchial hyperresponsiveness, edemas, abscesses, pneumo- and pyopneumothorax, pulmonary heart disease, maxillary sinusitis, liver cirrhosis, rectal prolapse, developmental impairments, sterility, diabetes mellitus, etc. [2].

According to the statistical data, about 650 newborns in Russia are diagnosed with CF every year [4], while the worldwide number is one diagnosis per 2,000–5,000 healthy newborns. The total number of CF cases in the United States and Europe is about 70,000 [5]. The disease affects males and females equally. Children are usually diagnosed with CF in their first years of life, because lesions to the affected organs (especially lungs and intestines) are clearly visible even at the early stages. Patients show multiple impairments in various systems, including the respiratory, digestive, locomotor, nervous, cardiovascular systems, etc. Exocrine pancreatic insufficiency (ductal dysfunction) is observed in 85–90% of cases. The average life expectancy for CF patients may be 30–40 years, with their quality of life directly depending on the scope of the specialized medical care they receive and the availability of symptomatic treatment. Despite that, up to 90% of CF patients die from pulmonary infections and associated complications [3].

Since CF is caused by a *CFTR* gene mutation, the disease is not fully reversible through the currently available methods. Until recently, CF management remained confined to symptomatic treatment; i.e., mucus thinning (mucolytics), bronchiectasis therapy, anti-inflammatory therapy, antibacterial therapy, and enzyme replacement therapy (in intestinal CF). All these therapies fail to increase the life expectancy of patients and only manage to temporarily improve their quality of life [6]. The development of *CFTR* modulator drugs (Vertex Pharmaceuticals) for pathogenetic therapy has significantly increased the life expectancy of CF patients, but the cause of the disease still could not be eliminated, and patients are condemned to expensive life-long therapy.

On the other hand, the use of gene therapy aimed at restoring the function of the *CFTR* gene in epithelial cells offers new opportunities in the management of CF and other severe hereditary diseases, where gene therapy has already proved to be safe and efficacious. Rapid developments in genome editing technology leave us hopeful for the development of etiotropic therapy, making it possible to correct the *CFTR* mutation causing mucoviscidosis and, through that, improve the quality of life and life expectancy of CF patients.

MOLECULAR-GENETIC MECHANISMS OF CF DEVELOPMENT

CFTR is a transmembrane protein localized on the apical surface of epithelial cells. ATP binding of this protein changes its conformation inside the channel protein ensuring extracellular transport of Cl^- ions. In turn, the termination of ATP hydrolysis leads to channel closing (*Fig. 1*).

It is known that maintaining normal osmotic pressure and fluid circulation in the intercellular space requires the presence of sodium and chlorine ions near the outer membrane. In addition, a controlled continuous flux of chlorine ions across the membrane is a necessary condition for proper functioning of epithelial cells in the lungs, intestines, sweat glands, and other organs. Impairment of the transmembrane transport of chlorine ions changes transmembrane conductance for water molecules and, as a result, causes dehydration and increased viscosity of the secretion. This is what determines the organs primarily affected by CF: a thick viscous secretion is formed on the epithelial surface and blocks bronchopulmonary airways and glandular lumens, which interferes with the normal functioning of the respective organs [2].

Secretion and absorption are two opposite processes associated with the transport of the electrolytes regulating the viscoelastic properties of the liquid component of exocrine secretions. According to available data, electrolyte transport dysfunctions in CF occur both at the level of salt absorption and at the level of fluid absorption and secretion, which are mediated by anions [8]. A decrease in chlorine ion content in the intercellular space activates the epithelial sodium channel (ENaC), which increases the Na content in the cell (*Fig. 2*). It, in turn, boosts the absorption of Cl^- ions and water and causes abnormalities in transepithelial electrical potential difference. As a result, the volume of fluid on the airway surface decreases, its viscosity increases significantly, and the clearance rate on the ciliated epithelial surface is sharply reduced (*Fig. 2*). Such processes in the lungs lead to dehydration of the airways and, subsequently, a reduction in the cleansing effect of epithelial cilia and mucosa in general. What is more, mucus congestion also favors the rapid development of infections [9].

The produced secretion is a polymeric mesh consisting of O-glycosylated glycoproteins (mucins) secreted as threads, forming a porous structure [11, 12]. The viscoelastic properties of the secretion and its structure under normal physiological conditions are specifically adapted to trap and remove inhaled particles and bacteria. Increased secretion viscosity in CF causes mucin plaques and a reduction in pore size

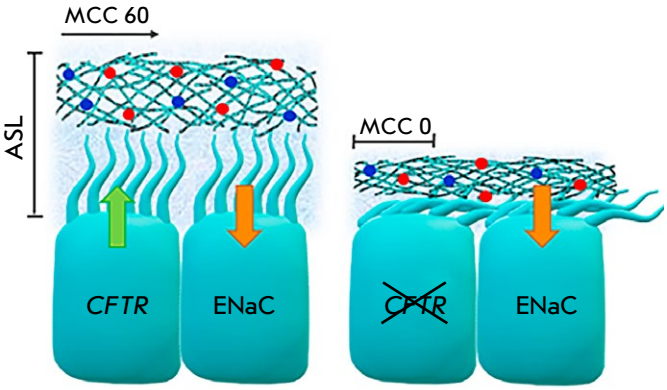

Fig. 2. In healthy individuals (left), the thickness of the airways mucosal layer (ASL, airway surface liquid) is a result of the normal functioning of the *CFTR* and ENaC channels. MCC – mucociliary clearance that is the airway clearance rate due to mucus movement (in μm/sec). In cystic fibrosis (right), due to a defective *CFTR*, a decrease in the number of chloride ions leads to excessive transport of sodium ions resulting in dehydration of the airway epithelium surface, increased secretion viscosity, and compression of the cilia. Weak secretion mobility triggers an inflammatory reaction, and it is also an ideal environment for the reproduction of pathogenic microorganisms [9, 10]

from 0.2–1 μm to under 0.1 μm. As a result, neutrophils acting as the first line of immune defense against bacteria are unable to migrate through the mucus. At the same time, the bacterial macrocolonies formed on the thick mucus are especially resistant to the immune response and antibiotics, which further complicates the therapy [13]. Chronic infections caused by unrestricted proliferation of bacteria on the airway surface are considered the main cause of death in CF [14].

CFTR GENE MUTATIONS

CF is an autosomal recessive disease caused by mutations in the *CFTR* gene identified in 1989 by a research team headed by Lap-Chee Tsui [15, 16]. The *CFTR* gene is localized on chromosome 7 and consists of 27 exons and codes for a protein composed of 1,480 amino acid residues. Over 2,000 mutations in the *CFTR* gene have currently been described, and the list is updated on a regular basis, but only 250–300 of these mutations have pathological consequences, and among those only 20 are relatively common (over 0.1% of patients) [17]. Five classes of mutations (seven, according to some authors) are identified based on the associated defects (*Fig. 3*). Class I–III (severe) muta-

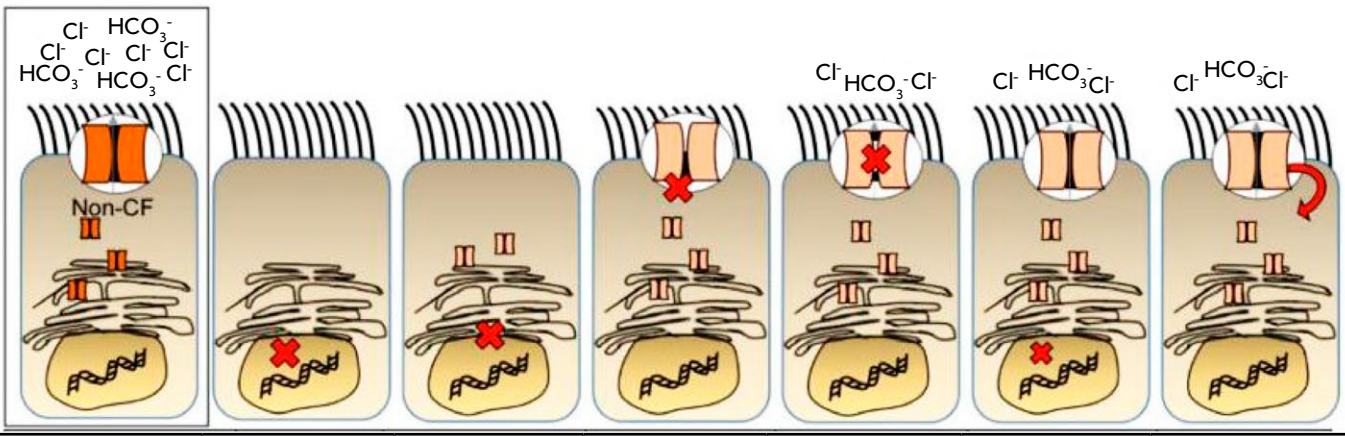

Class of *CFTR* mutation	I	II	III	IV	V	VI
Protein defect	Impaired protein synthesis	Impaired protein transport to the membrane	Impaired channel opening	Reduced Conductance	Reduced protein quantity	Protein instability
Most common mutation	G542X	F508del	G551D	R117H	3489+10kb C>T	4326delTC
% of people with at least one mutation	22	88	6	6	5	5
Therapy	–	VX-809, VX-661	VX-770	–	–	–

Fig. 3. Types of *CFTR* mutations and therapies approved by the FDA for the treatment of the conditions associated with these mutations. CF patients may have more than one mutation. *Fig.* adapted from [23]

tions are associated with a fundamental *CFTR* dysfunction; and class IV–V (mild) mutations, with the residual function of the *CFTR* protein [18]. Various mutations in the *CFTR* gene may impair the synthesis, processing, stability, and functioning of the *CFTR* protein, as well as its intracellular transport from the endoplasmic reticulum to the Golgi complex and degradation, which leads to a variety of phenotypic manifestations [19].

Class I mutations

Class I mutations (G542X, W1282X, R553X, 2143delT, 1677delTA) are observed in about 10% of CF patients. If the gene includes this type of mutation, then the *CFTR* protein is not synthesized at all or its shortened variant is synthesized and degraded. This class of mutations includes nonsense mutations, frameshift mutations, and splicing site mutations causing the generation of a stop codon, premature termination of protein synthesis, and production of an enzyme that can no longer function as the initially synthesized protein [19].

Class II mutations

Class II missense mutations (del F508, del I 507, N1303 K, S541 I, S549 R) are considered the most common in CF patients. Among those, F508del, i.e., deletion of phenylalanine residue in position 508, occurs most

often. About 70% of patients have mutations in both copies of the *CFTR* gene (homozygous), and 90% of patients have at least one mutant allele [20]. The most severe course of the disease affects homozygous patients, while heterozygous *CFTR*-F508del with one healthy copy of the gene show no signs of the disease.

The F508del mutation causes errors in protein folding and its further processing, which is why most mutant molecules are unable to reach the cellular membrane and are destroyed. It should be noted that about 1% of these molecules still manage to reach the cellular surface, but since the mutation impairs the mobility of the domains associated with opening and closing of the channel, protein effectiveness remains very low [21]. On top of that, the protein is removed from the surface and destroyed in a matter of several minutes [22].

Class III mutations

Class III missense mutations (G551 D, G1224 E, S1255 P) affecting the regulation of ion channel opening are observed in about 4–5% of CF patients. Proteins with this mutation reach the apical membrane, but conductance and permeability of the channel are impaired. Here, the conversion of the glycine residue in position 551 of NBD1 into aspartic acid (G551D) is the most common mutation. This mutation leaves the channel closed most of the time [19, 21].

Class IV mutations

Class IV mutations are the rarest ones (about 1.7%). These mutations (R117H, R334W, R347P) reduce chlorine ion transport through the open *CFTR* channel [9] and convert positively charged arginine residues in the *CFTR* channel into noncharged residues (presumably, the presence of positive charges in the channel is required for Cl^- ion transport). These mutations in CF patients are usually associated with a mild course of the disease, often without pulmonary or pancreatic signs.

Class V–VI mutations

In some cases, clinicians also identify class V–VI mutations, where the functional *CFTR* protein is produced, but its synthesis is inhibited and it is quickly removed from the cellular surface, which leads to insufficient content of the protein. These mutations are associated with a relatively mild course of the disease [17].

PATHOGENETIC THERAPY OF CYSTIC FIBROSIS

At present, the FDA (*Food and Drug Administration*) has approved a CF therapy using small molecules maintaining the normal functioning of chlorine channels (*CFTR* modulators). The Drugs Kalydeco (VX-770), Orkambi (VX-809), and Symdeco (VX-661) are being developed by the U.S.-based company Vertex Pharmaceuticals (*Fig. 3*). Kalydeco (ivacaftor) is approved in the United States, Canada, and the EU for managing CF patients aged above 6–12 months with one out of 10 *CFTR* gene mutations (G551D, S1255P, G178R, S549N, G1244E, S1251N, G1349D, S549R, G551S, or R117H). Orkambi (lumacaftor + ivacaftor) is used for managing patients above 12 years of age with two copies of the F508del mutation in the *CFTR* gene. Symdeco (tezakaftor + ivacaftor) is intended for patients above 6 years of age. The screening in bronchial epithelial cells in homozygous *CFTR-F508del* patients has shown that Symdeco combined with ivacaftor increases chloride transport to 15.7% of its adequate value. These are very expensive drugs (priced at least RUB 1 million for 1 package) that only act as supportive therapy and do not lead to complete recovery. Nevertheless, this therapy has brought about significant progress, since with it the average life expectancy of CF patients has more than doubled.

GENE THERAPY OF CF

The discovery of *CFTR* modulators that can correct the functioning of the defective protein has had a positive effect on life expectancy and quality of life and given hope to many CF patients. However, about 10% of patients are unresponsive to *CFTR* modulators because *CFTR* is not synthesized at all or is only synthesized in low quantities. In addition, clinical trials (CT) show that 10–20% of CF patients have individual intolerance to modulator drugs [24].

This taken into account, new approaches to CF management are being developed, including the ones using gene therapy methods to deliver nucleic acids to the affected cells to address the primary (genetic) cause of the pathology and, through that, mitigate the course of the disease. Even though multiple organs are affected by the CF, lungs are the main target of the gene therapy, since 90–95% of deaths from the disease are due to severe pulmonary lesions. The key strategy in CF gene therapy is to ensure that the *CFTR* gene is delivered to the airway epithelial cells. Here, the delivery method should be selected taking into account the significantly reduced efficacy of aerosol administration due to the thick secretion in the bronchioles. The latter also imposes additional restrictions on the gene therapy, since the vector should not only ensure the effective expression of the functional *CFTR* protein but should also penetrate submucosal glandular cells and the superficial mucosal epithelium covered by the thick secretion [2].

Table 1. Selected CTs of CF gene therapy*

CFTR delivery method	Administration method	Clinical trials	Reference
Adenovirus (Ad)	Nasal administration, endobronchial administration	NCT00004779 NCT00004287	[26–29]
Adeno-associated virus (AAV)	Maxillary gland administration, nasal administration, endobronchial administration	NCT00073463 NCT00004533	[30–32]
Lentivirus (LV)	Intranasal administration (perfusion)	Preparation stage	[33]
Nanoparticles (liposomes), synthetic polymers	Aerosol administration (nebulizer), intranasal administration	NCT01621867 NCT00789867 NCT00004471 NCT00004806	[34–38]
Single-stranded antisense RNA-oligonucleotide (QR-010)	Intranasal administration	NCT02564354 NCT02532764	[39]

*All CTs are completed.

CTs of gene therapy drugs, where the genes of interest are delivered to nasal and bronchial airway epithelium in CF patients using both viral and non-viral systems, have been taking place since 1993. So far, over 27 CTs of gene therapy in CF involving over 600 patients have been completed but none of them has shown significant success for one reason or another (*Table 1*).

It should be noted that continuous renewal of airway epithelium necessitates repeated delivery of the gene of interest, which restricts the use of viral vector systems, because the repeated administration often triggers an immune response resulting in vector elimination. In addition, the lack of adequate *in vivo* models for testing the efficacy of new vectors also hinders the progress in the research. Therefore, despite the initial enthusiasm, there is still no FDA-approved gene therapy for CF [25]. Nevertheless, advances in vector development, better understanding of various vector serotypes, and development of new *in vivo* CF models has sustained the search for more effective CF gene therapy [5].

Gene delivery using adenoviral (Ad) vectors

The first CTs of CF gene therapy were aimed at using Ad to deliver a healthy copy of a gene into airway epithelial cells (*Table 1*). Two CTs using first-generation Ad have been completed [26–28, 40, 41]. But despite the efficacy of the approach in cell models and *in vivo*, the CT results raised the issue of the questionable safety of the vectors for humans. Congenital and cellular immunity hindered the long-term effect of Ad-based vectors: observations showed increased alveolar inflammation, accompanied by an increase in serotype-specific neutralizing antibodies, which rendered the repeated administration of viral particles ineffective [23].

In later designs, the gene was delivered using an improved Ad platform in the form of a helper-dependent adenovirus (HD-Ad) devoid of viral genes, which made it possible to neuter the T cell response to the viral protein that was a feature of the first-generation Ad vectors. Nevertheless, the adaptive immune response of $CD8^+$ T cells with HD-Ad epitope presentation by dendritic cells remained present [42].

HD-Ad was used in the lungs in combination with lysophosphatidylcholine (LPC) with the intention to destroy the thick secretion layer and ensure better access to the basolateral cell surface for infection. This strategy resulted in lengthier gene expression *in vivo* compared to the first-generation Ad and demonstrated effective gene delivery to the airways in mice, pigs, and ferrets [43, 44].

A possible modification of the Ad platform is to use piggyBac transposons with their cut-and-paste mechanism for gene transfer. Transposase-mediated piggyBac insertion in the recombinant Ad produced a hybrid vector piggyBac/Ad, which made it possible to effectively express the gene of interest in the lungs of pigs [45].

Another approach to CF therapy, which is yet to be studied in detail, is the use of genome editing tools TALEN (Transcription Activator-Like Effector Nucleases) and CRISPR (Clustered Regulatory Interspaced Short Palindromic Repeats)/Cas9. These relatively recent molecular methods of genome editing have already proved their efficacy and reliability [46]. The relative safety and significant capsid size of HD-Ad vectors (36 kbp) make it possible to transfer several constructs at the same time, which allows for the use of site-specific nucleases for targeted insertion of a delivered gene at a desired locus. This specific insertion of a healthy gene copy is advantageous compared to the correction of the mutated protein, because here CF therapy no longer depends on the *CFTR* mutation type. An example of this approach is presented in Xia et al. [47], where an expression cassette with the *CFTR* gene was inserted at the *AAVS1* locus *in vitro* using a HD-Ad vector simultaneously carrying the TALEN nuclease. Expression of *CFTR* mRNA and restored protein function were observed in the cells transduced by the vector with this expression cassette [47]. A similar approach with an HD-Ad vector for precise delivery of CRISPR/Cas9 and a DNA copy at the GGTA1 locus in the genome of airway epithelial cells was used *in vitro* and *in vivo* in pigs. It transpired that the transduced cells expressed functional *CFTR* at mRNA and at the protein levels both in *in vitro* and in *in vivo* models. An engineered cell line CFTR$^{-/-}$ of pig epithelium was developed for *CFTR* protein expression assessment after transduction with CRISPR/Cas9. Measurement of *CFTR* channel activity in the transduced *CFTR*$^{-/-}$ cells showed restoration of the anion transport function [48, 49]. These data allow us to anticipate a new nuclease-based approach to CF gene therapy in the near future.

Gene delivery using adeno-associated viral (AAV) vectors

Replacement of a mutated CFTR protein gene with its functional copy turned out to be a rather complex undertaking, and following the failure with first-generation Ad vectors the search for alternative approaches in gene delivery to target cells was initiated. The reports from the CTs using the AAV2 vector (*Table 1*) showed that introduction of the vector into the lungs of CF patients did not cause significant side-effects, but the efficacy was disappointing, since none of the CTs demonstrated significant *CFTR* expression or correction of pathological CF manifestations. The lack of success could be explained by the insufficient efficacy of gene insertion (possibly due to the inability of viral particles to penetrate the thick secretion layer in the airways), insufficient promoter strength in the expression cassette, or immune response of the host to the introduction of the viral vector [50]. Hence the recent efforts to improve the tropism of AAV vectors, identify new serotypes, new promoters, new methods to enhance the expression of the target protein and its persistence in the lungs, as well as new approaches to immunogenicity reduction. At the same time, new *in vivo* models, including pigs [51], sheep [52], ferrets [53], and mice [54], were being developed, which, along with the conventional *in vitro* tests in human epithelial cells, would make it possible to carry out more effective preclinical trials for the CF gene therapy.

For example, the AAV virus with high airway epithelial tropism was selected based on *in vivo* experiments in pigs [51]. Improved AAV2H22 capsid based on AAV2 with five-point mutations made specific infection of airway epithelium in pigs 240 times as effective. One of the key parameters indicating phenotypic efficacy of the therapy is Cl^- transport. Introduction of AAV2H22-CFTR into the airways of *CFTR*-null pigs lacking a functional *CFTR* gene resulted in *CFTR* expression in epithelial cells, restoration of anion transport, and normalization of the pH of the secretion on the airway surface and its bactericide properties [51].

Gene expression efficacy was also increased using the AAV vector including the CFTRDR gene of the shortened protein driven by a short cytomegalovirus promoter CMV173. Transduction of organoids by AAV-CFTRDR resulted in restored *CFTR* function. In addition, changes in the potential difference on the epithelial cell membrane in nasal airways were recorded, which was an indication of the restoration of the normal phenotype in mice carrying the most common CF mutation, ΔF508 [54]. The problem of the limited size of the genetic construct packed in AAV2 may be solved by developing a short synthetic promoter [55] or obtaining a *CFTR* gene with partial deletion of the regulatory domain [56].

In addition, a new chimeric vector, AAV2/HBoV1, obtained by pseudotyping the AAV2 genome into a capsid of human bocavirus, HBoV1, infecting human airways and characterized by high tropism for the apical surface of airway epithelial cells in humans was tested [57]. The capsid size was increased as a result,

which made it possible to use a stronger promoter and a complete *CFTR* gene [58]. The ability of rAAV2/HBoV1 to transduce pulmonary epithelial cells in ferrets (*Mustela putorius furo*) made it possible to create *in vivo* models for preclinical trials [53].

Testing of nine characterized AAV vector serotypes in the epithelial cells and lungs of mice resulted in identification of the AAV6 vector with the highest tropism for pulmonary epithelial cells in mice and humans [59, 60]. It transpired that the transduction efficiency of AAV6 in the airway epithelial cells of mice reached 80% and that its immunogenicity was lower than that of the AAV2 vectors, which makes AAV6 a preferable vector for gene therapy of CF and other pulmonary diseases [61]. To further boost the transduction efficiency of the AAV6 vector in epithelial cells, a point mutation was introduced into the gene coding for an atypical amino acid residue, F129, usually present in the capsid protein. The resulting AAV6.2 vector showed higher transduction efficiency in both the airway cells of mice and HAEC (human airway epithelial cells) cultures. Stable expression of the transgene intranasally administered (2×10^{11} viral particles) to macaques for 72 days was observed [59]. The advantage of the AAV6 vector in penetrating mucus obtained from CF patients was also shown in the new mouse model most accurately mimicking the pulmonary pathophysiology in obstructive pulmonary diseases. The point mutation in the capsid protein seems to point to the potential mechanism used to avoid AAV6 adhesion to the polymeric mesh representing the mucus in CF and prompting the attack against other AAV vector serotypes [62].

It should be noted that only a few pharmaceutical companies are currently involved in the development of AAV-based CF gene therapy. According to Abeona Therapeutics [63], preclinical trials of ABO401, a new-generation capsid AAV204 developed by the company and carrying a functional copy of the human mini-*CFTR* gene, show that the product effectively restores the main phenotypic attribute of CF, i.e., chlorine channel functioning, in *in vitro* and *in vivo* models. In addition, AAV204 more specifically targets pulmonary cells and also transduces bronchial and nasal epithelial cells in CF patients (*CFTR* expression rate 3–5 times higher compared to the AAV6 vector).

In addition, Spiro-2101 by Spirovant Sciences, designed for CF therapy was certified by the FDA as an orphan drug in 2020, which allowed the company to accelerate its clinical trials and take the drug to the market. Spiro-2101 also includes a new AAV capsid with improved tropism for airway epithelial cells for the delivery of a functional copy of the *CFTR* gene.

Gene delivery using lentiviral vectors

Lentivirus-based vectors are widely used in gene therapy as well. Their beneficial aspects include low immunogenicity, ability to infect various cell types and integrate consistently into the genome to ensure long-term expression and preservation of the gene in cell division. Nevertheless, it should be mentioned that consistent integration into the genome may lead to insertional mutagenesis and, as a result, a risk of tumor transformation (oncogenesis) [64]. All existing approaches to CF therapy using lentiviral vectors (LV) are currently undergoing preclinical trials, but recent advances in the application of improved lentiviral vectors in various CTs have shown that they are safe to use in CF therapy [65].

Studies into the primary epithelial cultures of CF patients and animal models have shown the long-term phenotype correction and low immunogenicity carried by lentiviral vectors. In particular, the restoration of *CFTR* channel functioning in the airways of pigs after transduction with the feline immunodeficiency virus (FIV) pseudotyped with the GP64 protein to ensure apical tropism for HAE-ALI (human airway epithelium cultured on an air-liquid interface) cells was demonstrated in *in vivo* experiments. A significant increase in Cl^- transepithelial transport and normalization of the pH of the tracheal surface fluid and its bactericide properties were observed two weeks after FIV-CFTR aerosol administration into the nose and lungs [66].

Another experimental design involved the simian immunodeficiency virus (SIV) pseudotyped with the Sendai virus fusion protein (F), hemagglutinin, and neuraminidase (HN). Preclinical trials showed that *CFTR* gene transfer into the lungs using this vector ensured more efficient transduction of human bronchial epithelial cells and the pulmonary epithelium of mice *in vivo* compared to nonviral transfer and did not trigger any immune response [33].

In 2017, Alton et al. analyzed the results of several preclinical trials to select the most promising vector type for initiation and planning of the first-in-man CT using lentiviral transfer of the *CFTR* gene. A lentivirus vector rSIV.F/HN ensuring the expression of functional *CFTR* with efficacy of 90–100% in clinically relevant delivery devices was considered the lead candidate. These data support the idea of using this vector in the first CT in CF patients [33]. Yet the CT has not been initiated, probably a clue that the vector requires additional preclinical trials and proof of efficiency as a CF gene therapy.

Non-viral gene delivery using liposomes and polymeric nanoparticles

The benefits of liposomal gene transfer include simplicity in scaling up the final formulation of the product and a size suitable for large DNA molecules. In 2015, one of the largest CTs, where pGM169/GL67A liposomes were used for *CFTR* delivery, showed that the product was safe in CF [67]. Safety with repeated administrations of the product was confirmed in a later CT using pGM169/GL67A liposomes. It was shown for the first time that gene therapy is capable of slowing down the deterioration of the pulmonary function in CF patients but that the relief was still insufficient for researchers to recognize the therapy as efficient [34].

In recent years, research efforts have been directed toward increasing efficiency in liposome-based gene delivery (*Fig. 4*). In particular, it was discovered that the use of clinically relevant liposomal nanoparticles (LNP) for the packaging and delivery of chemically modified *CFTR* (cmCFTR) mRNA into the bronchial epithelial cells of CF patients increased the quantity of the *CFTR* localized on the membrane and restored the function of chlorine channels [68].

In addition, intranasal administration of LNP-cm*CFTR* resulted in restored Cl^- transport in the airway epithelium of CFTR-KO mice for 14 days. *CFTR* functional activity reached its peak on the 3rd day after transfection, which was supported by a restoration of Cl^- flux to 55% of that in healthy mice. These results are comparable in efficiency with Ivacaftor (*CFTR* modulator) and support the idea of using LNP-cmCFTR to correct for CF and other monogenic diseases [68].

There are also a number of polymer-based methods, including dense polyethylene glycol (PEG) coating of particles to ensure that they penetrate the thick mucus layer *in vitro* and, thus, increase transfection efficiency in the lungs of mice *in vivo* [69]. Also of interest is the use of biodegradable triplex-forming peptide nucleic acids (PNA) binding to genomic DNA and forming PNA/DNA/PNA triplexes that can stimulate the restoration of endogenous DNA. Delivery of these complexes, along with the corrective gene, results in site-specific gene correction [70]. In this case, introduction of the donor DNA *in vivo* into nasal sinuses and the lungs of homozygous ΔF508del mice caused significant mutation correction in airway epithelium and mitigated the course of the disease [71].

In addition, the first attempt at systemic introduction of the improved polymeric nanoparticles PNA LNP carrying DNA-editing agents and characterized by higher cell permeability and efficiency of mutation correction was described. I/V administration of these particles led to a more adequate biodistribution, with particles accumulating in the airways and gastrointestinal tracts of mice, and *CFTR* functions in epithelial cells fully restored. This was the first successful case of systemic introduction of nanoparticles as CF gene therapy [72].

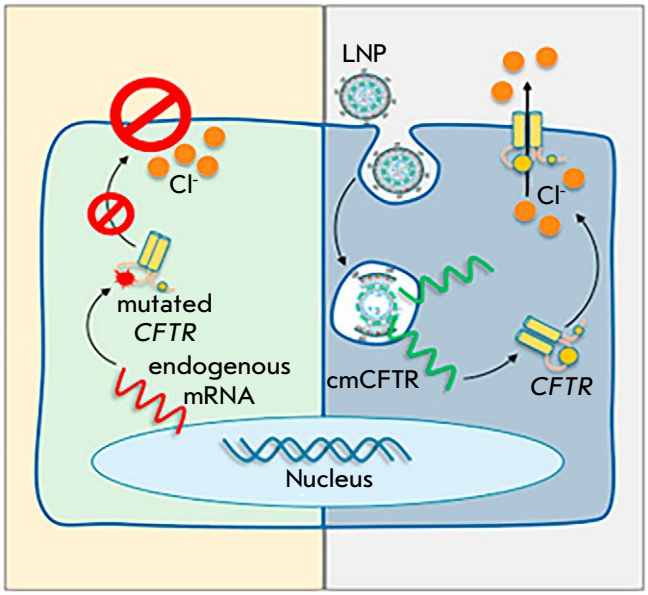

Fig. 4. LNP-cmCFTR delivery. *Fig.* adapted from [68]

Antisense oligonucleotides

It is known that oligonucleotides and their complexes have been used as therapeutic molecules for the restoration of DNA modifications (DNA repair) [73]. These oligomers, including RNA- and/or DNA-nucleotides, are used for site-specific repair of defective DNA.

Recently, ProQR Therapeutics have completed two CTs looking into the possibility of RNA-mediated *CFTR* gene correction. Intranasal administration of single-stranded antisense RNA (eluforsen, QR-010) designed for specific binding to the F508del domain in mRNA and the restoration of *CFTR* function in airway epithelium was used in the CTs. Preliminary *in vitro* and *in vivo* studies in mice showed that QR-010 was able to quickly diffuse through the CF-like secretion, presumably due to its small size and negative charge. QR-010 remained stable even when combined with conventional CF therapies and under bacterial infection. On top of that, positive changes in chloride transport were observed [74–77]. The CT results showed that QR-010 restored the *CFTR* function in

homozygous *CFTR*-F508del patients: A clinically significant improvement in the *CFTR* function, demonstrated by stabilization of the Cl and Na transport parameters, was observed after three intranasal doses for 4 weeks Cl and Na [78].

CONCLUSIONS

Using preclinical models and clinical trials in CF, it has been shown that some advances have already been made in the use of gene therapy methods for the delivery of functional *CFTR* gene copies. Nevertheless, the problem of inefficient *CFTR* gene delivery to bronchopulmonary airway epithelial cells still stands. No optimal approach has yet been found to ensure protein expression in epithelial cells in the quantities required for a pronounced therapeutic effect. It should be taken into account that viral delivery of genetic material may naturally trigger an immune response to the viral capsid upon repeated administration and, thus, a reduced therapeutic effect, while non-viral carriers possess enough permeability to penetrate a thick mucus layer. Despite the fact that there currently are no FDA-approved CF gene therapies, the critical factors that hobble therapeutic efficiency have already been identified and efforts have been initiated to overcome them. Based on the data available, more efficient delivery methods will appear, efficiency in the penetration through the thick secretion layer will increase, and the immune response to therapy will be minimized. The rapid developments in gene engineering technology of recent years provide hope that etiotropic CF therapy will become a reality in the near future. ●

REFERENCES

1. Classification of cystic fibrosis and related disorders. Report of a Joint Working Group of WHO/ICF (M)A/ECFS/ECFTN. World Health Organization. // J. Cyst. Fibros. 2002. V. 1. P. 5–8.
2. Orlov A.V., Simonova O.I., Roslavtseva E.A., Shadrin D.I. Cystic Fibrosis (clinical aspects, diagnostics, treatment, rehabilitation, clinical examination): Textbook for doctors. St. Petersburg: North-Western State Medical University. I.I. Mechnikov, 2014. 160 p.
3. Baranov A.A., Namazova-Baranova L.S., Simonova O.I., Kashirskaya N.Yu., Roslavtseva E.A., Gorinova Yu.V., Krasovskiy S.A., Selimzyanova L.R. // Pediatric pharmacology. 2015. V. 12. №5. P. 589–604.
4. Clinical recommendations. Cystic Fibrosis: microbiological diagnosis of chronic respiratory infection. Ministry of Health of the Russian Federation, 2020.
5. Yan Z., McCray P.B., Engelhardt J.F. // Hum. Mol. Genet. 2019. V. 28. № R1. P. R88–R94.
6. Smirnikhina S.A., Lavrov A.V. // Genes & Cells. 2018. V. 13. № 3. P. 23–31.
7. Bradley S.Q., Steven M.R. // BMJ. 2016. V. 352. P. i859.
8. Gembitskaya T.T., Chermensky A.G. // Pulmology and Allergology. 2011. V. 4. P. 35–39.
9. Clunes M.T., Boucher R.C. // Drug Discov. Today Dis. Mech. 2007. V. 4. P. 63–72.
10. Krasosvky S.A., Samoilenko V.A., Amelina E.L. // Practical Immunology. 2013. V. 1. P. 42–46.
11. Rubin B.K. // Paediatric Respir. Rev. 2007. V. 8. № 1. P. 4–7.
12. Ostedgaard L.S., Moninger T.O., McMenimen J.D., Sawin N.M., Parker C.P., Thornell I.M., Powers L.S., Gansemer N.D., Bouzek D.C., Cook D.P., et al. // Proc. Natl. Acad. Sci. USA. 2017. V. 114. № 26. P. 6842–6847.
13. Boucher R.C. // Trends Mol. Med. 2007. V. 13. P. 231–240.
14. Matsui H., Verghese M.W., Kesimer M., Schwab U.E., Randell S.H., Sheehan J.K., Grubb B.R., Boucher R.C. // J. Immunol. 2005. V. 175. № 2. P. 1090–1099.
15. Kerem B., Rommens J.M., Buchanan J.A., Markiewicz D., Cox T.K., Chakravarti A., Buchwald M., Tsui L.C. // Science. 1989. V. 245. № 4922. P. 1073–1080.
16. Rommens J.M., Iannuzzi M.C., Kerem B., Drumm M.L., Melmer G., Dean M., Rozmahel R., Cole J.L., Kennedy D., Hidaka N., et al. // Science. 1989. V. 245. № 4922. P. 1059–1065.
17. Fajac I., Wainwright C.E. // Presse Med. 2017. V. 46. № 6. Pt 2. P. e165–e175.
18. Welsh M.J., Smith A.E. // Cell. 1993. V. 73. № 7. P. 1251–1254.
19. Maiuri L., Raia V., Kroemer G. // Cell Death Differ. 2017. V. 24. № 11. P. 1825–1844.
20. Ameen N., Silvis M., Bradbury N.A. // J. Cyst. Fibros. 2007. V. 6. № 1. P. 1–14.
21. Meng X., Clews J., Martin E.R., Ciuta A.D., Ford R.C. // Biochem. Soc. Trans. 2018. V. 46. № 5. P. 1093–1098.
22. Meng X., Clews J., Kargas V., Wang X., Ford R.C. // Cell Mol. Life Sci. 2017. V. 74. № 1. P. 23–38.
23. Cooney A.L., McCray P.B., Sinn P.L. // Genes (Basel). 2018. V. 9. № 11. P. 538.
24. Burgener E.B., Moss R.B. // Curr. Opin. Pediatr. 2018. V. 30. № 3. P. 372–377.
25. Burney T.J., Davies J.C. // Appl. Clin. Genet. 2012. V. 5. P. 29–36.
26. Zabner J., Couture L.A., Gregory R.J., Graham S.M., Smith A.E., Welsh M.J. // Cell. 1993. V. 75. P. 207–216.
27. Crystal R.G., McElvaney N.G., Rosenfeld M.A., Chu C.S., Mastrangeli A., Hay J.G., Brody S.L., Jaffe H.A., Eissa, N.T., Danel, C. // Nat. Genet. 1994. V. 8. P. 42–51.
28. Boucher R.C., Knowles M.R., Johnson L.G., Olsen J.C., Pickles R., Wilson J.M., Engelhardt J., Yang Y., Grossman M. // Hum. Gene Ther. 1994. V. 5. P. 615–639.
29. Zuckerman J.B., Robinson C.B., McCoy K.S., Shell R., Sferra T.J., Chirmule N., Magosin S.A., Propert K.J., Brown-Parr E.C., Hughes J.V., et al. // Hum. Gene Ther.

1999. V. 10. № 18. P. 2973–2985.
30. Wagner J.A., Nepomuceno I.B., Messner A.H., Moran M.L., Batson E.P., Dimiceli S., Brown B.W., Desch J.K., Norbash A.M., Conrad C.K., et al. // Hum. Gene Ther. 2002. V. 13. № 11. P. 1349–1359.
31. Moss R.B., Milla C., Colombo J., Accurso F., Zeitlin P.L., Clancy J.P., Spencer L.T., Pilewski J., Waltz D.A., Dorkin H.L., et al. // Hum. Gene Ther. 2007. V. 18. № 8. P. 726–732.
32. Flotte T.R., Zeitlin P.L., Reynolds T.C., Heald A.E., Pedersen P., Beck S., Conrad C.K., Brass-Ernst L., Humphries M., Sullivan K., et al. // Hum. Gene Ther. 2003. V. 14. № 11. P. 1079–1088.
33. Alton E.W., Beekman J.M., Boyd A.C., Brand J., Carlon M.S., Connolly M.M., Chan M., Conlon S., Davidson H.E., Davies J.C., et al. // Thorax. 2017. V. 72. № 2. P. 137–147.
34. Alton E.W., Armstrong D.K., Ashby D., Bayfield K.J., Bilton D., Bloomfield E.V., Boyd A.C., Brand J., Buchan R., Calcedo R., et al. // Lancet Respir. Med. 2015. V. 3. № 9. P. 684–691.
35. Alton E.W., Stern M., Farley R., Jaffe A., Chadwick S.L., Phillips J., Davies J., Smith S.N., Browning J., Davies M.G., et al. // Lancet. 1999. V. 353. № 9157. P. 947–954.
36. Caplen N.J., Alton E.W., Middleton P.G., Dorin J.R., Stevenson B.J., Gao X., Durham S.R., Jeffery P.K., Hodson M.E., Coutelle C., et al. // Nat. Med. 1995. V. 1. № 1. P. 39–46.
37. Yoshimura K., Rosenfeld M.A., Nakamura H., Scherer E.M., Pavirani A., Lecocq J.P., Crystal R.G. // Nucl. Acids Res. 1992. V. 20. P. 3233–3240.
38. Ruiz F.E., Clancy J.P., Perricone M.A., Bebok Z., Hong J.S., Cheng S.H., Meeker D.P., Young K.R., Schoumacher R.A., Weatherly M.R., et al. // Hum. Gene Ther. 2001. V. 12. № 7. P. 751–761.
39. Sermet-Gaudelus I., Clancy J.P., Nichols D.P., Nick J.A., De Boeck K., Solomon G.M., Mall M.A., Bolognese J., Bouisset F., den Hollander W., et al. // J. Cyst. Fibros. 2019. V. 18. № 4. P. 536–542.
40. Knowles M.R., Hohneker K.W., Zhou Z., Olsen J.C., Noah T.L., Hu P.C., Leigh M.W., Engelhardt J.F., Edwards L.J., Jones K.R., et al. // N. Engl. J. Med. 1995. V. 333. P. 823–831.
41. Crystal R.G., Jaffe A., Brody S., Mastrangeli A., McElvaney N.G., Rosenfeld M., Chu C.S., Danel C., Hay J., Eissa T. // Hum. Gene Ther. 1995. V. 6. P. 643–666.
42. Kushwah R., Cao H., Hu J. // J. Immunol. 2008. V. 180. № 6. P. 4098–4108.
43. Yan Z., Stewart Z.A., Sinn P.L., Olsen J.C., Hu J., McCray P.B., Engelhardt J.F. // Hum. Gene Ther. Clin. Dev. 2015. V. 26. P. 38–49.
44. Cao H., Ouyang H., Grasemann H., Bartlett C., Du K., Duan R., Shi F., Estrada M., Seigel K.E., Coates A.L., et al. // Hum. Gene Ther. 2018. V. 29. P. 643–652.
45. Cooney A.L., Singh B.K., Loza L.M., Thornell I.M., Hippee C.E., Powers L.S., Ostedgaard L.S., Meyerholz D.K., Wohlford-Lenane C., Stoltz D.A., et al. // Nucl. Acids Res. 2018. V. 46. P. 9591–9600.
46. Nemudriy A.A., Valetdinova K.R., Medvedev S.P., Zakiyan S.M. // Acta Naturae. 2014. V. 6. № 3. P.20–42.
47. Xia E., Zhang Y., Cao H., Li J., Duan R., Hu J. // Genes (Basel). 2019. V. 10. № 1. P. 39.
48. Zhou Z.P., Yang L.L., Cao H., Chen Z.R., Zhang Y., Wen X.-Y., Hu J. // Hum. Gene Ther. 2019. V. 30. № 9. P. 1101–1116.
49. Zhou Z.P., Yang L.L., Cao H., Wen X.-Y., Hu J. // ASGCT meeting 2019. Mol. Therapy. V. 27. № 4S1.
50. Guggino W.B., Cebotaru L. // Expert Opin. Biol. Ther. 2017. V. 17. № 10. P. 1265–1273.
51. Steines B., Dickey D.D., Bergen J., Excoffon K.J., Weinstein J.R., Li X., Yan Z., Abou Alaiwa M.H., Shah V.S., Bouzek D.C., et al. // JCI Insight. 2016. V. 1. № 14. P. e88728.
52. McClain L.E., Davey M.G., Zoltick P.W., Limberis M.P., Flake A.W., Peranteau W.H. // J. Pediatr. Surg. 2016. V. 51. P. 879–884.
53. Yan Z., Feng Z., Sun X., Zhang Y., Zou W., Wang Z., Jensen-Cody C., Liang B., Park S.Y., Qiu J., et al. // Hum. Gene Ther. 2017. V. 28. P. 612–625.
54. Vidovic D., Carlon M.S., da Cunha M.F., Dekkers J.F., Hollenhorst M.I., Bijvelds M.J., Ramalho A.S., van den Haute C., Ferrante M., Baekelandt V., et al. // Am. J. Respir. Crit. Care Med. 2016. V. 193. P. 288–298.
55. Yan Z., Sun X., Feng Z., Li G., Fisher J.T., Stewart Z.A., Engelhardt J.F. // Hum. Gene Ther. 2015. V. 26. P. 334–346.
56. Ostedgaard L.S., Rokhlina T., Karp P.H., Lashmit P., Afione S., Schmidt M., Zabner J., Stinski M.F., Chiorini J.A., Welsh M.J. // Proc. Natl. Acad. Sci. USA. 2005. V. 102. P. 2952–2957.
57. Yan Z., Keiser N.W., Song Y., Deng X., Cheng F., Qiu J., Engelhardt J.F. // Mol. Ther. 2013. V. 21. P. 2181–2194.
58. Yan Z., Zou W., Feng Z., Shen W., Park S.Y., Deng X., Qiu J., Engelhardt J.F. // Hum. Gene Ther. 2019. V. 30. P. 556–570.
59. Limberis M.P., Vandenberghe L.H., Zhang L., Pickles R.J., Wilson J.M. // Mol. Ther. 2007. V. 15. № 1. P. S160. doi: 10.1016/S1525-0016(16)44621-6.
60. Kurosaki F., Uchibori R., Mato N., Sehara Y., Saga Y., Urabe M., Mizukami H., Sugiyama Y., Kume A. // Gene Ther. 2017. V. 24. P. 290–297.
61. Halbert C.L., Allen J.M., Miller A.D. // J. Virol. 2001. V. 75. № 14. P. 6615–6624.
62. Duncan G.A., Kim N., Colon-Cortes Y., Rodriguez J., Mazur M., Birket S.E., Rowe S.M., West N.E., Livraghi-Butrico A., Boucher R.C., et al. // Mol. Ther. Meth. Clin. Dev. 2018. V. 9. P. 296–304.
63. Wille P.T., Rosenjack J., Cotton C., Kelley T., Padegimas L., Miller T.J. // J. Cyst. Fibros. 2019. V. 18. P. S39. doi: 10.1016/S1569-1993(19)30241-3.
64. Cherenkova E.E., Islamov R.R., Rizvanov A.A. // Intern. J. Appl.& Fundam. Res. 2013. V. 11. № 2. P.57–58.
65. Marquez Loza L.I., Yuen E.C., McCray P.B. Jr. // Genes (Basel). 2019. V. 10. № 3. P. 218.
66. Cooney A.L., Abou Alaiwa M.H., Shah V.S., Bouzek D.C., Stroik M.R., Powers L.S., Gansemer N.D., Meyerholz D.K., Welsh M.J., Stoltz D.A., Sinn P.L., McCray P.B. Jr. // JCI Insight. 2016. V. 1. № 14. P. e88730.
67. Alton E.W., Boyd A.C., Porteous D.J., Davies G., Davies J.C., Griesenbach U., Higgins T.E., Gill D.R., Hyde S.C., Innes J.A., et al. // Am. J. Respir. Crit. Care Med. 2015. V. 192. P. 1389–1392.
68. Robinson E., MacDonald K.D., Slaughter K., McKinney M., Patel S., Sun C., Sahay G. // Mol. Ther. 2018. V. 26. № 8. P. 2034–2046.
69. Mastorakos P., da Silva A.L., Chisholm J., Song E., Choi W.K., Boyle M.P., Morales M.M., Hanes J., Suk J.S. // Proc. Natl. Acad. Sci. USA. 2015. V. 112. P. 8720–8725.
70. Quijano E., Bahal R., Ricciardi A., Saltzman W.M., Glazer P.M. // J. Biol. Med. 2017. V. 90. № 4. P. 583–598.
71. McNeer N.A., Anandalingam K., Fields R.J., Caputo C., Kopic S., Gupta A., Quijano E., Polikoff L., Kong Y., Bahal

R., et al. // Nat. Commun. 2015. V. 6. P. 6952.
72. Piotrowski-Daspit A.S., Barone C., Kauffman A.C., Lin C.Y., Nguyen R., Gupta A., Glazer P.M., Saltzman W.M., Egan M.E. // J. Cyst. Fibros. 2021. V. 20. P. S277. doi: 10.1016/S1569-1993(21)02005-1.
73. Papaioannou I., Simons J.P., Owen J.S. // Expert Opin. Biol. Ther. 2012. V. 12. № 3. P. 329–342.
74. Beumer W., Swildens J., Henig N., Anthonijsz H., Biasutto, P., Teresinha L., Ritsema T. // J. Cyst. Fibros. 2015. V. 14. P. S1. doi: 10.1016/S1569-1993(15)30002-3
75. Brinks V., Lipinska K., Koppelaar M., Matthee B., Button B.M., Livraghi-Butrico A., Henig N. // J. Cyst. Fibros. 2016. V. 15. № 1. P. S31. doi: 10.1016/S1569-1993(16)30168-0.
76. Beumer W., Swildens J., Leal T., Noel S., Anthonijsz H., van der Horst G., Kuiperij-Boersma H., Potman M., van Putten C., Biasutto P., et al. // PLoS One. 2019. V. 14. № 6. P. e0219182.
77. Brinks V., Lipinska K., Jager M., Beumer W., Button B., Livraghi A., Henig N., Matthee B. // J. Aerosol Med. Pulmonary Drug Delivery. 2019. V. 32. № 5. P. 303–316.
78. Sermet-Gaudelus I., Clancy J.P., Nichols D.P., Nick J.A., De Boeck K., Solomon G.M., Mall M.A., Bolognese J., Bouisset F., den Hollander W., et al. // J. Cyst. Fibros. 2019. V. 18. № 4. P. 536–542.

MALAT1 Long Non-coding RNA and Its Role in Breast Carcinogenesis

M. M. Tsyganov[1,2*], M. K. Ibragimova[1,2,3]
[1]Cancer Research Institute, Tomsk National Research Medical Center, Russian Academy of Sciences, Tomsk, 634050 Russian Federation
[2]Siberian State Medical University, Tomsk, 634050 Russian Federation
[3]National Research Tomsk State University, Tomsk, 634050 Russian Federation
*E-mail: TsyganovMM@yandex.ru
Received December 26, 2022; in final form, March 2, 2023
DOI: 10.32607/actanaturae.11905

ABSTRACT **Our genome consists not only of protein-coding DNA, but also of the non-coding part that plays a very important role in the regulation of all cellular processes. A part of the non-coding genome comes with non-coding RNAs (ncRNAs), and disruption of the functional activity of these RNAs may be associated with oncogenesis in various cancer types. There exist two types of ncRNAs: small and long non-coding RNAs, which are classified according to their transcript length. Long non-coding metastasis-associated lung adenocarcinoma transcript 1, *MALAT1* RNA (*NEAT2*), is a long non-coding RNA of particular interest. The aforementioned transcript takes part in the regulation of numerous cellular processes and pathogenesis of different malignant tumors, including breast tumors. This review focuses on experimental and clinical studies into the role of MALAT1 in carcinogenesis and the progression of breast cancer.**
KEYWORDS **MALAT1, NEAT2, breast cancer, long non-coding RNAs, carcinogenesis.**
ABBREVIATIONS **snRNA – small nuclear RNA; BC – breast cancer; TNBC – triple-negative breast cancer; EMT – epithelial–mesenchymal transition; Δsv-MALAT1 – small variant MALAT1; ER1 – estrogen receptor 1; MALAT1 – metastasis-associated lung adenocarcinoma transcript 1; mascRNA – MALAT1-associated small cytoplasmic RNA; MMTV-PyMT – mouse mammary tumor virus-polyomavirus middle T-antigen; ncRNA – non-coding RNA; sh-MALAT1 – short hairpin RNA; siMALAT1 – MALAT1 small interfering RNA.**

INTRODUCTION

Breast cancer (BC) remains one of the most common malignant tumors affecting women [1]. Breast cancer is highly heterogeneous, which makes it different in how sensitive it is to therapy, its prognosis and risk of metastatic spread and recurrence, thus, reducing treatment effectiveness. Therefore, personalized preoperative therapy moves to the forefront in breast cancer patients [2]. Molecular markers for breast cancer such as tumor cell membrane receptors, the p53 protein, antigen Ki-67, the *BRCA1* and *BRCA2* genes, various microRNAs, etc. are currently well-understood, which allows one to classify tumors and predict treatment outcome [3]. Five molecular biological subtypes of breast cancer are recognized today: ER^+ luminal A breast cancer (HER2-negative, low Ki-67 expression ($\leqslant$ 20%), and high progesterone receptor (PR) level ($\geqslant$ 20%)); HER2-negative luminal B breast cancer: ER^+, $HER2^-$, one of the following factors is present: high Ki-67 expression ($\geqslant$ 30%) or low PR level ($<$ 20%); HER2-positive luminal B breast cancer: ER-positive, HER2-positive, any level of Ki-67 expression, any PR level; $HER2^+$: $HER2^+$, ER^- and PR^-, any level of Ki-67 expression; and triple negative breast cancer (TNBC): ER^-, PR^-, $HER2^-$ [4]. However, almost no target is effective in triple-negative breast cancer.

The advances in genome sequencing technology have revealed that, along with protein-coding RNAs, the human genome encodes nontranslating (non-coding) RNAs (ncRNAs) constituting most of the genome (~ 98%) [5]. Non-coding RNAs are involved in genetic and epigenetic regulation; therefore, their functions and participation in tumor progression are being currently vigorously studied [6]. ncRNAs are subdivided into small (micro-) and long non-coding RNAs (miRNAs and lncRNAs, respectively). Long non-coding RNAs, which perform many different functions in the cell and take part in various processes, are of particular interest [6, 7]. The functions of 2% of lncRNAs have been identified thus far. There are three categories of functions performed by lncRNAs. They act as signaling molecules, regulate transcription by participating in the assembly of RNA polymerases in the enhancer domain, initiate RNA cleavage, and are

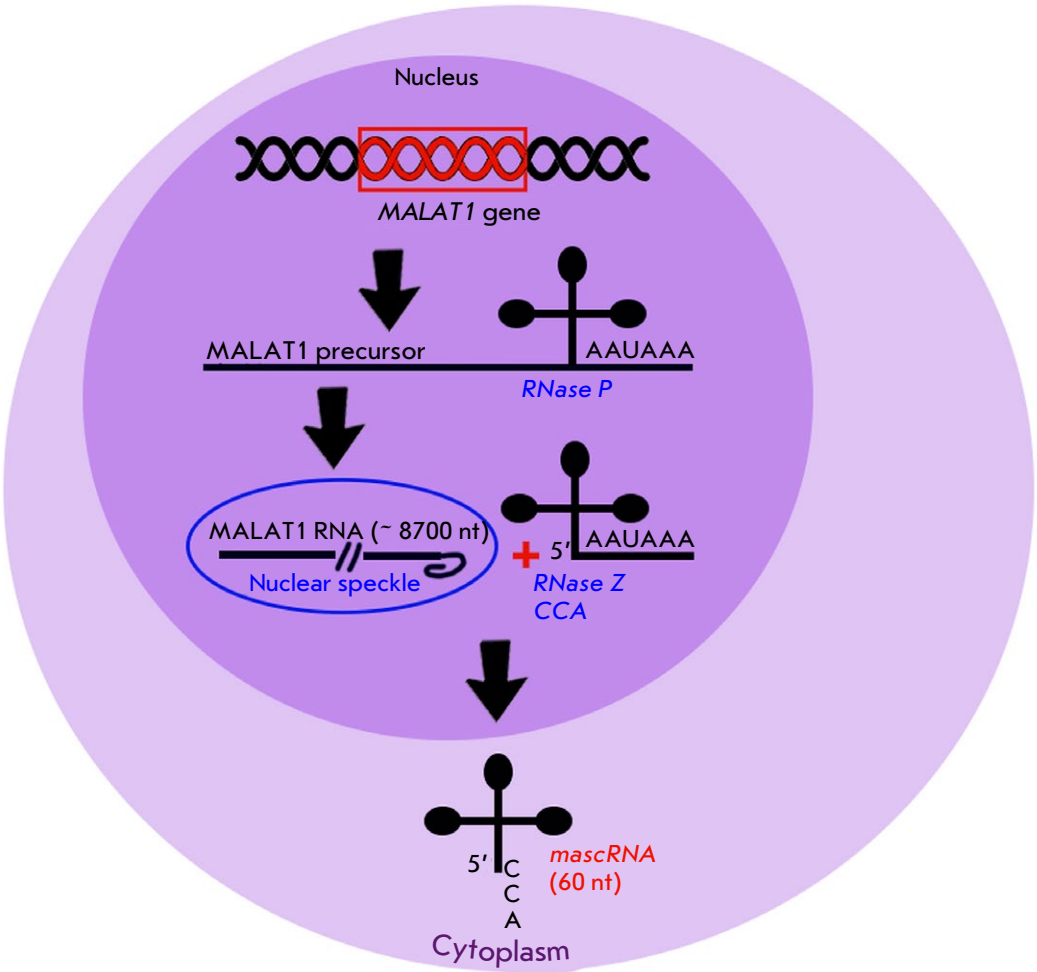

Fig. 1. Scheme of the synthesis of MALAT1 long non-coding RNA in a cell

associated with pluripotency and cellular reprogramming. lncRNAs act as miRNA traps or guides binding proteins and delivering them to the regions where they become involved in the *trans*- and *cis*-regulation of gene expression by binding to DNA:RNA heteroduplexes or RNA:DNA:DNA triplexes and interact with Polycomb group and Trithorax group proteins, thus preventing them from performing histone modification and exerting any degree of epigenetic regulation and chromatin remodeling. lncRNAs initiate the assembly of the RNA complexes that act as protein assembly sites and control the protein function under stress conditions [6, 8–12]. MALAT1 RNA associated with metastatic lung adenocarcinoma is one of the interesting lncRNAs [13].

MALAT1 LONG NON-CODING RNA

MALAT1 RNA was first discovered when studying gene expression in metastatic non-small cell lung cancer (NSCLC) [13]. MALAT1, also known as NEAT2 (nuclear-enriched abundant transcript 2), resides in the nucleoplasm in nuclear speckles (structures performing various functions, the main one being the regulation of pre-mRNA splicing and transcription) [14]. The intronless *MALAT1* gene localized in the 11q13.1 locus encodes the ~ 8700-nt-long transcript [15, 16]. The *MALAT1* gene is located in a region characterized by a high density of genes with very high synthetic evolutionary conservation [17]. Thus, a unique feature of *MALAT1* is that its nucleotide sequence is conserved (in vertebrates, the overall conservation of the 3'-terminal sequence is > 50% and 80%) [18]. The MALAT1 transcript usually has a long half-life: it remains stable for 16 h in human B cells and for 9–12 h in tumor cells [19]. The half-life of MALAT1 is longer than that of other lncRNAs, probably because of the triple helical structure present on its 3'-end [20].

MALAT1 is transcribed by RNA polymerase II from the long arm of human chromosome 11 (11q13) (*Fig. 1*). Formation of this lncRNA depends on tRNA

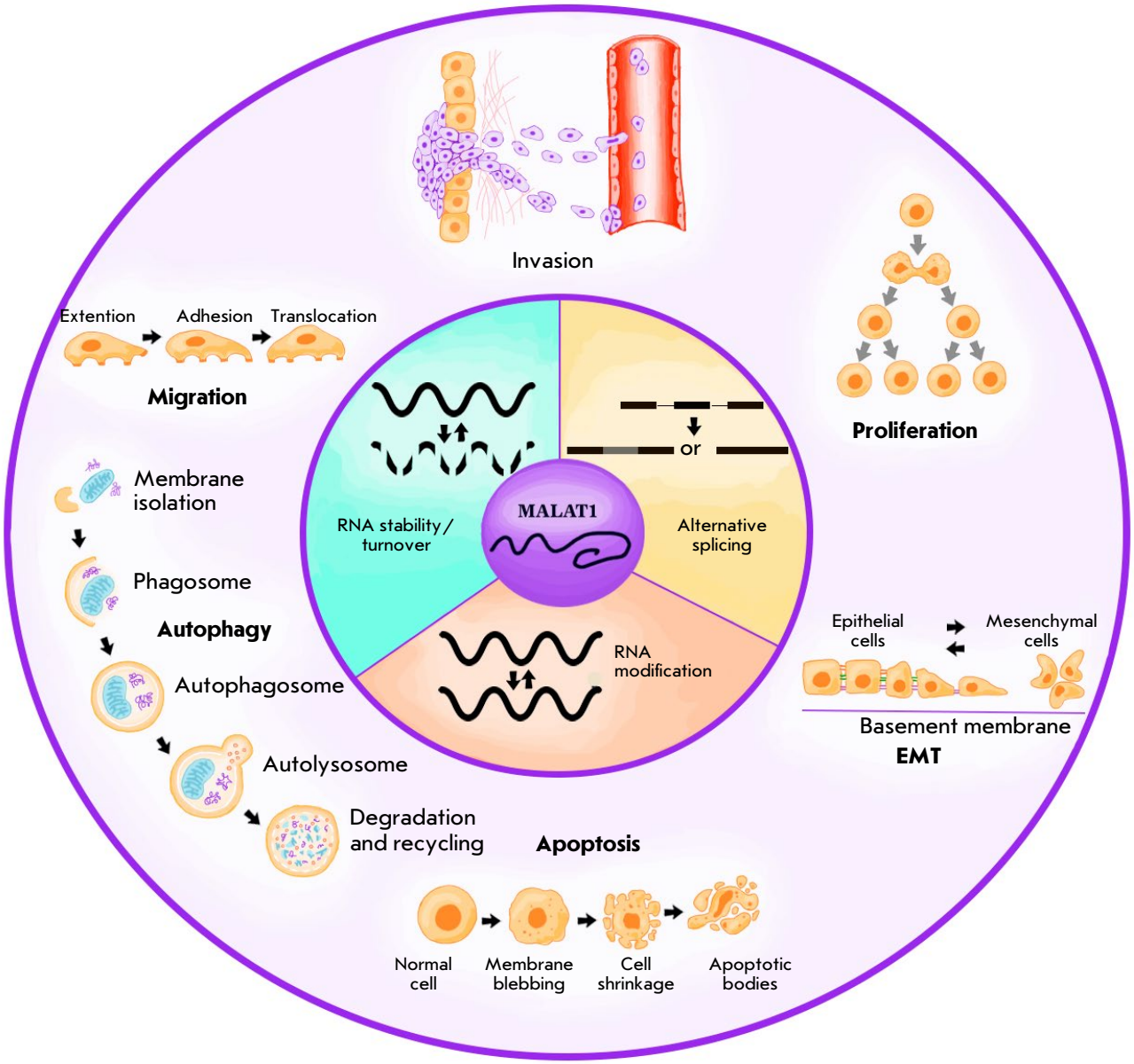

Fig. 2. The main functions of MALAT1 long non-coding RNA in a cell

processing that produces two non-coding RNAs from the same locus, which reside in different subcellular compartments and perform different functions [21]. The RNase P endonuclease recognizes this tRNA-like structure and cleaves it to simultaneously generate the mature 3'-end of the MALAT1 long transcript and the 5'-end of the tRNA-like small RNA. Additional enzymes, which are involved in tRNA biogenesis, including RNase Z and the CCA-adding enzyme, then process small RNA to form the 61-nt-long mature transcript known as mascRNA (*MALAT1*-associated small cytoplasmic RNA). Once the MALAT1 primary transcript is processed, mascRNA is exported to the cytoplasm while the long transcript remains in the nucleus in the form of nuclear speckles [22].

MALAT1 long non-coding RNA accumulates in the nucleus, where it plays a crucial role in cancer progression and the formation of nuclear paraspeckles.

MALAT1 has many different functions (*Fig. 2*): it (1) acts as a nuclear scaffold at the speckle periphery for trans-acting protein factors such as SR proteins, leading to the modulation of pre-splicing and alternative splicing; (2) is involved in the post-transcriptional regulation of the genes associated with cellular motil-

ity [23]; and (3) participates in the regulation of many processes, together with microRNAs [24–27], as well as in epigenetic regulation; e.g., MALAT1 binds to the promoter of the *EEF1A1* gene encoding eukaryotic translation elongation factor 1 alpha 1 (EEF1A1), resulting in the methylation of histone H3 [28].

Not only does MALAT1 play a regulatory role, but it also participates in various signaling pathways (e.g., in the TGF-β/Smad and p53 pathways) [11, 29]. Interestingly, MALAT1 can bind to other ncRNAs and pre-mRNAs, mostly exclusively through mediator proteins, and bind to chromatin exclusively within the region of actively spliced genes [14].

Alternative splicing is also worth mentioning: changes to it are increasingly often recognized as a potential pathogenic mechanism of carcinogenesis. Alternative splicing is the post-transcriptional mechanism that enhances the transcriptome complexity by expressing many of the different mRNAs of individual genes, thus potentially generating different protein isoforms [30]. The screening of the Database of Expressed Sequence Tags (dbEST) undertaken by Meseure et al. discovered Δsv-MALAT1 (the small variant MALAT1 transcript), which was the main product of the alternative splicing of MALAT1. Breast tumors are mostly characterized by low Δsv-MALAT1 expression levels [31].

THE ROLE OF MALAT1 IN BREAST CARCINOGENESIS

It is exciting to study the role played by MALAT1 in carcinogenesis, because this RNA is involved in the regulation of numerous cellular processes. Thus, expression of the *MALAT1* transcript is unstable in patients with different types of cancer and in tumors of different localizations [32]. MALAT1 was first found to be involved in carcinogenesis in patients with non-small cell lung cancer and was shown to be associated with a higher risk of metastatic disease and unfavorable outcome in patients with squamous cell cancer and adenocarcinoma of the lung [13]. Weber et al. [33] suggested that the serum level of MALAT1 in lung cancer patients could be a potential biomarker for this disease. Moreover, MALAT1 overexpression is observed in human hepatocellular carcinoma, breast cancer, pancreatic cancer, and colorectal cancer cells [32]; it is also involved in the expression regulation of some genes associated with metastatic ability [10, 34] and tumor progression in breast cancer patients [27]. According to Liu et al. [35], MALAT1 expression is positively correlated with metastatic lung cancer and negatively correlated with disease prognosis; it is an important prognostic marker for patients with NSCLC. The data on MALAT1 involvement in tumor processes have aroused a keen interest in studying the oncogenic role of MALAT1 and its involvement in metastatic breast tumor. Thus, it has been established that MALAT1 plays a critically important role in the regulation of transcription and the cell cycle, epigenetic regulation, as well as in the inflammation and metastatic processes in tumor (*Fig. 2*) [36]. MALAT1 affects the initiation and progression of tumors of various localizations, including laryngeal cancer, cancer of the laryngopharynx, as well as thyroid, esophageal, lung, liver, and ovarian cancers [37–40]. Therefore, MALAT1 is among the key factors contributing to the regulation of the molecular pathways that lead to phenotypic manifestations of cancer [16]. Below, the role of MALAT1 in breast cancer will be discussed in more detail.

In vitro studies

The mechanisms causing cell migration and invasion and research into the metastatic cascade in breast cancer patients are of significant interest. Many studies have confirmed that MALAT1 is involved in the regulation of cells' migration and invasion ability. MALAT1 was previously reported to regulate the proliferation of cervical and gastric cancer cells, as well as their cisplatin resistance through the PI3K/Akt pathway [41, 42]. The epithelial–mesenchymal transition (EMT) of tumor cells is one of the first steps in metastatic spread [43]. Xu et al. [23] studied the role of MALAT1 in EMT in breast cancer patients and found that MALAT1 promotes *in vitro* migration and invasion of breast cancer cells (MDA-MB-231, MDA-MB-453, MCF10A, SK-BR-3, and BT549); the lower MALAT1 expression level is associated with metastatic breast cancer; i.e., MALAT1 acts as an EMT inducer by activating the PI3K-Akt pathway [23]. Similar findings were also made by Wu et al. [44], who demonstrated that the PI3K/Akt pathway mediating FOXO1 binding to the *MALAT1* promoter can be the mechanism through which *MALAT1* induces EMT and reduces the trastuzumab sensitivity of $HER2^+$ breast cancer cells [44]. A distinctive feature of this study was that MALAT1 expression was evaluated in seven breast cancer cell lines that included cell lines of the $ER^+/HER2^-$, $ER^+/HER2^+$, $ER^-/HER2^+$, and TNBC subtypes. Among these cell lines, the highest MALAT1 expression level was detected in metastatic triple-negative breast cancer cells and trastuzumab-resistant $HER2^+$ cells [44]. Cell cultures of triple-negative breast cancer (MDA-MB-231, primary TNBC cells, Hs578T, and HCC1806) were characterized by lower MALAT1 levels compared to ER^+ cells (MCF-7, primary ER^+ tumor cells, and T-47D) [27, 45, 46]. It was found that metastasis-associated MALAT1 overexpression can be negatively correlated with the

expression of the Nisch product, a tumor suppressor protein whose expression is downregulated in breast cancer patients [47]. In 231-GFP-Nisch cell cultures (MDA-MB-231 with Nisch overexpression), Nisch expression levels are associated with the MALAT1 expression levels: knockout of the *Nisch* gene transcript in these cells increases their proliferation and migration [47].

Zhang et al. [48] showed that tumor cells secrete MALAT1 in recipient cells in order to regulate the proliferation of receptor cells in the tumor microenvironment. MALAT1 expression levels in breast cancer cells are significant: MDA-MB-231 exosomes substantially increase the proliferation of MDA-MB-231 and ZR-75-1 cells; however, exosomes from MDA-MB-231 cells treated with MALAT1-siRNA (small interfering RNA or siRNA targeting MALAT1) reduce cell proliferation in breast cancer patients. Earlier, Jin et al. [45] showed that *MALAT1* in TNBC cells suppresses cells' proliferation and invasion ability and triggers apoptosis, which is achieved through reverse regulation of the miR-1 RNA transcriptome and its target protein promoting epithelial–mesenchymal transition, Slug [45]. The mechanism of functioning of this process has been described more thoroughly for the MDA-MB-231 and MCF-7 cultures, using the plasmid transfection method. MALAT1 overexpression enhances cells' migration and invasion ability by binding to miR-1 and reducing the level of Cdc42, the protein involved in EMT [26]. Furthermore, it was revealed using siMALAT1-mediated inhibition of MALAT1 and, conversely, by inserting the MALAT1 overexpression vector into a breast cancer cell line that MALAT1 expression directly affects the expression of miR-124, a microRNA associated with the suppression of breast cancer progression and that MALAT1 overexpression suppresses the inhibitory effect of miR-124 on breast tumor growth, thus increasing its size [25].

For the culture of 4T14T1 cells, the highly metastatic breast cancer cell line derived from spontaneous mammary tumor in BALB/c mice, Li et al. [49] discovered a new mechanism through which MALAT1 could participate in the regulation of EMT in mammary tumors. The transcript was shown to exhibit pro-inflammatory activity and be able to regulate the lipopolysaccharide-induced inflammation and cellular EMT. An antisense transcript of the *MALAT1* gene, transcribed from the opposite strand and named TALAM1, was also discovered [50]. Having conducted their own study based on this discovery, Gomes et al. showed that overexpression of these transcripts is typical of breast cancer cell lines and that there exists a positive correlation between their expression levels in the studied cell lines. MALAT1 and TALAM1 work together: TALAM1 mediates MALAT1 activity in the presence of TGF-β cytokine [51], a well-known EMT inducer. Nevertheless, it is rather difficult to assess the effect of MALAT1 on cells' metastatic ability, since different authors have provided different descriptions of this mechanism. The main reasons for the lack of consistency in the data on MALAT1 activity are still to be identified. Differences in the results obtained for tumor cell cultures can probably be assigned to the features of protein expression in different types of cells, as well as to the fact that the MALAT1 transcript forms complexes with different proteins, thus causing opposite effects [47]. Other plausible explanations include the use of cell lines having different genetic backgrounds or differences in culture conditions.

It is notable that the effect of MALAT1 on cell function was uncovered in studies using the A549 lung cancer cell line. A549 cells were transfected with MALAT1 siRNA1 and MALAT1 siRNA2; the control cells were transfected with control siRNA1 and siRNA2, respectively. *MALAT1* knockdown by siRNA reduced MALAT1 levels by 70–80%, which significantly affected cell motility (this parameter decreased compared to that in the cells transfected with control siRNA). In addition, *MALAT1* knockdown reduced the cell migration rate. However, no effect on cell proliferation was observed [52].

In vivo studies using model objects

The *in vivo* functions of *MALAT1* have mainly been studied by xenotransplantation of human tumors or cell cultures into thymus-deficient mice. The *in vitro* studies in cell cultures and studies using tumor xenografts have revealed the contradictory effects of *MALAT1* on tumor cell growth and invasion. Targeted inactivation of the *MALAT1* gene in a breast cancer model in transgenic mice without altering the expression of neighboring genes was shown to promote lung metastasis, and this phenotype can be reversed by genetic insertion of *MALAT1*. Identically, *MALAT1* knockout in human breast cancer cells confers metastatic ability, which is eliminated by *MALAT1* re-expression [53]. Furthermore, MALAT1 stimulates mammary tumor growth: transfecting siMALAT1 into MDA-MB-231 and ZR-75-1 cell cultures suppressed the proliferation ability of cells, whereas subcutaneous injection of transfected tumor cells to mice also reduced tumor growth rate and size [48]. According to the results obtained for cell cultures (*MALAT1* knockdown resulted in inhibition of the proliferation and invasion ability and triggered apoptosis in TNBC cell cultures), Jin et al. [45] subcutaneously injected *MALAT1* knockout tumor xenografts to mice and obtained similar results:

tumor growth was inhibited; tumor size decreased; MALAT1 hypoexpression triggered apoptosis of tumor cells and reduced their proliferation rate and the number of Ki-67-positive cells in the tumor. In a model of xenografts with siMALAT1, an influenced miR-124 inhibitor and miR-124+ inhibitor showed that MALAT1 overexpression is associated with CDK4 expression and cell proliferation, all controlled by the CDK4/E2F1 signaling pathway in breast cancer [25]. It is also worth noting that Yang et al. developed a mouse tumor xenograft model for detecting the *MALAT1* function in $HER2^+$ breast cancer: MALAT1 expression was significantly upregulated in $HER2^+$ breast cancer both in cells and in tissues. *MALAT1* silencing suppressed the proliferation of $HER2^+$ breast cancer cells. The results seemed to suggest that MALAT1 could be a potential biomarker and a therapeutic target in $HER2^+$ breast cancer [54].

Several studies have addressed the feasibility of targeting MALAT1 in order to improve the treatment of malignant neoplasms. Research into RNA therapy currently allows one to design RNA-based therapeutics, namely, antisense oligonucleotides (ASOs), which are small sequences complementary to mRNA carrying information about the protein under study, which can inhibit its synthesis [55]. Examination of the role of MALAT1 in breast cancer progression in the MMTV (mouse mammary tumor virus)-PyMT model showed that *MALAT1* knockdown subcutaneously delivered ASO and reduced the metastasis rate. *MALAT1* knockdown (20–80%) was achieved in mice injected with MALAT1-specific ASO1 or ASO2 compared to control mice that received the scrambled ASO (ScASO) control. The tumor growth rate was also reduced by 50% in mice in the experimental group compared to that in control mice injected with ScASO [56].

In vivo studies in breast cancer patients

The published data suggest that MALAT1 utilizes different mechanisms for different molecular subtypes of breast cancer [2]. *MALAT1* expression is upregulated in patients with TNBC, and those with elevated MALAT1 expression levels have a poor overall survival chance. Thus, Samir et al. investigated not only MALAT1 lncRNA, but also the X-inactive specific transcript (XIST). They successfully demonstrated that although miR-182-5p exhibited oncogenic activity, XIST had a preponderant effect on the regulation of the PD-L1 signaling pathway by inhibiting the oncogenic function of MALAT1 [57]. This fact can explain the findings obtained by Xiping et al. showing that MALAT1 suppression downregulates PD-L1 expression. This study demonstrated that MALAT1 gene editing can efficiently suppress the proliferation and invasion ability of triple negative and $HER2^+$ breast cancer cells [2]. MALAT1 expression levels are much higher in TNBC samples than they are in $HER2^+$ breast cancer samples. Lin et al. [32] showed that the downregulated or absent expression of MALAT1 is typical mostly of normal tissue, while MALAT1 overexpression is characteristic of breast, pancreatic, liver, lung, colorectal, and prostate cancers. MALAT1 mRNA expression proved also significantly upregulated in breast cancer tissues. These results are consistent with the findings made in earlier studies demonstrating that MALAT1 lncRNA can also promote cell proliferation and invasion in TNBC and lung cancer [57]. It follows from these data that MALAT1 can be used as a promising biomarker in the clinical diagnosis and prognosis of aggressive breast cancer tumors. In other words, it is clear that MALAT1 activation plays a crucial role in breast carcinogenesis. However, it is interesting to note that the serum levels of MALAT1 can also be a potential diagnostic oncomarker of breast cancer. In their *in vitro* study, Miao et al. showed that suppression of MALAT1 lncRNA significantly inhibited the proliferation, migration, and invasion of breast cancer cells, induced apoptosis and G1-phase cell cycle arrest, which has also been repeatedly shown in other independent studies. Furthermore, the serum level of MALAT1 in breast cancer patients was significantly higher than in patients having benign breast conditions ($p < 0.001$) [58].

On the other hand, when analyzing the RNA sequencing data (The Cancer Genome Atlas), Kim encountered the lowest MALAT1 expression levels in more aggressive tumors; MALAT1 expression in breast cancer cells was lower than that in normal tissue. This finding contradicted the results reported in other studies: in most cases, overexpression of the MALAT1 transcript in breast cancer cells compared to normal tissue was observed [25, 28, 45, 46, 59–61]. Kim et al. used the CRISPR-Cas9 genome editing tool to achieve *MALAT1* knockout and observed an increased metastasis rate. Such differences in the results most probably had to do with the differences in the approaches used to obtain MALAT1 knockdown mice. Thus, according to the published data, MALAT1 overexpression is observed in the tumors of the ER+ and PR+ subtypes, as well as TNBC [27, 31, 46, 62]. Comparison of the expression levels of the transcript in TNBC and HER2-enriched breast cancer cells revealed MALAT1 overexpression in triple-negative cancer cells, which may be an indication that MALAT1 expression is correlated with the metastatic ability and that the differences are associated with the mediated participation of MALAT1 in different

cellular processes [2]. MALAT1 overexpression is believed to be associated with poor tumor differentiation and resistance to hormone therapy [59, 62], while low expression might be associated with the relatively high five-year overall survival rate of breast cancer patients [63].

CLINICAL SIGNIFICANCE OF MALAT1

Not only is *MALAT1* usually overexpressed in different types of cancer, but it also frequently undergoes mutation. Some researchers have reported a high frequency of mutations in the *MALAT1* locus (e.g., translocation in *MALAT1* in renal cell carcinoma and gastroblastoma cells is established) [17]. Today, there are very few studies focusing on the association between *MALAT1* mutations and breast cancer progression and the clinicopathological parameters of the tumor; so, it remains an open question whether this gene is a driver gene in breast carcinogenesis or not [64]. Kandoth et al. reported a low rate (1.1%) of *MALAT1* mutations in breast cancer patients compared to other types of malignancies [31, 65]. However, the genome-wide association study of tumors collected from breast cancer patients conducted by Nik-Zainal et al. revealed a high rate of *MALAT1* mutations (single nucleotide substitutions, insertions, and deletions), but it still remained unclear whether these mutations were driver mutations or resulted from the high tumor mutation burden in this genomic region [66].

MALAT1 was shown to belong to the group of genes of the luminal B breast cancer subtype: *MALAT1* mutations are associated with such clinicopathologic parameters as a high tumor grade and high Ki-67 expression level. *MALAT1* deletions and high frequency of insertion and deletion mutations (that most likely had arisen during transcription) were also observed in patients with the luminal subtypes of breast cancer [67]. This study also mentioned that *MALAT1* mutations were unrelated to changes in gene expression levels; they probably had arisen during transcription as well [64]. The probability of activating the oncogenic effect of MALAT1 on cells can hardly be associated with gene amplification. This conclusion was drawn by Meseure et al., since the *MALAT1* gene resides in the chromosome locus that is rarely amplified [31]. According to our data [68], the frequency of deletions in the locus where *MALAT1* resides in luminal B breast tumors amounts to 18%. Amplification at the 11q13.1 locus was observed in 10% of patients; in the vast majority of cases (72%), tumor cells had a normal copy number at this locus [68].

Furthermore, the MALAT1 lncRNA rs619586 polymorphism was shown to be associated with the response to platinum-based chemotherapy [69]. In the dominant genotypic model, the presence of the wild-type genotype (A/A) was found to be associated with a high chance of responding to chemotherapy by patients with non-small cell lung cancer (OR 0.60; 95% CI 0.36–0.97; $p = 0.04$), especially by patients younger than 57 years (OR 0.49; 95% CI 0.24–0.98; $p = 0.04$), males (OR 0.53; 95% CI 0.31–0.92; $p = 0.02$), smokers (OR 0.46; 95% CI 0.24–0.89; $p = 0.02$), and patients with squamous cell carcinoma of the lung (OR 0.24; 95% CI 0.10–0.60; $p < 0.001$) [69].

MALAT1 as a prognostic factor

According to the data reported previously, MALAT1 can be used as a promising biomarker in the clinical diagnosis and prognosis of aggressive breast cancer. Findings on the MALAT1 expression level can be a prognostic factor. An analysis of the data reported in 14 studies revealed that MALAT1 overexpression was associated with poor patient survival (HR = 1.95; 95% CI 1.57–2.41; $p < 0.001$) [48, 70, 71]. The low relapse-free survival rates associated with MALAT1 overexpression were also characteristic of patients with the ER-negative profile of tumor expression (HR = 2.83; 95% CI 1.02–7.83; $p = 0.045$) and for the group of patients having the luminal subtypes of breast cancer (ER+) and receiving tamoxifen therapy (HR = 2.56; 95% CI 1.04–6.0; $p = 0.034$) [62]. Similar results were obtained for patients with the TNBC and $HER2^+$ subtypes of breast cancer having no lymphatic metastases; elevated MALAT1 levels correlated with a worse prognosis [27]. Elbasateeny et al. [72] arrived at a conclusion that not all TNBC patients have a poor prognosis; patients negative for one of the MALAT1 and BACH1, or both, have a satisfactory prognosis and so can be managed by breast oncoplastic conserving surgery. These data can explain the inconclusiveness of the findings obtained in independent studies. Later, Wang et al. conducted a meta-analysis, with special emphasis placed on metastatic spread, and showed that MALAT1 overexpression is associated with poor disease prognosis. The relapse-free survival of breast cancer patients with upregulated expression of this gene was lower in 95% of cases (HR = 1.97; 95% CI 1.25–3.09; $p = 0.003$), and no association between MALAT1 expression and lymphatic metastasis was detected (OR = 1.32; 95% CI 0.34–5.21) [73]. However, for the TNBC and $HER2^+$ breast cancer samples, Xiping et al. revealed a positive correlation between the increased expression level of the MALAT1 transcript and the number of metastatic lymph nodes, as well as an inverse relationship between its expression level and the relapse-free survival rate of patients with the $HER2^+$ subtype of

breast cancer [2]. A different effect was reported for the metastasis-free survival rate of breast cancer patients: the decreased MALAT1 expression in these patients was associated with worse survival rates (HR = 0.81; 95% CI 0.67–0.99, p = 0.0420; HR = 0.65; 95% CI, p = 0.005) [23]. However, in this case, the conclusion was based on experimental results demonstrating that MALAT1 acts as an EMT inducer in breast cancer patients by activating the PI3K-Akt pathway. Therefore, there is no direct evidence of correlations between a low MALAT1 expression level and a worse prognosis.

In addition, a recent meta-analysis showed that high MALAT1 expression levels are associated with the PR+ tumor profile (95% CI 1.18–1.82; p = 0.0006) and, moreover, with decreased immune cell infiltration into the tumor, which may be one of the reasons for the poor survival prognosis in breast cancer patients with MALAT1 overexpression [71]. Finally, we would like to mention that Meseure et al. showed that both the expression level of the full-length MALAT1 transcript and the expression level of the alternatively spliced MALAT1 transcript (Δsv-MALAT1) carrying two deletions can be used as prognostic factors: Δsv-MALAT1 hypoexpression in the tumor was observed in 19% of cases and was positively correlated with a large tumor size, ER-negative, PR-negative, triple-negative subtypes of breast cancer, and a poor metastasis-free survival chance [31]. Hence, it is fair to assume that alterations in gene expression affect the direction of tumor progression.

Importantly, MALAT1 is also a prognostic marker in human tumors of other localizations. Thus, according to the results of a study of prostate cancer cells resistant to enzalutamide (an antiandrogen used in prostate cancer treatment), the *MALAT1/AR-v7* axis (androgen receptor splice variant 7, AR) can be a promising therapeutic marker. The relationship between the expression of *AR-v7*, which contributes to the development of enzalutamide resistance, and the *MALAT1* expression has been emphasized [74]. The expression levels of both genes in EnzR-PCa cells (the enzalutamide-resistant cell line) were higher than those in drug-susceptible cells. Administration of MALAT1 siRNA and/or ASC-J9 (5-hydroxy-1,7-bis(3,4-dimethoxyphenyl)-1,4,6-heptatrien-3-one) suppressed the progression of EnzR-PCa tumor cells. AR was shown to bind to androgen response elements (AREs) on the *MALAT1* promoter. This interaction was inhibited in the presence of enzalutamide, thus boosting the activity of the *MALAT1* promoter. In turn, MALAT1-siRNA inhibited *AR-v7* expression [74].

Hence, the MALAT1 expression level can be used as a prognostic factor in breast cancer. The revealed patterns give grounds for inferring that MALAT1 lncRNA may indeed be a good predictive marker for selecting this treatment option.

CONCLUSIONS

An analysis of the role of lncRNAs in the carcinogenesis of different types of tumors appears to be important, since new data on the principles of action of long non-coding RNAs would reveal the role played by the non-coding part of the genome in tumor pathogenesis, as well as supplement our knowledge about potential prognostic markers in cancer; breast cancer in particular. The metastasis-associated lung adenocarcinoma transcript 1 (MALAT1), which was recently discovered during a study of the mechanisms of metastasis in lung cancer, is of interest. This RNA is involved in numerous cellular processes such as transcription, splicing, metastatic spread, cell proliferation, etc. It can be inferred from a number of studies that a high level of this transcript is a marker of a poor survival likelihood for breast cancer patients and it can also be involved in the regulation of the mechanisms of EMT, invasion, and metastatic spread. For this reason, collecting data on this ncRNA is important in the search for more efficient methods to diagnose and treat malignant breast tumors. Further research into the functions of MALAT1 will allow one to understand the key mechanisms of tumor neoplasm initiation and progression. ●

Conflict of Interest. The authors have no conflicts of interest to declare.

This work was supported by the Russian Science Foundation (grant No. 22-15-00169 "The Phenotype of BRCA-like Tumors During Carcinogenesis and Treatment".)

REFERENCES

1. Sung H., Ferlay J., Siegel R.L., Laversanne M., Soerjomataram I., Jemal A., Bray F. // CA: Cancer J. Clinicians. 2021. V. 71. № 3. P. 209–249.
2. Xiping Z., Bo C., Shifeng Y., Feijiang Y., Hongjian Y., Qihui C., Binbin T. // Oncotarget. 2018. V. 9. № 2. P. 2255–2267.
3. Wang D., Xu J., Shi G., Yin G. // J. Cancer Res. Therapeutics. 2015. V. 11. № 5. P. 11–15.
4. Tyulyandin S.A., Artamonova E.V., Zhukova L.G., Kislov N.V., Koroleva I.A., Parokonnaya A.A. // Malignant tumors. 2022. V. 12. № 3s2-1. P. 155–197.
5. Wang J., Ye C., Xiong H., Shen Y., Lu Y., Zhou J., Wang L. // Oncotarget. 2017. V. 8. № 3. P. 5508–5522.

6. Alahari S., Eastlack S., Alahari S. // Internat. Rev. Cell Mol. Biol. 2016. V. 234. № 1. P. 229–254.
7. Sanchez Calle A., Kawamura Y., Yamamoto Y., Takeshita F., Ochiya T. // Cancer Sci. 2018. V. 109. № 7. P. 2093–2100.
8. Wright C.M. // Epigenetic Cancer Therapy. 2015. P. 91–114.
9. Tsai M.-C., Manor O., Wan Y., Mosammaparast N., Wang J.K., Lan F., Shi Y., Segal E., Chang H.Y. // Science. 2010. V. 329. № 5992. P. 689–693.
10. Gutschner T., Hämmerle M., Eißmann M., Hsu J., Kim Y., Hung G., Revenko A., Arun G., Stentrup M., Groß M. // Cancer Res. 2013. V. 73. № 3. P. 1180–1189.
11. Zhang J., Han C., Song K., Chen W., Ungerleider N., Yao L., Ma W., Wu T. // PLoS One. 2020. V. 15. № 1. P. e0228160.
12. Schmitt A.M., Chang H.Y. // Cancer Cell. 2016. V. 29. № 4. P. 452–463.
13. Ji P., Diederichs S., Wang W., Böing S., Metzger R., Schneider P.M., Tidow N., Brandt B., Buerger H., Bulk E. // Oncogene. 2003. V. 22. № 39. P. 8031–8041.
14. Galganski L., Urbanek M.O., Krzyzosiak W.J. // Nucl. Acids Res. 2017. V. 45. № 18. P. 10350–10368.
15. van Asseldonk M., Schepens M., de Bruijn D., Janssen B., Merkx G., van Kessel A.G. // Genomics. 2000. V. 66. № 1. P. 35–42.
16. Goyal B., Yadav S.R.M., Awasthee N., Gupta S., Kunnumakkara A.B., Gupta S.C. // Biochim. Biophys. Acta (BBA) – Rev. Cancer. 2021. V. 1875. № 2. P. 1–13.
17. Arun G., Aggarwal D., Spector D.L. // Noncoding RNA. 2020. V. 6. № 2. P. 1–22.
18. Johnsson P., Lipovich L., Grandér D., Morris K.V. // Biochim. Biophys. Acta (BBA) –Gen. Subjects. 2014. V. 1840. № 3. P. 1063–1071.
19. Tani H., Nakamura Y., Ijiri K., Akimitsu N. // Drug Discov. Therapeut. 2010. V. 4. № 4. P. 235–239.
20. Brown J.A., Bulkley D., Wang J., Valenstein M.L., Yario T.A., Steitz T.A., Steitz J.A. // Nat. Struct. Mol. Biol. 2014. V. 21. № 7. P. 633–640.
21. Amodio N., Raimondi L., Juli G., Stamato M.A., Caracciolo D., Tagliaferri P., Tassone P. // J. Hematol. Oncol. 2018. V. 11. № 1. P. 1–19.
22. Wilusz J.E. // Biochim. Biophys. Acta (BBA) – Gene Regulatory Mechanisms. 2016. V. 1859. № 1. P. 128–138.
23. Xu S., Sui S., Zhang J., Bai N., Shi Q., Zhang G., Gao S., You Z., Zhan C., Liu F. // Internat. J. Clin. Exp. Pathol. 2015. V. 8. № 5. P. 4881–4891.
24. Liu R., Li J., Lai Y., Liao Y., Liu R., Qiu W. // Internat. J. Biol. Macromol. 2015. V. 81. P. 491–497.
25. Feng T., Shao F., Wu Q., Zhang X., Xu D., Qian K., Xie Y., Wang S., Xu N., Wang Y. // Oncotarget. 2016. V. 7. № 13. P. 16205–16216.
26. Chou J., Wang B., Zheng T., Li X., Zheng L., Hu J., Zhang Y., Xing Y., Xi T. // Biochem. Biophys. Res. Commun. 2016. V. 472. № 1. P. 262–269.
27. Jadaliha M., Zong X., Malakar P., Ray T., Singh D.K., Freier S.M., Jensen T., Prasanth S.G., Karni R., Ray P.S. // Oncotarget. 2016. V. 7. № 26. P. 40418–40436.
28. Li X., Chen N., Zhou L., Wang C., Wen X., Jia L., Cui J., Hoffman A.R., Hu J.-F., Li W. // Am. J. Cancer Res. 2019. V. 9. № 4. P. 714–729.
29. Zhang T., Wang H., Li Q., Fu J., Huang J., Zhao Y. // Cell. Physiol. Biochem. 2018. V. 50. № 6. P. 2216–2228.
30. Black D.L. // Annu. Rev. Biochem. 2003. V. 72. № 1. P. 291–336.
31. Meseure D., Vacher S., Lallemand F., Alsibai K.D., Hatem R., Chemlali W., Nicolas A., De Koning L., Pasmant E., Callens C., et al. // Br. J. Cancer. 2016. V. 114. № 12. P. 1395–1404.
32. Lin R., Maeda S., Liu C.a., Karin M., Edgington T. // Oncogene. 2007. V. 26. № 6. P. 851–858.
33. Weber D.G., Johnen G., Casjens S., Bryk O., Pesch B., Jöckel K.-H., Kollmeier J., Brüning T. // BMC Res. Notes. 2013. V. 6. № 1. P. 1–9.
34. Ren D., Li H., Li R., Sun J., Guo P., Han H., Yang Y., Li J. // Oncol. Lett. 2016. V. 11. № 3. P. 1621–1630.
35. Liu C., Li H., Jia J., Ruan X., Liu Y., Zhang X. // Med. Sci. Monitor: Internat. Med. J. Exp. Clin. Res. 2019. V. 25. P. 5143–5149.
36. Qiao Y., Peng C., Li J., Wu D., Wang X. // Curr. Neurovasc. Res. 2018. V. 15. № 3. P. 211–219.
37. Kyurkchiyan S.G., Popov T.M., Stancheva G., Rangachev J., Mitev V.I., Popova D.P., Kaneva R.P. // J. BUON. 2020. V. 25. № 1. P. 357–366.
38. Xu E., Liang X., Ji Z., Zhao S., Li L., Lang J. // Eur. Arch. Oto-Rhino-Laryngol.. 2020. V. 277. № 2. P. 611–621.
39. Wang S., Wang T., Liu D., Kong H. // Cancer Manag. Res. 2020. V. 12. P. 10735–10747.
40. Zhao L., Lou G., Li A., Liu Y. // Mol. Med. Rept. 2020. V. 22. № 2. P. 1449–1457.
41. Wang N., Hou M., Zhan Y., Shen X., Xue H. // Eur. Rev. Med. Pharmacol. Sci. 2018. V. 22. № 22. P. 7653–7659.
42. Dai Q., Zhang T., Li C. // Cancer Management and Research. 2020. V. 12. № 1. P. 1929–1939.
43. Bill R., Christofori G. // FEBS Lett. 2015. V. 589. № 14. P. 1577–1587.
44. Wu Y., Sarkissyan M., Ogah O., Kim J., Vadgama J.V. // Cancers. 2020. V. 12. № 7. P. 1918.
45. Jin C., Lu Q., Lin Y., Ma L. // Tumor Biol. 2016. V. 37. № 6. P. 7383–7394.
46. Latorre E., Carelli S., Raimondi I., D'Agostino V., Castiglioni I., Zucal C., Moro G., Luciani A., Ghilardi G., Monti E. // Cancer Res. 2016. V. 76. № 9. P. 2626–2636.
47. Eastlack S.C., Dong S., Mo Y.Y., Alahari S.K. // PLoS One. 2018. V. 13. № 6. P. 1–13.
48. Zhang P., Zhou H., Lu K., Lu Y., Wang Y., Feng T. // OncoTargets. Therapy. 2018. V. 11. P. 291–299.
49. Li Z., Xu L., Liu Y., Fu S., Tu J., Hu Y., Xiong Q. // Am. J. Translat. Res. 2018. V. 10. № 10. P. 3186–3197.
50. Zong X., Nakagawa S., Freier S.M., Fei J., Ha T., Prasanth S.G., Prasanth K.V. // Nucl. Acids Res. 2016. V. 44. № 6. P. 2898–2908.
51. Gomes C.P., Nóbrega-Pereira S., Domingues-Silva B., Rebelo K., Alves-Vale C., Marinho S.P., Carvalho T., Dias S., de Jesus B.B. // BMC Cancer. 2019. V. 19. № 1. P. 1–11.
52. Takahashi D.T., Gadelle D., Agama K., Kiselev E., Zhang H., Yab E., Petrella S., Forterre P., Pommier Y., Mayer C. // Nat. Commun. 2022. V. 13. № 1. P. 1–11.
53. Kim J., Piao H.-L., Kim B.-J., Yao F., Han Z., Wang Y., Xiao Z., Siverly A.N., Lawhon S.E., Ton B.N. // Nat. Genet. 2018. V. 50. № 12. P. 1705–1715.
54. Yang C., Zhu H., Tan Y., Zhu R., Wu X., Li Y., Wang C. // Curr. Cancer Drug Targets. 2021. V. 21. № 10. P. 860–869.
55. Chen Q., Zhu C., Jin Y. // Front Genet. 2020. V. 11. № 93. P. 1–9.
56. Arun G., Diermeier S., Akerman M., Chang K-C., Wilkinson J.E., Hearn S., Kim Y., MacLeod A.R., Krainer A.R., Norton L., et al. // Genes Dev. 2016. V. 30. № 1. P. 34–51.
57. Samir A., Tawab R.A., El Tayebi H.M. // Oncol. Lett.

2021. V. 22. № 2. P. 1–12.
58. Miao Y., Fan R., Chen L., Qian H. // Ann. Clin. Lab. Sci. 2016. V. 46. № 4. P. 418–424.
59. Guffanti A., Iacono M., Pelucchi P., Kim N., Soldà G., Croft L.J., Taft R.J., Rizzi E., Askarian-Amiri M., Bonnal R.J. // BMC Genomics. 2009. V. 10. № 1. P. 1–17.
60. Arshi A., Sharifi F.S., Ghahfarokhi M.K., Faghih Z., Doosti A., Ostovari S., Maymand E.M., Seno M.M.G. // Mol. Therapy–Nucle. Acids. 2018. V. 12. P. 751–757.
61. Huang X.J., Xia Y., He G.F., Zheng L.L., Cai Y.P., Yin Y., Wu Q. // Oncology Reports. 2018. V. 5. P. 2683–2689.
62. Huang N.-S., Chi Y.-Y., Xue J.-Y., Liu M.-Y., Huang S., Mo M., Zhou S.-l., Wu J. // Oncotarget. 2016. V. 7. № 25. P. 37957–37965.
63. Sun Z., Liu J., Liu J. // Cell. Mol. Biol. 2020. V. 66. № 3. P. 72–78.
64. Rheinbay E., Nielsen M.M., Abascal F., Wala J.A., Shapira O., Tiao G., Hornshøj H., Hess J.M., Juul R.I., Lin Z. // Nature. 2020. V. 578. № 7793. P. 102–111.
65. Kandoth C., McLellan M.D., Vandin F., Ye K., Niu B., Lu C., Xie M., Zhang Q., McMichael J.F., Wyczalkowski M.A. // Nature. 2013. V. 502. № 7471. P. 333–339.
66. Nik-Zainal S., Davies H., Staaf J., Ramakrishna M., Glodzik D., Zou X., Martincorena I., Alexandrov L.B., Martin S., Wedge D.C. // Nature. 2016. V. 534. № 7605. P. 47–54.
67. Ellis M.J., Ding L., Shen D., Luo J., Suman V.J., Wallis J.W., van Tine B.A., Hoog J., Goiffon R.J., Goldstein T.C. // Nature. 2012. V. 486. № 7403. P. 353–360.
68. Ibragimova M.K., Tsyganov M.M., Slonimskaya E.M., Litvyakov N.V. // Bull. Sib. Med. 2020. V. 19. № 3. P. 22–28.
69. Gong W.-J., Yin J.-Y., Li X.-P., Fang C., Xiao D., Zhang W., Zhou H.-H., Li X., Liu Z.-Q. // Tumor Biol. 2016. V. 37. № 6. P. 8349–8358.
70. Tian X., Xu G. // BMJ. 2015. V. 5. № 9. P. 1–11.
71. Wang Y., Zhang Y., Hu K., Qiu J., Hu Y., Zhou M., Zhang S. // Biosci. Rep. 2020. V. 40. № 8. P. 1–11.
72. Elbasateeny S.S., Yassin M.A., Mokhtar M.M., Ismail A.M., Ebian H.F., Hussein S., Shazly S.A., Abdelwabab M.M. // Internat. J. Breast Cancer. 2022. V. 2022. № 1. P. 1–13.
73. Wang Y., Xue D., Li Y., Pan X., Zhang X., Kuang B., Zhou M., Li X., Xiong W., Li G. // J. Cancer. 2016. V. 7. № 8. P. 991–1001.
74. Wang R., Sun Y., Li L., Niu Y., Lin W., Lin C., Antonarakis E.S., Luo J., Yeh S., Chang C. // Eur. Urol. 2017. V. 72. № 5. P. 835–844.

Relationship between the Gene Expression of Adenosine Kinase Isoforms and the Expression of CD39 and CD73 Ectonucleotidases in Colorectal Cancer

G. A. Zhulai[1*], M. I. Shibaev[2]
[1]Institute of Biology, Karelian Research Centre, Russian Academy of Sciences, Petrozavodsk, 185910 Russian Federation
[2]Endoscopic Department, Baranov Republican Hospital, Petrozavodsk, 185910 Russian Federation
*Email: zhgali-111@yandex.ru
Received: December 07, 2022; in final form, April 03, 2023
DOI: 10.32607/actanaturae.11871

ABSTRACT **Tumor cells have the capacity to create an adenosine-rich immunosuppressive environment, which can interfere with antitumor immunotherapy. Approaches are currently being developed with a view to suppressing the production of adenosine or its signals. Such approaches include the use of antibodies to inhibit CD39, CD73, and adenosine-receptor antagonists. However, the abundance of enzymatic pathways that control the ATP-adenosine balance, as well as the still poorly understood intracellular adenosine regulation, makes the hoped-for success unlikely. In the present study, the enzyme adenosine kinase (ADK) needed to convert adenosine to adenosine monophosphate, thereby regulating its levels, was investigated. To do so, peripheral blood samples from patients with colorectal cancer (CRC) (n = 31) were collected with blood samples from healthy donors (n = 17) used as controls. ADK gene expression levels and those of its long (*ADK-L*) and short (*ADK-S*) isoforms were measured. The relationship between the levels of *ADK* gene expression and that of *CD39*, *CD73*, and *A2aR* genes was analyzed. It turned out that in the group of CRC patients (stages III-IV), the level of *ADK-L* mRNA was lower ($p < 0.0011$) when compared to that of the control. For the first time, an average correlation was found between the level of expression of *CD39* and *ADK-S* (r = -0.468 at p = 0.043) and between *CD73* and *ADK-L* (r = 0.518 at p = 0.0232) in CRC patients. Flow cytometry was used to assess the content of CD39/CD73-expressing $CD8^+$, $CD4^+$ and Treg lymphocytes, as well as their relationship with the level of ADK gene expression in CRC patients. But no significant correlations were found.**
KEYWORDS **adenosine kinase, ADK-S, ADK-L, CD39, CD73, $CD8^+$ T cells, $CD4^+$ T cells, Treg cells, colorectal cancer.**
ABBREVIATIONS **ADK – adenosine kinase; ADK-L – long isoform of ADK; ADK-S – short isoform of ADK; CD39 – ecto-nucleoside triphosphate diphosphohydrolase, ENTPD1; CD73 – ecto-5'-nucleotidase, 5'NT; A2aR – adenosine receptor A2a; CRC – colorectal cancer.**

INTRODUCTION

The role of extracellular adenosine in the tumor microenvironment has been sufficiently researched [1]. Adenosine can regulate the innate and adaptive immune responses [2] by inhibiting the activity of the effector component and stimulating the immunosuppressive component. Thus, extracellular adenosine acts as a barrier for antitumor immunotherapy. The therapeutic potential of enzyme blockade, specifically that of the ectonucleotidases CD39 (ectonucleoside triphosphate diphosphohydrolase, ENTPD1) and CD73 (ecto-5'-nucleotidase, 5'NT) involved in ATP breakdown to adenosine and inhibition of adenosine receptors (primarily A2a) was demonstrated in preclinical trials and is now being tested in oncological patients in clinical trials I/II [3]. However, the hoped-for efficacy, based on preclinical trials, is yet to be achieved [4].

Numerous pathways controlling the ATP-adenosine balance still remain understudied. Approaches to the blockade of the adenosine signaling pathway are usually developed with little attention paid to the intracellular adenosine regulation. Aside from the "classical" extracellular adenosine synthesis pathway from ATP by ectonucleotidases CD39-CD73, recent discus-

sions have tended to focus on the role of the alternative pathway involving extracellular nicotinamide adenine dinucleotide (NAD^+) in cancer progression [5]; so, a study into other adenosine metabolism components in developing tumors seems relevant.

The adenosine content is regulated by adenosine-converting enzymes; i.e., adenosine kinase (ADK) and adenosine deaminase [6, 7]. ADK adds a phosphoric acid residue to adenosine and converts it into AMP. Adenosine deaminase removes amino groups from adenosine molecules, with inosine as a by-product. On top of that, the adenosine level may be regulated by the way it is delivered to the extracellular space by bidirectional nucleotide transporters.

Of special interest here is adenosine kinase regulating the availability of adenosine while also being involved in complex homeostatic and metabolic networks [8]. The balance between adenosine and ADK is strictly maintained in healthy cells, while changes in enzyme expression lead to various degrees of activation of adenosine receptors, which often determines the role of ADK in the development of the pathology [9]. Apart from purine metabolism, ADK is also involved in the regulation of transmethylation. A relationship between ADK expression and DNA methylation has also been demonstrated. The use of specific ADK inhibitors may reduce the global DNA methylation level in HeLa cells in a dose-dependent fashion [10]. Human ADK is represented by two isoforms with different molecular masses and, presumably, functions. The short isoform ADK-S localized in the cytoplasm ensures routine metabolic removal of adenosine under normal conditions by means of its phosphorylation into AMP. The key function of ADK-S is to regulate the level of extracellular tissue adenosine. The long isoform ADK-L localized in nuclei has a direct biochemical link to S-adenosylmethionine-dependent transmethylation pathway-controlling DNA and histone methylation. High levels and degree of activity of ADK-L are associated with increased global DNA methylation [1].

The role of ADK in carcinogenesis is poorly studied. The available data [10–15] suggests that there is a potential role for ADK in the development of colorectal cancer (CRC) [14], as well as breast [15] and liver cancer [12]. Other evidence of possible ADK involvement in tumor development includes the relationship between ADK and angiogenic activity and cellular proliferation during ontogenesis, as well as the changes in ADK expression in tumor tissue and its association with epigenetic regulation [8].

CRC is a common malignant disease and a major cause of cancer-related deaths. The adenosinergic pathway closely related to adaptive immunity suppression plays a significant part in CRC pathogenesis [16]. However, the relationship between ADK and immune mechanisms in CRC has not been properly studied. Given that, the goal of the present paper was to study the mRNA levels in *ADK, ADK-L*, and *ADK-S* and their relationship to the contents of CD39/CD73-expressing T cells in the peripheral blood of CRC patients.

EXPERIMENT

The test material included vein blood samples collected into tubes with K3EDTA. In the present study, 31 blood samples from patients with colon adenocarcinoma 65 ± 12.4 years were analyzed. All patients were diagnosed through clinical investigations with histological confirmation. Their clinical characteristics are presented in *Table 1*. The inclusion criteria were age of over 18 and large colon cancer as a confirmed diagnosis. The exclusion criteria were neoadjuvant therapy administration and reports of autoimmune and inflammatory diseases in the recent three months. We also analyzed 17 blood samples from healthy donors of comparable age (56.10 ± 17.70) as the controls. The study was carried out in compliance with the requirements of the Declaration of Helsinki and approved by the Medical Ethics Committee of the Ministry of Healthcare and Social Development of the Republic of Karelia and Petrozavodsk State University (protocol No. 25 dated February 12, 2013). All participants gave their informed consent in writing prior to inclusion in the study.

Table 1. Patient characteristics

Parameter		CRC patients	Healthy donors
Sample size		31	17
Sex	M	11 (35.5%)	6 (35.3%)
	F	20 (64.5%)	11 (64.7%)
Median age (min–max)		65.0 (45–78)	55.0 (28–79)
CRC stage	1–2	16 (51.6%)	–
	3–4	15 (48.3%)	
Tumor grade	G1	3 (9.7%)	–
	G2	23 (74.2%)	
	G3	5 (16.1%)	

Table 2. The nucleotide sequences of the primers used in this study

Gene	Primer ' → 3'	
	Forward	Reverse
ADK	TTACTACGAGCAGAATGAGCAG	TGGCAGCAGCAAGATTAGC
ADK-L	TGTAGAGCCAAAGTGGGGTG	GCCTCCACCTTCAGCTTTTTG
ADK-S	AAGCAGTTGCTGTGGTACCTG	AGCAGAGGATTTCCCATTCCA
A2AR	CTTGGGTTCTGAGGAAGCAG	CAGCAGCTCCTGAACCCTAG
CD39	AGCAGCTGAAATATGCTGGC	GAGACAGTATCTGCCGAAGTCC
CD73	ATTGCAAAGTGGTTCAAAGTCA	ACACTTGGCCAGTAAAATAGGG
GAPDH	GGTGGTCTCCTCTGACTTCAACAG	GTTGCTGTAGCCAAATTCGTTGT

Gene expression analysis

The total RNA was isolated from the blood using TRIzol LS reagent (ThermoFisher Scientific, the United States), DNA contamination was removed, and the samples were treated with DNase I (Lucigen, the United States). The quantity and quality of the obtained RNA was assessed using SmartSpec Plus spectrophotometer (Bio-Rad, the United States). Synthesis of cDNA was performed using random hexaprimers and reverse transcriptase MMLV (Evrogen, Russia). Amplification of the cDNA and analysis of the amplification products with real-time PCR was run using the master mix with a SYBR Green I intercalating dye (Evrogen, Russia), in accordance with the manufacturer's manual on the iCycler amplifier with an iQ5 optical system (Bio-Rad, the United States), in duplicates with no template control. Expression of the genes of interest was normalized to the expression of the reference gene *GAPDH*. The primers used for the expression assessment of the genes *ADK, ADK-L, ADK-S, A2AR, CD39*, and *CD73* (Syntol, Russia) are presented in *Table 2*. The optimal annealing temperature was determined by temperature gradient setup. The protocol for *ADK, ADK-L,* and *ADK-S* was as follows: cDNA denaturation for 5 min, at 95°C; 40 cycles: denaturation at 95°C, 30 s; annealing at 61°C, 30 s; elongation at 72°C, 30 s. The protocol for *A2AR, CD39*, and *CD73* was as follows: cDNA denaturation for 5 min, at 95°C; 40 cycles: denaturation at 95°C, 30 s; annealing at 64°C, 30 s; elongation at 72°C, 30 s. PCR specificity was controlled by analyzing melting curves. Relative gene expression levels were calculated using the $2^{-\Delta\Delta Ct}$ method, where Ct is the threshold cycle and ΔCt is the difference between the threshold cycle values for the reference and target genes. The total gene expression level was calculated with respect to the control (healthy donors), with the expression level of each gene of interest in the control taken as 1. The data are presented in per-unit notation and calculated as the mean value ± standard error (M ± SE).

Flow cytometry

The whole blood samples were stained with antibodies and incubated for 20 min at room temperature in the dark in accordance with the manufacturer's protocol. RBCs were lysed by BD FACS Lysing Solution (BD Biosciences, the United States). In the present study, the following monoclonal antibodies were used: CD3-PC5 (UCHT1 clone), CD4-FITC (OKT4 clone), CD4-PC7 (OKT4 clone), CD8-PC7 (RPA-T8 clone), CD25-PC5 (BC96 clone), CD127-PC7 (EBIORDR5 clone), CD73-PE (AD2 clone), CD39-PE (EBIOA1 clone), CD39-FITC (EBIOA1 clone) (eBioscience, the United States), as well as the respective isotype controls. All events were acquired using a Cytomics FC500 cytometer (Beckman Coulter, the United States). At least 30,000 events per sample were analyzed in the lymphocyte gate based on forward and side scatter. The data were presented as M ± SD.

Statistical analysis

The statistical processing and parameter calculation were performed using the GraphPad Prism v.7 software. The significance of the differences between the quantitative parameters was calculated using the nonparametric Mann–Whitney test. The differences were considered significant at $p < 0.05$. The correlation between parameters was estimated using Spearman's test.

RESULTS

Expression level of adenosine kinase mRNA in the peripheral blood in CRC patients

The data on ADK gene expression in CRC tissue are available in the literature [14], but it is yet to be stud-

ied how the ADK gene and its isoforms are expressed in the peripheral blood of CRC patients and how it is related to the clinical signs of the disease. We have estimated the relative content of mRNA of the *ADK* gene and its isoforms in the peripheral blood of CRC patients. The comparison of CRC patients with healthy donors showed a reduced *ADK-L* mRNA level ($p = 0.002$) in CRC. No differences from the control group were observed in the mRNA contents for the *ADK* gene and *ADK-S* isoform. Blood samples from patients with CRC stages III–IV showed reduced *ADK-L* mRNA levels ($p < 0.001$) as compared to healthy donors (*Fig. 1*). Meanwhile, no significant differences were observed in *ADK-L* mRNA levels between patients at early stages (I–II) and the control group. Finally, mRNA contents for the *ADK* gene and *ADK-S* isoform in the blood samples of CRC patients at both early and late stages were close to those in healthy donors.

In this study, the relationship between the mRNA levels of the gene of interest and the clinical signs of the disease was analyzed. A moderate negative correlation was established between the *ADK-L* mRNA content and tumor size (T2–T4), with a value of 0.508 at $p = 0.038$. However, no significant correlation was found between the *ADK-L* mRNA level and the disease stage. The differences in the *ADK* mRNA levels in CRC patients with and without distant metastases (M0–M1) or metastases to regional lymph nodes (N0–N2) were not statistically significant.

The extracellular adenosine level is regulated by the enzyme network, with the CD39 and CD73 ectonucleotidases playing a major part in carcinogenesis [17]. It has been demonstrated that the peripheral blood of CRC patients shows an increased *CD39* mRNA level, whereas the *CD73* mRNA level remains the same as that in healthy donors [18]. We have analyzed the relationship between the relative expression of the genes *CD39, CD73*, and *A2AR* and the expression of the *ADK* gene and its isoforms in the peripheral blood of CRC patients. This has yielded new data on a correlation between gene expression levels: a negative correlation appears to exist between the *ADK-S* and *CD39* mRNA levels. A positive correlation was identified between the *ADK-L* and *CD73* mRNA levels (*Table 3*).

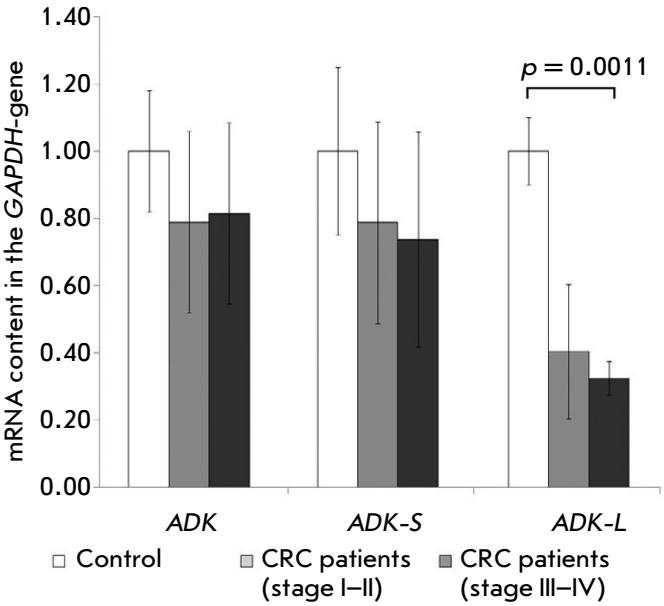

Fig. 1. Changes in the relative level of mRNA of the *ADK*, *ADK-S*, *ADK-L* genes in the peripheral blood leukocytes of CRC patients if compared to healthy donors. The relative level of control mRNA was taken as 1. The normalization was performed according to *GAPDH*-gene mRNA

Table 3. Correlation coefficient values between mRNA levels for the *ADK* gene and its isoforms *ADK-S* and *ADK-L* and mRNA levels for the *CD39*, *CD73*, and *A2AR* genes in CRC patients

mRNA level	*ADK*		*ADK-S*		*ADK-L*	
	r_s	p	r_s	p	r_s	p
A2AR	-0.284	0.21	0.02	0.9346	0.406	0.0843
CD39	-0.038	0.097	**-0.468**	**0.043**	-0.329	0.168
CD73	-0.033	0.889	-0.16	0.511	**0.518**	**0.0232**

Note. Statistically significant parameters are highlighted in bold.

Relationship between the *ADK* gene expression level and CD39$^+$/CD73$^+$ T cell content

The established relationship between the mRNA levels for the ADK and CD39/CD73 ectonucleotidases in the peripheral blood implies that there is a relationship between ADK and CD39/CD73 expressing immune cells. The balance between CD8$^+$ and CD4$^+$ effector T cells and immunosuppressive regulatory T cells (Treg) is the key parameter of the antitumor immune response. Similarly to many other cells, these lymphocytes are sensitive to the adenosine effect primarily mediated by the A2aR adenosine receptor and may be involved in adenosine production through the expression of the CD39 and/or CD73 on their surfaces [3]. To probe for a relationship between the *ADK* expression level and the number of T cells involved in adenosine generation, the relative contents

of $CD39^+/CD73^+$ effector T cells ($CD4^+$ T helpers and $CD8^+$ cytotoxic cells) and suppressive Treg cells were analyzed in CRC patients (n = 20) and healthy donors (n = 17) (*Fig. 2*).

CD39-positive cells prevailed in Treg cells in both healthy donors and CRC patients, whereas CD73 expression was more characteristic of $CD8^+$ T cells (*Fig. 3*). The same observations have been made by other authors [19]. Since the population of $CD4^+$ effector T cells includes 3–5% of Treg cells characterized by increased CD25 expression, the $CD4^+CD25^{-/int}$ phenotype was analyzed to exclude the contribution of Treg cells to CD39/CD73 expression by T helpers.

It was discovered that about 64% of all Treg cells in the blood of CRC patients were $CD39^+$, which was at significant variance with the Treg cell frequency in the blood of healthy donors (p = 0.0008), where $CD39^+$ cells only accounted for 42% of all Treg cells. Significant differences were also observed for $CD4^+CD39^+$ T helpers (p = 0.037). The population of $CD8^+$ T cells in CRC patients showed a reduced frequency of CD73-positive cells (p = 0.024). The frequency of $CD73^+$ Treg cells, $CD73^+CD4^+$ T cells, and $CD39^+CD8^+$ T cells in CRC patients was no different from the control.

To estimate the correlation between ADK and the $CD39^+/CD73^+$ T cell frequency, we analyzed the possible relationships between the mRNA levels for *ADK* the gene and its isoforms *ADK-L* and *ADK-S* and the frequency of CD39/CD73-expressing T cells in the peripheral blood of CRC patients: no statistically significant correlations were found (*Table 4*).

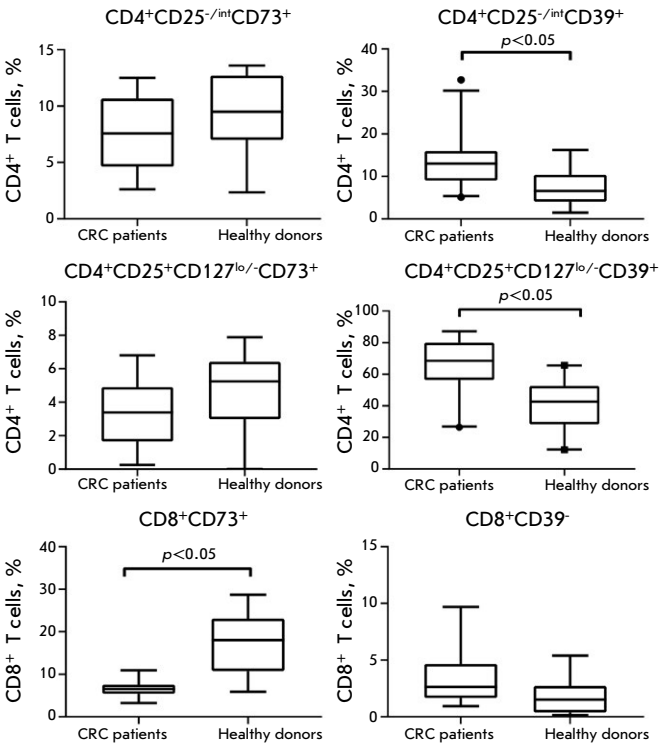

Fig. 2. $CD39^+$ and $CD73^+$ T cells frequency in the peripheral blood samples of CRC patients and healthy donors

DISCUSSION

The adenosinergic pathway has gained in interest as a promising target for antitumor therapy. The key actors in this pathway – CD39/CD73/A2aR – show increased expression levels and activity in tumor tissue and are often associated with clinical signs of the disease and unfavorable prognosis in some cancer types [17]. Clinical trials produced a preliminary optimal safety profile for the A2aR and CD73 blockers and showed an increased overall response rate to them [4, 20]. Nevertheless, the positive results achieved through both monotherapy and combination therapy fell mostly below the expectations engendered by the pre-clinical trials. This is an indication that we need a

Table 4. Correlation coefficient values between mRNA levels for the *ADK* gene and its isoforms *ADK-S* and *ADK-L* and relative contents of $CD39^+$ and $CD73^+$ T cells in the blood of CRC patients

T cells	*ADK*		*ADK-S*		*ADK-L*	
	r_s	p	r_s	p	r_s	P
$CD8^+CD73^+$	0.107	0.840	0.178	0.713	-0.036	0.951
$CD8^+$ $CD39^+$	0.033	0.948	-0.217	0.581	0.126	0.295
$CD4^+CD25^{-/int}CD73^+$	-0.217	0.581	-0.300	0.437	0.393	0.295
$CD4^+CD25^{-/int}CD39^+$	-0.021	0.929	0.255	0.278	0.002	0.995
$CD4^+CD25^+CD127^{lo/-}CD73^+$	-0.381	0.359	-0.381	0.360	0.256	0.549
$CD4^+CD25^+CD127^{lo/-}CD39^+$	0.051	0.827	0.278	0.235	-0.151	0.522

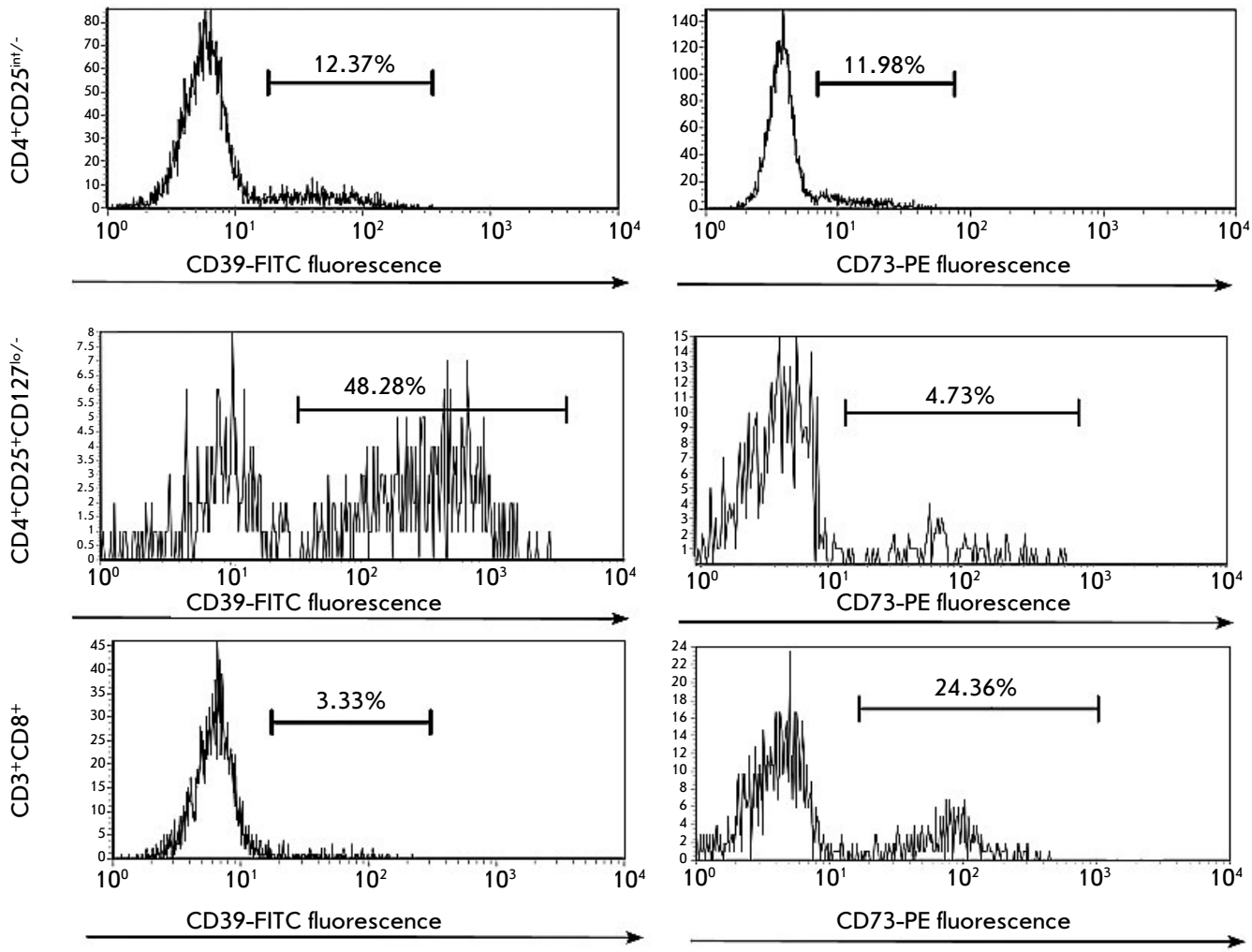

Fig. 3. An example of CD39 and CD73 expression distribution histograms on the surface of $CD8^+$ and $CD4^+$ T cells in a healthy donor. The X-axis shows the fluorescence intensity of FITC and PE fluorochromes conjugated with antibodies against CD39 and CD73, respectively. The Y-axis shows the number of events in the lymphocyte gates. On the right, under the horizontal line, the cells expressing CD39/CD73 are marked; on the left are cells that are negative for CD39/CD73 expression

more refined patient selection process or need to use biomarkers to better predict and optimize therapy results [4, 20].

The ADK enzyme regulates the adenosine level by converting it into AMP. We currently lack a clear understanding of the role of ADK in tumor development. Earlier papers show increased *ADK* gene expression levels [14] and enzymatic activity [21] in tumor tissue of CRC patients compared to healthy tissue. On the other hand, liver cancer patients show lower ADK protein levels compared to healthy tissue. In addition, a decrease in the ADK level in the liver resulted in higher sensitivity to the acute toxic effects of the carcinogen (diethylnitrosamine) in the experimental model [12]. Inhibition of tumor cell proliferation and induction of apoptosis after ADK inhibitor treatment, particularly in the colorectal cancer cell line HT-29, have been described in a series of experimental papers [22]. Information on the role of ADK isoforms in carcinogenesis is rather scarce. For instance, Shamloo et al. [15] have pointed to a more significant role for the long ADK isoform in breast cancer. The events caused by the respective gene knockdown point toward an involvement of this isoform in mitogenesis, carcinogenesis, and tumor cell invasion. ADK expression in peripheral blood and the relationship between ADK and the activation of the key lymphocyte populations associated with the antitumor immune response ($CD8^+$/$CD4^+$ T cells and Treg cells) in CRC patients remains poorly studied.

The results obtained in the present study confirm the changes in *ADK* expression in CRC pathogenesis. According to the published data, tumor tissue shows a local increase in ADK activation, possibly due to adenosine accumulation in the tumor microenvironment and its active metabolism. On the other hand, a decrease in the *ADK-L* mRNA level was observed in the peripheral blood in the group of patients with CRC stage III–IV compared with healthy donors, an inverse relationship was uncovered between the *ADK-L* mRNA levels in cancer patients with tumor extent T2–T4, and the *ADK-S* levels remained unchanged when compared to the controls.

It has been established that some leukocytes populations express CD39/CD73 ectonucleotidases and may be involved in adenosine generation [23], which may lead to immune suppression and tumor growth, particularly in CRC [3, 24]. In this study, we have discovered significant correlations between *CD39* and the *ADK-S* mRNA levels in the peripheral blood (r = -0.468 at p = 0.043), as well as *CD73* and the *ADK-L* mRNA levels (r = 0.518 at p = 0.0232) in CRC patients. Apart from that, no correlation has been found between the expression level of the *ADK* gene and its isoforms and the changes in the expression levels of the gene coding for the A2aA adenosine receptor, whose activation on lymphocytes boosts immune suppression.

In this paper, for the first time, the relationship between the frequency of the key effector and suppressive lymphocyte populations expressing CD39/CD73 on their surfaces and the changes in the *ADK* expression levels in CRC patients has been analyzed. The analysis of $CD4^+$ and $CD8^+$ T cells, as well as Treg cell, frequency in the peripheral blood showed that the changes in the $CD39^+$ T cell frequency were most significant in CRC (*Table 3*). For the first time, we have analyzed the relationship between the $CD39^+$ and $CD73^+$ T cell frequency and mRNA levels for the *ADK* gene and its isoforms in the peripheral blood of CRC patients: No significant correlations were found.

It is currently recognized as a fact that not only T cells can carry CD39 and CD73 ectonucleotidases on their surfaces, but also neutrophils, which are the most common leukocytes in the peripheral blood, B cells, monocytes, and endothelial cells [22, 25]. In this study, RNA for expression analysis was isolated from the whole blood. It is possible that identification of a relationship between the parameters of interest will require a more in-depth assessment with the use of a mononuclear cell fraction (lymphocytes and monocytes) as test material for gene expression analysis and increased sample size.

CONCLUSIONS

The data obtained in this study and available in the literature show changes in the ADK expression levels in CRC pathogenesis. The relationship between the expression of long and short *ADK* isoforms and the expression of the *CD39/CD73* ectonucleotidases involved in extracellular adenosine generation has been determined. It is indicated that the *ADK-L* mRNA level shows promise as a CRC biomarker. However, no correlation between the expression levels of the *ADK* gene and its isoforms *ADK-L* and *ADK-S* and the contents of CD39/CD73-expressing T cells in the peripheral blood of CRC patients has been found. ●

This research was supported by the Russian Science Foundation (project No. 21-75-00013).

REFERENCES

1. Boison D., Yegutkin G.G. // Cancer Cell. 2019. V. 36. № 6. P. 582–596.
2. Sek K., Mølck C., Stewart G., Kats L., Darcy P., Beavis P. // IJMS. 2018. V. 19. № 12. P. 3837.
3. Churov A., Zhulai G. // Human Immunol. 2021. V. 82. № 4. P. 270–278.
4. Thompson E.A., Powell J.D. // Annu. Rev. Med. 2021. V. 72. № 1. P. 331–348.
5. Horenstein A.L., Chillemi A., Zaccarello G., Bruzzone S., Quarona V., Zito A., Serra S., Malavasi F. // OncoImmunology. 2013. V. 2. № 9. P. e26246.
6. Park J., Gupta R.S. // Cell. Mol. Life Sci. 2008. V. 65. № 18. P. 2875–2896.
7. Bagheri S., Saboury A.A., Haertlé T. // Internat. J. Biol. Macromolecules. 2019. V. 141. P. 1246–1257.
8. Zhulai G., Oleinik E., Shibaev M., Ignatev K. // Biomolecules. 2022. V. 12. № 3. P. 418.
9. Boison D. // Pharmacol. Rev. 2013. V. 65. № 3. P. 906–943.
10. Wahba A.E., Fedele D., Gebril H., AlHarfoush E., Toti K.S., Jacobson K.A., Boison D. // ACS Pharmacol. Transl. Sci. 2021. V. 4. № 2. P. 680–686.
11. Xu Y., Wang Y., Yan S., Zhou Y., Yang Q., Pan Y., Zeng X., An X., et al. // EMBO Mol. Med. 2017. V. 9. № 9. P. 1263–1278.
12. El-Kharrag R., Owen R., Boison D. // J. Caffeine Adenosine Res. 2019. V. 9. № 1. P. 4–11.
13. Huang J., He Y., Chen M., Du J., Li G., Li S., Liu W., Long X. // Mol. Med. Repts. 2015. V. 12. № 5. P. 6509–6516.
14. Giglioni S., Leoncini R., Aceto E., Chessa A., Civitelli S., Bernini A., Tanzini G., Carraro F., Pucci A., Vannoni D. // Nucleosides. Nucleotides Nucl. Acids. 2008. V. 27. № 6–7. P. 750–754.
15. Shamloo B., Kumar N., Owen R.H., Reemmer J., Ost J., Perkins R.S., Shen H. // Oncotarget. 2019. V. 10. № 68. P. 7238–7250.
16. Hajizadeh F., Masjedi A., Heydarzedeh Asl. S., Karoon Kiani F., Peydaveisi M., Ghalamfarsa G., Jadidi-Niaragh

F., Sevbitov A. // Internat. Immunopharmacol. 2020. V. 87. P. 106853.
17. Baghbani E., Noorolyai S., Shanehbandi D., Mokhtarzadeh A., Aghebati-Maleki L., Shahgoli V.K., Brunetti O., Rahmani S., Shadbad M., Baghbanzadeh M., et al. // Life Sci. 2021. V. 282. P. 119826.
18. Zhulai G.A., Oleinik E.K., Churov A.V., Romanov A.A., Kravchenko (Semakova) P.N., Oleinik V.M. // Med immunol. 2017. V. 19 № 1. P. 89–94.
19. Golovkin A.S., Serebryakova M.K., Zhiduleva E.V., Murtazalieva P.M., Titov V.A., Irtuga O.B., Moiseeva O.M., Krobinec I.I., Kudryavtsev I.V. // Transl med. 2017. V. 4. № 5. P. 46–60.
20. Willingham S.B., Hotson A.N., Miller R.A. // Curr. Opin. Pharmacol. 2020. V. 53. P. 126–133.
21. Vannoni D., Bernini A., Carlucci F., Civitelli S., Di Pietro M.C., Leoncini R., Rosi F., Tabucchi A., Tanzini G., Marinello E. // Med. Oncol. 2004. V. 21. № 2. P. 187–195.
22. Luo H.Y., Shen H.Y., Perkins R.S., Wang Y.X. // Front. Pharmacol. 2022. V. 13. P. 908882.
23. Antonioli L., Pacher P., Vizi E.S., Haskó G. // Trends Mol. Med. 2013. V. 19. № 6. P. 355–367.
24. Wu X.R., He X.S., Chen Y.F., Yuan R.X., Zeng Y., Lian L., Zou Y., Lan N., Wu X., Lan P. // J. Surg. Oncol. 2012. V. 106. № 2. P. 130–137.
25. Pulte E.D., Broekman M.J., Olson K.E., Drosopoulos J.H.F., Kizer J.R., Islam N., Marcus A.J. // Thrombosis Res. 2007. V. 121. № 3. P. 309–317.

mmp-9 mRNA Expression and Bridging Fibrosis Progression in Toxic Liver Injury

E. I. Lebedeva[1*], A. S. Babenka[2], A. T. Shchastniy[1]
[1]Vitebsk State Order of Peoples' Friendship Medical University, Vitebsk, 210009 Republic of Belarus
[2]Belarussian State Medical University, Minsk, 220116 Republic of Belarus
[*]E-mail: lebedeva.ya-elenale2013@yandex.ru
Received: March 22, 2023; in final form, May 30, 2023
DOI: 10.32607/actanaturae.17856

ABSTRACT **Developing liver disease treatments, in which fibrosis is a key pathogenetic link, still remains an urgent problem in hepatology. In the present study, the level of *mmp-9* mRNA expression and the number of FAP$^+$, α-SMA$^+$, CD45$^+$ cells were analyzed at nine time points of fibrosis and cirrhosis. It was found that in the case of liver fibrosis, the choice of the optimal reference gene depended on the stage of fibrogenesis. When studying the specific stages rather than the entire process in a long-term experiment, it was shown that choosing an optimal reference gene has to be done additionally. In this case, the *mmp-9* mRNA expression level should be considered as a marker of liver fibrosis initiation and development but not as that of cirrhosis progression. In the liver, two morphologically heterogeneous populations of myofibroblasts were simultaneously identified as able to synthesize various types of immunohistochemical markers. It was found that the FAP+ cells were the main contributor to the development of portal fibrosis and the initial stages of bridging fibrosis. In the selected experimental model, fibrosis initiation and the development stages preceding parenchyma restructuring were accompanied by a low level of inflammation.**
KEYWORDS **rats, liver, *mmp-9* mRNA, immunohistochemistry, FAP$^+$, α-SMA$^+$, CD45$^+$ cells.**
ABBREVIATIONS **HSCs – stellate cells; PFs – portal fibroblasts; TAA – thioacetamide; RT-PCR – real-time polymerase chain reaction.**

INTRODUCTION

The MMP-9 protein, also known as type IV collagenase (gelatinase B), belongs to a large family of matrix zinc-dependent proteinases (MMPs). Almost all members of this family play an important role in liver regeneration and in the control over the number of extracellular matrix proteins. They also participate in fibrosis, cirrhosis, carcinogenesis, and other processes [1]. Many years of studying the molecular mechanisms of liver fibrosis development have made it clear that the MMP-2 and MMP-9 proteins are involved in this pathological process at almost all stages and perform a key function in its progression [2, 3]. At the same time, the number of MMPs in blood plasma is a marker of fibrosis and some therapeutic approaches are aimed at MMP-9 as a specific target [4–7].

Some researchers have noted an increase in the expression of the MMP-9 protein and corresponding mRNA in the presence of progressing liver fibrosis, while the etiological factors causing fibrosis are not that important. An increase in MMP-9 expression has been observed in toxic damage to the liver, as well as in the presence of viral hepatitis [8, 9]. As fibrosis develops, an increase in the specific amount of connective tissue occurs and, in some cases, a correlation between this process with an increase in the level of *mmp-9* mRNA has been reported. In normal conditions, it is metalloproteinase that stands responsible for the degradation of connective tissue, collagen renewal, and maintenance of the optimal level of extracellular matrix proteins [10, 11]. However, the relationship between an increased level of *mmp-9* mRNA and the progression of liver fibrosis has yet to be studied [1–3]. In addition, existing experimental animal models have been designed to investigate specific key positions that are rather far apart from each other (norm, fibrosis and cirrhosis, or fibrogenesis) and they are usually studied within a relatively short time period. These limitations may cause the models to miss the important details relative to *mmp-9* level dynamics [8–11].

Stellate cells (HSCs) are considered to be the main cell population synthesizing the intercellular substance in liver pathologies. In the scientific litera-

ture, they are known under different names, such as fat-accumulating cells, lipocytes, perisinusoid cells, hepatic stellate cells, Ito cells, and pericytes [12–15]. Under physiological conditions, HSCs are localized in the perisinusoidal space; they regulate the blood flow in the sinusoids, functioning as pericytes, and possess low proliferative capacity and the ability to secrete collagens [13, 15]. Liver lesions of predominantly viral and toxic etiology stimulate HSC activation and transdifferentiation into a myofibroblastic phenotype, with an overexpression of α-SMA [12, 14–16]. The activation and transdifferentiation processes are not yet fully understood, which is why an effective antifibrotic therapy has not yet been developed. The source of resting and activated HSCs has also not been established yet. Their pool is assumed to be replenished by bone marrow cells, but it cannot be ruled out that this is a self-sustaining cell population [12, 16–18].

These are resident portal fibroblasts (PFs) that are considered to be the source of myofibroblasts in cholestatic liver diseases [13], but their role in the development of cholestatic fibrosis remains debatable. In the studies using Col-GFP and Mdr2$^{-/-}$mice, PFs served as the source of myofibroblasts at the initial stages of cholestatic fibrogenesis, whose further progression led to HSC transdifferentiation into a fibrogenic phenotype [16]. Other authors note that cholestatic fibrosis is accompanied by simultaneous PF and HSC activation [16–18].

For the purposes of this study, we had hypothesized that the increase in the level of *mmp-9* mRNA might be associated with the rate of connective tissue formation in fibrogenesis; so, the objective of our investigation was to probe for new data on the level of *mmp-9* mRNA expression and fibrogenic cell population at different stages of toxic liver fibrosis.

EXPERIMENT

The design of the experiment was approved at a meeting of the Commission on Bioethics and Humane Treatment of Laboratory Animals of Vitebsk State Order of Peoples' Friendship Medical University (Minutes No. 6 of 01/03/2019) and involved mature male Wistar rats weighing 190–210 g. Liver fibrosis and cirrhosis were modeled by chronic intoxication with thioacetamide (TAA; Acros Organics). A freshly prepared TAA solution was administered intragastrically through a tube at a dose of 200 mg/kg of body weight twice a week for 17 weeks. The rats comprising the control group (n = 12) received TAA-free water in the same volume. The animals were randomized into 8 groups (n = 12 in each) depending on TAA exposure duration: 3 weeks (Group 1), 5 weeks (Group 2), 7 weeks (Group 3), 9 weeks (Group 4), 11 weeks (Group 5), 13 weeks (Group 6), 15 weeks (Group 7), and 17 weeks (Group 8).

Applied histological and morphometric methods

After guillotine decapitation under short-term ether anesthesia, samples of 5–10 mm in diameter were taken from the large left lobe of rat liver to be fixed for 24 h in a 10% neutral formalin phosphate buffer solution (Biovitrum, Russia). The fixed material was embedded in paraffin using an STP-120 spin tissue processor (Thermo Fisher Scientific, Germany) and an EC350 modular paraffin embedding center (Thermo Fisher Scientific). From each animal, one preparation was obtained for each staining method and using an HM340E rotary microtome (MICROM, Laborgerate GmbH, Germany). An average of 3–4 sections with a thickness of 4 μM were prepared and placed on glass slides. To get the overview histological preparations, the liver sections were stained with hematoxylin and eosin; and to identify connective tissue, they were stained as per Mallory in an HMS70 staining machine (Thermo Fisher Scientific) [19].

Immunohistochemical study was performed on paraffin sections [20]. Such markers as rabbit polyclonal antibodies FAP (FAP-alpha, FAP prolyl endopeptidase, dilution 1 : 100) were applied for activated PFs; activated HSC - mouse monoclonal antibodies (alpha-SMA, ASTA2, dilution 1 : 1000) for α-SMA, and hematopoietic stem cells for rabbit polyclonal antibodies (CD45, dilution 1 : 200). The antibodies were manufactured by Wuman Elabscience Biotechnology Incorporated Company, catalog number E-AB-32870 (FAP), E-AB-22155 (α-SMA), E-AB-16319 (CD45). For investigation purposes, we also employed a 2-step Plus Poly-HRP Anti Rabbit/Mouse IgG Detection System with the DAB Solution kit; Retrieve-All Antigen (Unmasking System Basic), Antibody Dilution Buffer (BioLegend), Tween-20 (Glentham Life Sciences), and PBS (Melford). For better orientation in the preparation and correct identification of the cells containing the desired antigens, the sections were counterstained with Mayer's hematoxylin for 1 min. For an objective interpretation of the results for each group in the study, both positive and negative controls were utilized: immunohistochemical staining was assessed as positive only in the absence of staining in the negative control and, conversely, as negative when staining was detected in the positive control.

Morphometric analysis

Histological preparations were examined using the ImageScope Color and cellSens Standard software. The connective tissue area was determined as a percentage of the total section area [21]. The measure-

Table 1. Stages of liver fibrosis as scaled by K.G. Ishak

Scaled liver fibrosis stages	Morphological characteristics of fibrosis severity
F0	No fibrosis
F1	Fibrous enlargement of the portal zones with and without short fibrous septa
F2	Fibrous expansion of most portal zones with and without short fibrous septa
F3	Fibrous expansion of most portal zones with single bridging portoportal septa
F4	Fibrous expansion of most portal zones with pronounced bridging portoportal and portocentral septa
F5	Numerous bridge-like septa with single nodules (incomplete cirrhosis)
F6	Cirrhosis

ments were carried out using an OLYMPUS XC30 digital camera (Japan) based on an OLYMPUS BX51 microscope (Japan) of 20× magnification to take microphotographs of the random vision fields (at least 3 in each histological section) of the liver preparations. The number of FAP^+-positive cells (FAP^+ cells), α-SMA-positive cells (α-SMA^+ cells), and CD45-positive cells ($CD45^+$ cells) was counted in the three vision fields of each histological section at a 40× magnification. The degree of fibrosis was assessed using the semi-quantitative scale devised by K.G. Ishak (*Table 1*) [22, 23].

mmp-9-gene mRNA relative level estimation

To investigate *mmp-9* mRNA, the liver samples were placed in cryovials and then in liquid nitrogen for storage before the start of a total RNA isolation procedure. The total RNA fraction was isolated as per the manufacturer's instructions for the ArtRNA MiniSpin kit (ArtBioTech, Belarus). cDNA was synthesized using oligo(dT) primers and the ArtMMLV Total kit (ArtBioTech) according to the manufacturer's instructions. In each reaction, 200 ng of the total RNA fraction was used. Oligonucleotide primers and real-time polymerase chain reaction (RT-PCR) probes were selected using the free online application Primer3 v. 0.4.0 (http://bioinfo.ut.ee/primer3-0.4.0/). *Hes1, sdha,* and *hprt* were chosen as reference gene candidates. The oligonucleotide sequences are presented in *Table 2*.

Real-time PCR (RT-PCR) was performed using reagents manufactured by Primetech, Belarus. The final volume of the reaction mixture was 25 μl and contained all the necessary components in the following concentrations: 2 mM of magnesium chloride; 0.1 mM of a mixture of deoxynucleotide triphosphates; 500 nM of oligonucleotides, including a real-time PCR probe; and 1.25 units of thermostable Taq-DNA polymerase in the appropriate buffer solution. Thermal cycling included one 2-min cycle at 95°C followed by 40 5-second cycles at 95°C and a 45-second cycle at 60°C. FAM channel detection was performed after each cycle. To perform the PCR, the CFX96 Touch Real-Time PCR Detection System was

Table 2. Oligonucleotide primers and fluorescently labeled markers used in the study

Oligonucleotide	Nucleotide sequence, 5' → 3'	Marker, 5'	Marker, 3'
mmp-9F	CTACTCGAGCCGACGTCAC		
mmp-9R	AGAGTACTGCTTGCCCAGGA		
mmp-9P	GATGTGCGTCTTCCCCTTCG	FAM	BHQ1
hes1F	GAAAGATAGCTCCCGGCATT		
hes1R	CGGAGGTGCTTCACTGTCAT		
hes1P	CCAAGCTGGAGAAGGCAGACA	FAM	BHQ1
hprtF	GGACAGGACTGAAAGACTTGCT		
hprtR	ACAGAGGGCCACAATGTGAT		
hprtP	CATGAAGGAGATGGGAGGCC	FAM	BHQ1
sdhaF	CCCACAGGTATCTATGGTGCT		
sdhaR	TTGGCTGTTGATGAGAATGC		
sdhaP	CATCACAGAAGGGTGCCGTG	FAM	BHQ1

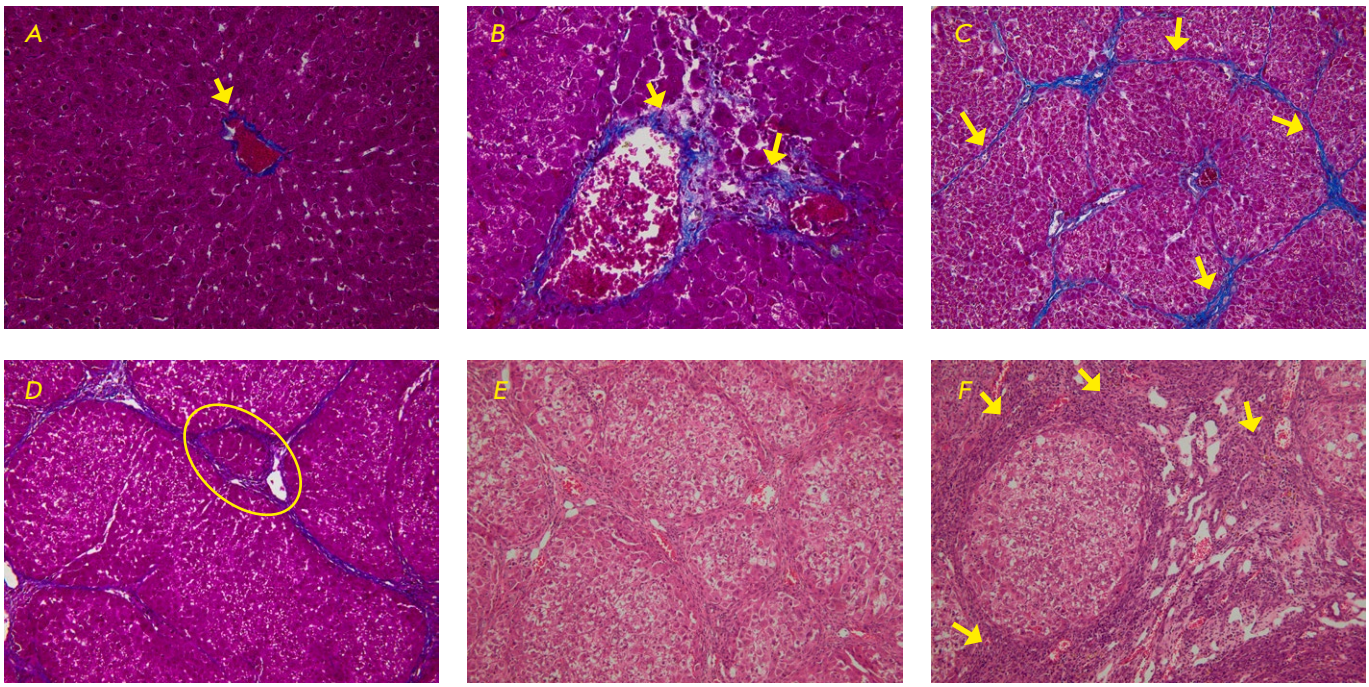

Fig. 1. Fragments of the liver of the control group rats: (*A*) at 3 weeks, (*B*) at 7 weeks, (*C*) at 9 weeks, (*D*) at 13 weeks, (*E*) at 17 weeks, (*F*) before the beginning of the experiment. Mallory staining ×40 (*A*, *B*); ×20 (*C*, *D*). Hematoxylin-eosin staining ×20 (*E*, *F*). (*A*) – a small amount of connective tissue in the central vein region (marked with an arrow); (*B*) – connective tissue in the portal zone (marked with arrows); (*C*) – connective tissue septa between portal zones (marked with arrows); (*D*) – neoformed false hepatic lobule (marked with an oval frame); (*E*) – neoformed false hepatic lobules; (*F*) – pronounced liver destruction with clearly visualized lymphoid-histiocytic infiltrate cells (marked with arrows)

employed (BioRad, USA). The efficiency of the reactions was determined using the standard curve method and series of dilutions of concentrated cDNA samples. RT-PCR of each sample was carried out in three repetitions. In each experimental and in the control group, each of the 12 samples was analyzed separately to achieve the highest reliability and account for the intragroup variation and phenotypic heterogeneity of the gene expression level.

Statistical analysis

The obtained results were processed in Statistica 10.0 (StatSoft, Inc.) and Microsoft Office Excel (Microsoft Corp.). For each sample, the normality of the frequency distribution of each feature was determined. Since the samples were not small ($n = 60>50$), the tests were carried out with application of the Lilliefors criterion. The data were presented as arithmetic means (M) and corresponding confidence intervals (95% CI), a median, and the 15th and 85th percentile values (Me (15%; 85%)). The level of statistical significance of the differences in the studied characteristics in the groups with normal data distribution was assessed using the Student's t-test; if the samples differed from the normal distribution, the Mann–Whitney U-test was used. For clarity, the results of the statistical analysis were presented as graphs of a one- and two-factor parametric variance analysis that was permissible to apply, since all groups had the same number of studied characteristics [24].

RESULTS

Pathological analysis of rat liver

In the animals of the intact group, a small amount of connective tissue was found around the interlobular vessels and bile ducts of the portal zones, as well as the central and collecting veins (F0, *Fig. 1A*). It is noteworthy that as liver fibrosis progressed, the rate of connective tissue growth varied (*Fig. 2*).

By the 3rd week into the experiment, a moderate formation of fibrous connective tissue was observed in the portal zones (F1, *Fig. 1B*). In the 5th week, the formation of fibrous tissue slowed down, but at the same time it was simultaneously detected both in the portal zones and in the parenchyma (bridging fibrosis, F2/F3). By the 7th week, the intensity of connective tissue synthesis remained almost at the same level as in the 5th one (F3/F4, *Fig. 1C*). At the stage of transition from fibrosis to cirrhosis, an increased formation of connective tissue similar to that in the 3rd week of the experiment was observed, again.

In nine weeks, in the portal zones, the formation of false hepatic lobules occurred, a morphological criterion for initial fibrosis to cirrhosis transition (F4/F5, *Fig. 1D*). In the period from the 11th to 17th week, connective-tissue proliferation reached its maximum value (F6, *Fig. 1E,F*).

In the liver of the intact animals, cells of the lymphoid-histiocytic infiltrate were practically absent, which was an indication of either extremely low inflammation severity or its complete absence. Contrary to popular belief that the inflammation level increases as fibrosis develops, by the 3rd week and then at the 5 and 7th weeks, we did not observe morphologically significant inflammation foci. That was the clue that, before the start of parenchyma restructuring, fibrosis initiation and development were accompanied in this toxic model by a low level of inflammation. Starting from the 9th week at the stage of active transition of fibrosis to cirrhosis, diffuse inflammation foci were observed in the connective tissue septa and the portal zones. By the 11th week (stage of incomplete cirrhosis), the level of inflammation was assessed as moderate; so, the number of lymphoid-histiocytic cells increased. From the 13 to 17th week at the stage of advanced cirrhosis, the level of inflammation rapidly increased, to be regarded as high (*Fig. 1E,F*).

Changes in the number of cells expressing FAP, α-SMA, and CD45 markers

The cells synthesizing the FAP$^+$ marker were absent in the livers of the intact animals (*Fig. 3A*). No α-SMA$^+$ cells were observed in the sinusoids (*Fig. 3B*), but in some cases they were detected in the walls of the interlobular arteries, as well as in the interlobular and sublobular veins. CD45$^+$ cells were almost never found in the lumens of the blood vessels and sinusoids; however, they were not visualized in the parenchyma, either (*Fig. 3C*).

Starting from week three, the number of cells bearing these markers increased, and the number of α-SMA$^+$-, CD45$^+$ cells began to exceed that of FAP$^+$-cells (*Fig. 4*). At the 5th week, the number of cells carrying the target markers increased while the gap between the FAP$^+$ and α-SMA$^+$ cells narrowed, and the increase in CD45$^+$ cells became minimal. Then, the situation with FAP$^+$- and α-SMA$^+$-cells repeated itself in the 7th and 9th weeks. In the 7th week, the increase in the number of α-SMA$^+$ cells, in percentage terms, was more pronounced, while in the 9th week the gap between the number of FAP$^+$ and α-SMA$^+$ cells had narrowed again. The number of CD45$^+$ cells grew as well, but, as fibrosis progressed, its rate dropped, making this parameter a minor one in growth-rate terms. From the eleventh to the thirteenth weeks, while transition from fibrosis to cirrhosis was under way, the gap in the growth rate of FAP+- and α-SMA$^+$-cells again appeared, in addition to which a slight decrease in the number of CD45$^+$-cells was recorded. Despite the observed increase, their share at the 15th and 17th weeks remained the lowest when compared to the FAP$^+$- and α-SMA$^+$-cells, while the number of α-SMA+ cells had increased rapidly. At all time, a statistically significant strong correlation was found between the area of connective tissue and the number of FAP$^+$-, α-SMA$^+$-, and CD45$^+$-cells.

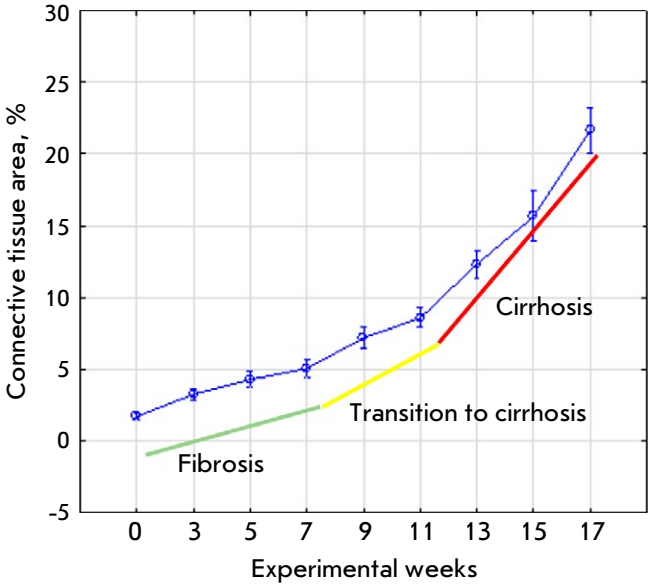

Fig. 2. Changes in the connective tissue area at different stages of the study

In the histological preparations, rounded α-SMA+ cells were observed in the sinusoids and necrotizing foci before the onset of the fibrosis to cirrhosis transition (9th week). From the 11th to 17th week, they were located both in the sinusoids and in the connective tissue septa (*Fig. 3D*). At the first stage of the experiment, rounded FAP$^+$ cells were localized around the interlobular vessels and near the interlobular bile ducts of the portal zones and from the 7th week they were detected in the connective tissue septa and sinusoids (*Fig. 3D*).

Using Mallory's staining method, we observed the directed growth of fibrous connective tissue fibers with FAP$^+$ cells from two portal zones through the liver parenchyma towards each other, predetermining the path for bridging fibrosis that is a formation of pathological tissue and connective tissue bridges. The CD45$^+$ cells were diffusely localized among other cells of the lymphoid-histiocytic infiltrate in the connective tissue septa and portal zones, as well as in the blood

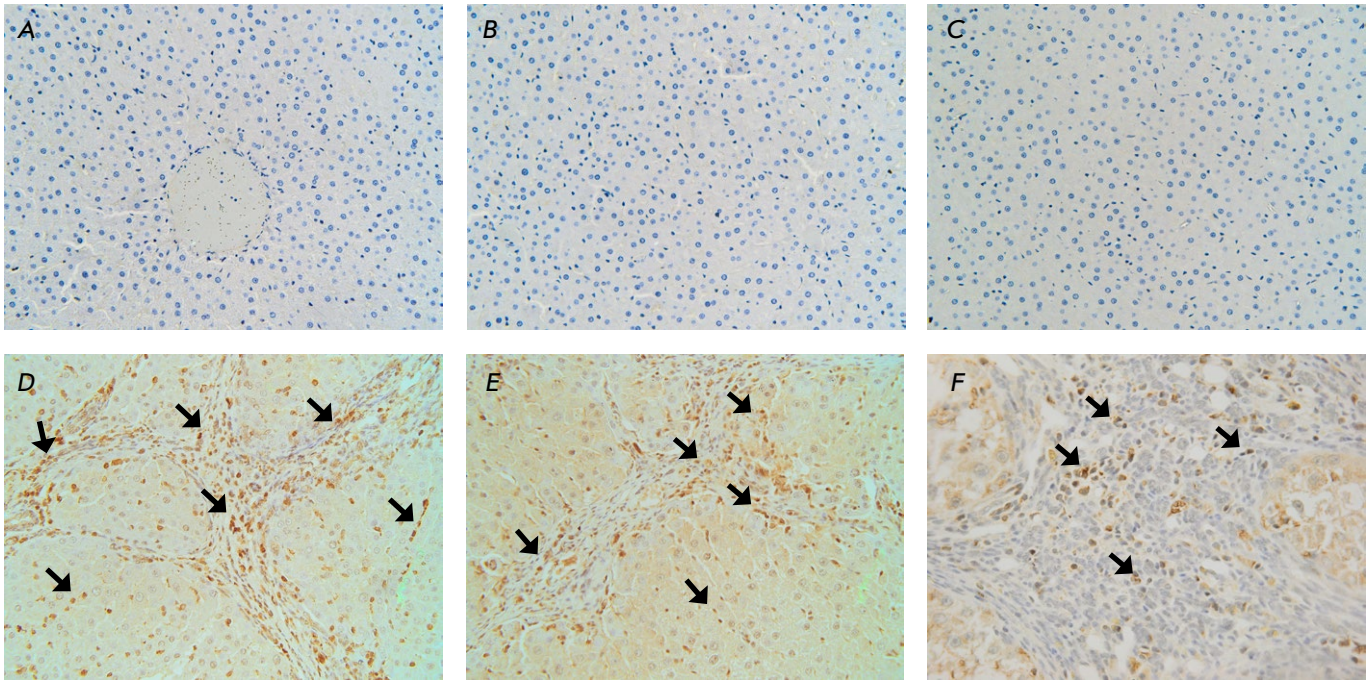

Fig. 3. Fragments of the liver of the control group rats: (*A*, *B*, *C*) at 15 weeks, (*D*, *E*) at 17 weeks, (*F*) before the beginning of the experiment. Immunohistochemical staining (restained with Mayer's hematoxylin): for FAP (*A*, *D*); for α-SMA (*B*, *E*); for CD45 (*C*, *F*). Magnification ×40: (*A*) no FAP^+-cells are found; (*B*) no α-SMA^+-cells are found in the sinusoids; (*C*) no $CD45^+$-cells are found in the parenchyma; (*D*) α-SMA^+-cells (marked with arrows); (*E*) FAP^+-cells (marked with arrows); (*F*) $CD45^+$-cells in the connective tissue (marked with arrows)

vessel lumens (*Fig. 3F*). Less commonly, they were detected in the sinusoids of false hepatic lobules.

mmp-9 mRNA expression level

To normalize the RT-PCR data, the *hes1* gene was chosen as a reference one, since its expression level proved the most stable throughout the experiment. The use of *hprt1* and *sdha* as reference genes was considered inappropriate due to the high variability of their mRNA levels. RT-PCR efficiency for the target (*mmp-9*) and the reference gene differed by less than 1% [25]; so, the relative mRNA level was assessed using the standard Livak and Schmittgen's method [26]. The data on a normalized level of *mmp-9* mRNA expression are shown in *Fig. 5*.

The analysis included all values obtained within the study, not excluding the "outliers" with a low level of *mmp-9* mRNA observed at the control point (intact rats). It is noteworthy that by the 3rd week into the experiment, in the presence of developing fibrosis, the relative *mmp-9* level did not increase and even slightly decreased when compared to the control value. At the same time, it increased over a relatively short interval between the 5th and 9th weeks to subsequently drop to its initial level. In the presence of increased *mmp-9* mRNA expression, the fibrosis to cirrhosis transition occurred. Starting from the 11th week, the level of *mmp-9* mRNA began to drop and, as a result, already from the 13th to 17th weeks, it had matched the initial one at the control point.

It is important to note that an increase in the level of *mmp-9* mRNA while fibrogenesis is underway has been noted in many studies performed on laboratory animals [27, 28]. However, researchers rarely insist on both a detailed analysis of all fibrosis stages and on choosing an appropriate reference gene for RT-PCR data normalization. *Figure 6* shows our data normalized using the two other reference genes (*hprt1, sdha*), whose range of Ct values in the experiment was higher than that of the target gene (*mmp-9*). In other words, *Fig. 6* exemplifies an inadequate use of reference genes for RT- PCR data normalization; e.g., when applying *hprt1*, an average increase in the *mmp-9* mRNA level was recorded that also decreased in the 3rd week. Given that relative characteristics vary widely, we believe the accuracy of such measurements can be sufficient only for a small number of experimental control points; so, we do not recommend using *hprt1* for a detailed analysis of fibrosis stages. Applying *sdha*, on the other hand, made it impossible to register a drop in the *mmp-9* level at the 3rd week and at the beginning of the 11th

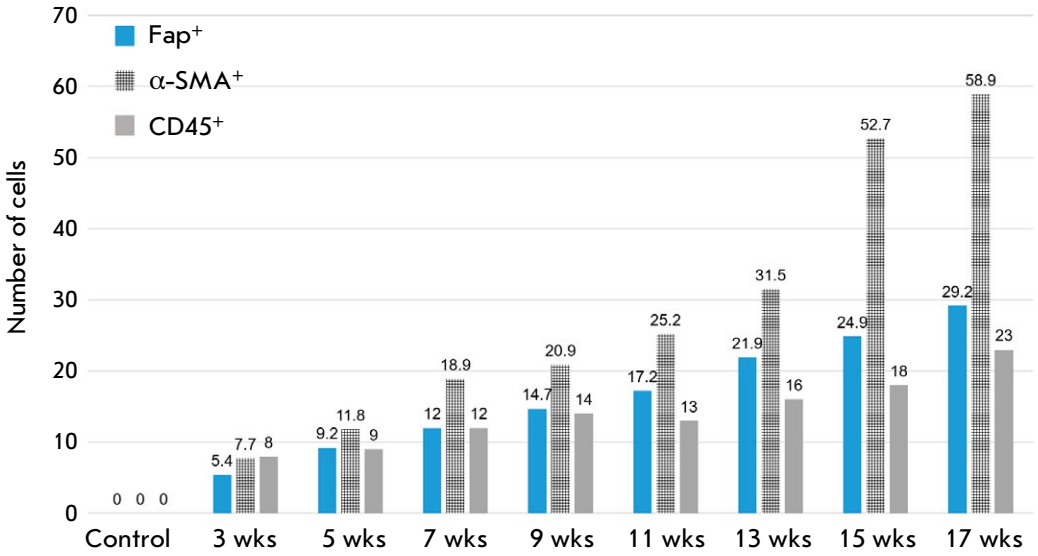

Fig. 4. Changes in the number of FAP+-, α-SMA+-, and CD45+-cells at different stages of the study

week. Here, it is noteworthy that the choice of an optimal reference gene depends on the stage of fibrosis. In a detailed study of its specific stages, rather than that of the entire process in a long-term experiment, one should make sure to additionally select an optimal reference gene [19].

DISCUSSIONS

In the framework of this study, we did not assess the level of the MMP-9 protein and cannot state which cells synthesize it, for this will be the subject of further research. In our study, MMP-9 was shown to be secreted in the liver mainly by Kupffer cells (resident macrophages) [29, 30]. MMP-9 activates latent TGFβ (transforming growth factor beta) and, thus, promotes HSC transdifferentiation into the myofibroblastic phenotype and further progression of liver fibrosis [31-33]. At the same time, Atta H. et al. note that MMP-9 can promote apoptosis of transformed HSCs at a low level of TIMP1 (tissue inhibitor of matrix metalloproteinases) and Kupffer cells play an important role in this process [29, 30, 34]; so, these contradictory data make it difficult to understand the role of Kupffer cells in liver fibrogenesis, which indicates the need for basic research.

At the early stages of liver fibrosis initiation and development (3rd week of the experiment), an increase in the area of connective tissue was observed. At the same time, the *mmp-9* mRNA level slightly decreased when compared to the control group. Probably, this decrease can be considered as one of the factors behind the relatively rapid accumulation of extracellular matrix proteins. The decreased *mmp-9* mRNA level may be also associated with a general toxic effect in response to TAA exposure and more complex processes. First, fibrosis development is characterized by

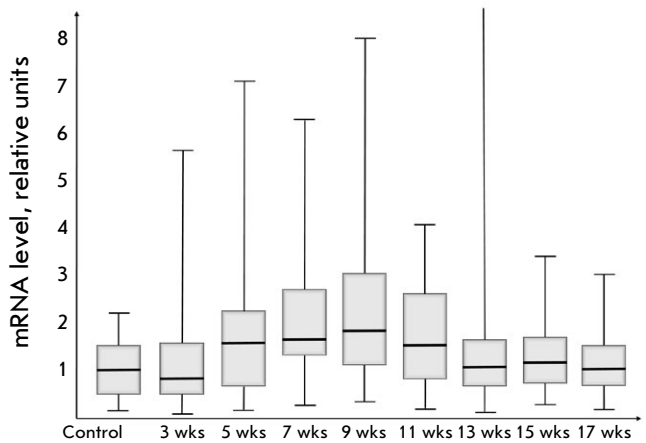

Fig. 5. Relative level of *mmp-9* mRNA

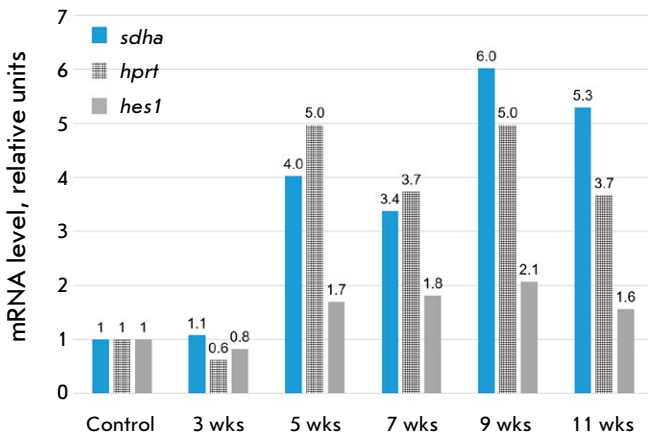

Fig. 6. Relative *mmp-9* mRNA level for different genes used to normalize RT-PCR data

an imbalance between the production of metalloproteinases and the corresponding inhibitors (TIMP family proteins). It is likely that the inhibitors are induced before the cells begin to produce more metalloproteinases in response to toxic damage. Second, *mmp-9* expression is controlled by epigenetic mechanisms and the increase in its expression may take some time and/or be inhibited at the transcriptional level.

By the 5th week of the experiment and in the presence of an increased *mmp-9* mRNA level, the rate of connective tissue formation significantly decreased, which was probably due to the increased expression of the corresponding protein, leading to an effective destruction of collagen and other proteins of the extracellular matrix. Such a reaction can be considered an attempt by the organ to counteract fibrosis progression through metalloproteinase hyperactivation; so, a similar situation was observed at the 7th week as well. In the presence of a slight increase in the *mmp-9* mRNA level when compared to the 5th week, the rate of connective tissue synthesis continued to decrease. Hence, compared with the control group, the increase in the connective tissue area by the 3rd week amounted to 2.1 times (201%, $p < 0.05$), 26.6% by the 5th week ($p < 0.05$), and only 5.2% by the 7th week ($p < 0.05$).

At the onset of the fibrosis to cirrhosis transition, the level of *mmp-9* mRNA reached its maximum having increased 2.07 times ($p < 0.05$) against that of the control group. However, the growth of connective tissue increased markedly only by the 9th week to amount to approximately 50% ($p < 0.05$) when compared to its amount registered by the 7th week. It seems that at this stage a role reversal takes place and the *mmp-9* level ceases to be an important factor in curbing the development of fibrosis. It is possible that these are inflammation-associated factors that move to the fore, since their role noticeably increases, which is confirmed by the increased number of diffuse foci in the lymphoid-histiocytic infiltrate.

By the 11th week at the stage of incomplete cirrhosis, the *mmp-9* mRNA level had decreased and probably ceased to play an important role in regulating the growth rate of the connective tissue area; so, its decrease was to do with some alternative protection/regeneration mechanisms. The *mmp-9* mRNA level increased only by 13% ($p < 0.05$) compared to the 9th week. At the same time, the signs of inflammation became more pronounced, significantly increasing the number of lymphoid-histiocytic infiltrate cells in the septa and portal zones.

At the stage of developed cirrhosis (weeks 13–17), the *mmp-9* mRNA level reached that of the control group while the inflammation level in the liver reached its maximum.

Applying the immunohistochemical method has enabled us to simultaneously detect two morphologically heterogeneous myofibroblast populations in the liver of rats, which expressed different marker types. It is remarkable that in the early stages of fibrosis, the α-SMA+ cells were not lumped together with the FAP^+ cells; before the onset of the fibrosis to cirrhosis transformation, α-SMA^+ cells were noted in the sinusoids of the liver and necrosing foci only to be later localized both in the sinusoids and in the connective tissue septa. At the stage of portal fibrosis, the FAP^+ cells were located near the interlobular vessels and interlobular bile ducts of the portal zones, and in the 7th week, they were detected in the connective tissue septa and sinusoids.

The low level of inflammation before the fibrosis to cirrhosis transition suggests that the function of the cells producing the CD45 marker is to participate in the regulation of the functions of the polymorphic cells of pathological septa. But confirming this statement requires further and more detailed research.

CONCLUSION

The results of our study have demonstrated that, when investigating liver fibrogenesis, the choice of an optimal reference gene depends on the fibrosis stage. If one is studying its specific stages and not the entire process in a long-term experiment, the optimal reference gene should be selected additionally, while the *mmp-9* mRNA expression level should be considered as a marker for liver fibrosis development initiation and not as that for cirrhosis progression.

Applying the immunohistochemical method has enabled us to simultaneously uncover two morphologically heterogeneous myofibroblast populations that synthesize different marker types. The FAP^+ cells have been found to be the main contributor to the development of the portal and initial stages of bridging fibrosis. They can be considered as one of the myofibroblast populations in thioacetamide-induced liver fibrogenesis. In the selected experimental model, fibrosis initiation and development before the start of parenchymal restructuring has proceeded at a low inflammation level. ●

Conflict of interest: The authors declare no conflict of interest.

This study was performed within the framework of State Research Program Fundamental and Applied Sciences for Medicine initiated by the Ministry of Healthcare of the Republic of Belarus; Task 2.89 Investigating The Role of NOTCH- and TWEAK-Signaling Pathway Gene Expression in Proliferation and Differentiation of Normal and Toxically -Defeated Liver Cells (Reg. No. 20190107).

REFERENCES

1. Tsomidis I., Notas G., Xidakis C., Voumvouraki A., Samonakis D.N., Koulentaki M., Kouroumalis E. // Biomedicines. 2022. V. 10. № 12. P. 3179. https://doi: 10.3390/biomedicines10123179.
2. Rezaeian A.A., Yaghobi R., Geramizadeh B. // Trop. Biomed. 2018. V. 35. № 3. P. 839–848.
3. Wanninger J., Walter R., Bauer S., Eisinger K., Schäffler A., Dorn C., Weiss T.S., Hellerbrand C., Buechler C. // Mol. Pathol. 2011. V. 91. № 2. P. 603–607. https://doi: 10.1016/j.yexmp.2011.07.001.
4. Lachowski D., Cortes E., Rice A., Pinato D., Rombouts K., Del Rio Hernandez A. // Sci. Rep. 2019. V. 9. № 1. P. 7299. https://doi: 10.1038/s41598-019-43759-6.
5. Roeb E. // Matrix. Biol. 2018. V. 68–69. P. 463–473. https://doi: 10.1016/j.matbio.2017.12.012.
6. Boeker K.H.W., Haberkorn C.I., Michels D., Flemming P., Manns M.P., Lichtinghagen R. // Clin. Chim. Acta. 2002. V. 316. № 1–2. P. 71–81. https://doi: 10.1016/s0009-8981(01)00730-6.
7. Craig V.J., Zhang L., Hagood J.S., Owen C.A. // Am. J. Respir. Cell. Mol. Biol. 2015. V. 53. № 5. P. 585–600. https://doi: 10.1165/rcmb.2015-0020TR.
8. Lu L., Zhang Q., Wu K., Chen X., Zheng Y., Zhu C., Wu J. // Cancer Lett. 2015. V. 356(2 Pt B). P. 470–478. https://doi: 10.1016/j.canlet.2014.09.027.
9. Crespo I., San-Miguel B., Fernández A., de Urbina J.O., González-Gallego J., Tuñón M.J. // Transl. Res. 2015. V. 165. № 2. P. 346–357. https://doi: 10.1016/j.trsl.2014.10.003.
10. Su F., Zhang W., Chen Y., Ma L., Zhang H., Wang F. // Exp. Ther. Med. 2014. V. 8. № 6. P. 1677–1682. https://doi: 10.3892/etm.2014.1989.
11. Gadd V.L., Melino M., Roy S., Horsfall L., O'Rourke P., Williams M.R., Irvine K.M., Sweet M.J., Jonsson J.R., Clouston A.D., Powell E.E. // Liver Int. 2013. V. 33. № 4. P. 569–579. https://doi: 10.1111/liv.12050.
12. Luo N., Li J., Wei Y., Lu J., Dong R. // Physiol. Res. 2021. V. 70. № 6. P. 821–829. https://doi: 10.33549/physiolres.934755.
13. Baglieri J., Brenner D.A., Kisseleva T. // Int. J. Mol. Sci. 2019. V. 20. № 7. P. 1723. https://doi:10.3390/ijms20071723.
14. Lay A.J., Zhang H.E., McCaughan G.W., Gorrell M.D. // Front. Biosci. (Landmark Ed). 2019. V. 24. № 1. P. 1–17. https://doi: 10.2741/4706.
15.Dhar D., Baglieri J., Kisseleva T., Brenner D.A. // Exp. Biol. Med. (Maywood). 2020. V. 245. № 2. P. 96–108. https://doi: 10.1177/1535370219898141.
16. Fuji H., Miller G., Nishio T., Koyama Y., Lam K., Zhang V., Loomba R., Brenner D., Kisseleva T. // Front. Mol. Biosci. 2021. V. 8. P. 790032. https://doi: 10.3389/fmolb.2021.790032.
17. Wells R.G. // Curr. Pathobiol. Rep. 2014. V. 2. № 4. P. 185–190. https://doi: 10.1007/s40139-014-0054-y.
18. Sun Y., Liu B., Xie J., Jiang X., Xiao B., Hu X., Xiang J. // Mol. Med. Rep. 2022. V. 25. № 5. P. 181. https://doi:10.3892/mmr.2022.12697.
19. Lebedeva E.I., Shchastniy A.T., Babenka A.S. // Molecular medicine. 2022. V. 20. № 2. P. 53–62. https://doi 10.29296/24999490-2022-02-08.
20. Theoretical foundations and practical application of immunohistochemistry methods / Ed. Korzhevsky D.E. St. Petersburg: SpecLit, 2014. 119p.
21. Zheng C., Luo J., Yang Y., Dong R., Yu F.X., Zheng S. // Front Pediatr. 2021. V. 8. P. 618226. https://doi: 10.3389/fped.2020.618226.
22. Everhart J.E., Wright E.C., Goodman Z.D., Dienstag J.L., Hoefs J.C., Kleiner D.E., Ghany M.G., Mills A.S., Nash S.R., Govindarajan S., et al. // Hepatology. 2010. V. 51. № 2. P. 585–594. https:// doi.org/10.1002/hep.23315.
23. Lebedeva E.I., Shchastniy A.T., Krasochko P.A., Babenka A.S. // Veterinary Journal of Belarus. 2022. V. 1. № 16. P. 105–110.
24. Zhizhin K.S. Medical statistics: Textbook. Rostov n/a: Phoenix, 2007. 160p.
25. A-Z of Quantitative PCR / Ed. Bustin S. La Jolla: International University Line, 2004. 882 p.
26. Livak K.J., Schmittgen T.D. // Methods. 2001. V. 4. P. 402–408. https://doi: 10.1006/meth.2001.1262.
27. Mirzavand S., Rafiei A., Teimoori A., Khorsandi L., Bahreini A., Motamedfar A., Beiromvand M. // Parasitol. Res. 2020. V. 119. P. 2177–2187. https://doi: 10.1007/s00436-020-06700-9.
28. Ebrahim H.A., Kamar S.S., Haidara M.A., Abdel Latif N.S., Abd Ellatif M., ShamsEldeen A.M., Al-Ani B., Dawood A.F. // Naunyn Schmiedebergs Arch. Pharmacol. 2022. V. 395. № 9. P. 1087–1095. https://doi: 10.1007/s00210-022-02264-w.
29. Tacke F., Trautwein C. // J. Hepatol. 2015. V. 63. № 4. P. 1038–1039. https://doi: 10.1016/j.jhep.2015.03.039.
30. Murphy F.R., Issa R., Zhou X., Ratnarajah S., Nagase H, Arthur M.J.P., Benyon C., Iredale J.P. // J. Biol. Chem. 2002. V. 277. № 13. P. 11069–11076. https://doi: 10.1074/jbc.M111490200.
31. Wang Q., Liu X., Zhang J., Lu L., Feng M., Wang J. // Mol. Med. Rep. 2019. V. 20. № 6. P. 5239-5248. https://doi: 10.3892/mmr.2019.10740.
32. Kobayashi T., Kim H., Liu X., Sugiura H., Kohyama T., Fang Q., Wen F., Abe S., Wang X. // Am J. Physiol. Lung. Cell. Mol. Physiol. 2014. V. 306. № 11. P. L1006–10015. https://doi: 10.1152/ajplung.00015.2014.
33. Lo R.C., Kim H. // Clin. Mol. Hepatol. 2017. V. 23. № 4. P. 302–307. https://doi: 10.3350/cmh.2017.0078.
34. Atta H., El-Rehany M., Hammam O., Abdel-Ghany H., Ramzy M., Roderfeld M., Roeb E., Al-Hendy A., Abdel Raheim S., Allam H., Marey H. // PLoS One. 2014. V. 9. № 11. P. e112384. https://doi: 10.1371/journal.pone.0112384.

EGFR Suppression Inhibits the Sphere Formation of MCF7 Cells Overexpressing EGFR

D. D. Novak[1≠], O. S. Troitskaya[1≠*], A. A. Nushtaeva[1], M. V. Zhilnikova[1,2], V. A. Richter[1], M. I. Meschaninova[1], O. A. Koval[1,2]

[1]Institute of Chemical Biology and Fundamental Medicine, Siberian Branch of the Russian Academy of Sciences, Novosibirsk, 630090 Russian Federation

[2]Department of Natural Sciences, Novosibirsk State University, Novosibirsk, 630090 Russian Federation

[≠]Authors who contributed equally to this work.

[*]E-mail: troitskaya_olga@bk.ru

Received: March 23, 2023; in final form, April 18, 2023

DOI: 10.32607/actanaturae.17857

ABSTRACT **The epidermal growth factor receptor (EGFR) is an oncogenic tyrosine kinase that is involved in tumor initiation and progression, making EGFR inhibitors and monoclonal antibodies to this receptor essential for anti-tumor therapy. We have previously shown that EGFR transgene expression in the human breast adenocarcinoma cell line MCF7 (MCF7-EGFR) stimulates the 3D spheroid-like growth. The primary focus of our present work was to investigate whether EGFR inhibition could affect the assembly of spheroids or lead to the destruction of pre-existing spheroids. We compared the effects of anti-EGFR siRNA, the anti-EGFR monoclonal antibody cetuximab, and the tyrosine kinase inhibitor AG1478 on dissociated and spheroid MCF7-EGFR cells. MCF7-EGFR cells were found to have a 2.5-fold higher sensitivity towards the cytotoxic effects of cetuximab and AG1478 compared with the parental MCF7 cell line. The suppression of EGFR mRNA with siRNA was found to reduce the sphere formation, whereas treating the pre-existing spheroids had no such effect. Treatment of dissociated spheroids with cetuximab and AG1478 was also found to inhibit the MCF7-EGFR sphere formation. We suggest that EGFR expression is important, at least, during the spheroid formation stage. The transition of a MCF7wt adherent cell culture to MCF7-EGFR spheroids was accompanied by a considerable increase in N-cadherin adhesion proteins. The level of N-cadherin decreased when MCF7-EGFR cells were treated with siRNA and cetuximab. Thus, we have demonstrated that N-cadherin is involved in the EGFR-dependent formation of MCF7-EGFR spheroids. Accordingly, MCF7-EGFR spheroids can be considered a suitable model for studying aggressive hormone-positive breast tumors.**

KEYWORDS **3D cell culture, spheroids, MCF7, EGFR, siRNA, cetuximab, AG1478.**

ABBREVIATIONS **EGFR – epidermal growth factor receptor; siRNA – small interfering RNA; LF – Lipofectamine 3000, PI – propidium iodide; wt – wild type; AG – EGFR inhibitor (AG1478); DMSO – dimethyl sulfoxide; FDA – fluorescein diacetate; SD – standard deviation; IC50 – drug concentration, at which cell death reaches 50%.**

INTRODUCTION

The interaction between various growth factors and their receptors is known to regulate the autonomous growth of cancer cells [1]. Hence, the epidermal growth factor (EGF) and its receptor (EGFR) play a crucial role in the pathogenesis and progression of various types of malignant tumors [2]. EGFR (or HER1) is a member of the ErbB family of receptor tyrosine kinases, which also includes HER2, HER3, and HER4. The EGFR composition includes an extracellular domain, a hydrophobic transmembrane domain, an intracellular catalytic tyrosine kinase domain, and several intracellular tyrosine residues [3].

Currently, two types of ErbB inhibitors are used in tumor therapy. There are monoclonal antibodies against the EGFR or HER2 extracellular domain, including cetuximab, matuzumab, panitumumumab, trastuzumab, and pertuzumab, as well as tyrosine kinase inhibitors that compete with ATP molecules for binding to the EGFR tyrosine kinase domain, such as gefitinib, erlotinib, lapatinib, AEE788 [4]. In 2004, the FDA first approved cetuximab for metastatic colorec-

tal cancer, and in 2011, it was approved for head and neck cancer therapy [5, 6]. The competitive specific binding of cetuximab to EGFR was found to be effective in inhibiting receptor phosphorylation, which in turn impedes the EGFR signaling pathway and results in tumor cell proliferation [7].

Knockdown of therapeutically relevant target genes is also considered an effective strategy for tumor therapy. Inhibition of mRNA processing by small interfering RNA (siRNA) is regarded as one way to block a specific target. RNA interference is a protective mechanism against exogenous nucleic acids entering the cell, such as viral RNA [8]. Currently, preclinical and clinical trials are under way on several siRNA-based agents for the treatment of brain and prostate cancer [9].

Earlier, we obtained an MCF7 human breast adenocarcinoma cell line that manifested an increased expression of EGFR. The study revealed that excessive EGFR in MCF7 cells led to the spontaneous formation of spheres under standard culture conditions [10, 11]. MCF7-EGFR spheroids have a round shape with a well-defined outer boundary and a median diameter of 100 μm, with the size of large spheroids likely to exceed 400 μm. Given that EGFR production has been demonstrated to affect the adhesive properties of MCF7-EGFR cells, inhibition of EGFR may be believed to cause disruption of the formed spheroids or inhibit the assembly of spheroids from individual cells. To verify this hypothesis, we examined the effects of anti-EGFR siRNA, cetuximab, and the tyrosine kinase inhibitor AG1478 on the structure and formation of MCF7-EGFR spheroids.

EXPERIMENTAL PART

Cell lines

The human breast adenocarcinoma cell lines MCF7wt (#ACC 115, Germany) and MDA-MB-231 (#ACC 732, Germany) were investigated. The cells were cultured as a monolayer in a IMDM or DMEM medium, containing 10% FBS and 1% penicillin-streptomycin-amphotericin (hereafter, complete medium), respectively, as described earlier [12].

The human breast adenocarcinoma cell line MCF7-EGFR forming spheroids was described in the previous study [10]. MCF7-EGFR spheroids were cultured under standard conditions on non-adhesive-coated plates (Nest Bio-technology Co., China).

Spheroid formation and counting

For spheroid formation kinetic curves to be generated, the cells were dissociated using Stempro™ Accutase™ reagent (Gibco, USA), seeded at 3×10^4 cells/well into a 48-well, non-adhesive-coated plate (Eppendorf, Germany), and cultured under standard conditions, as described above. The spheroids were counted in three or six independent wells of the plate using an inverted microscope (Eclipse Ti, Nikon, Japan) at 40× magnification. All free-floating spheroids larger than 30 μm were counted in the light field. Then, the average number of spheroids per well and the standard deviation (SD) were calculated. Preliminary counts in all experiments were performed using the ImageJ software (version 1.52a, USA) (data not shown). The exact number of spheroids was calculated manually.

Anti-EGFR siRNA construction

To evaluate the EGFR inhibition on MCF7-EGFR spheroids, we constructed siRNAs based on the sequences described in [13]. The oligonucleotides were synthesized in the laboratory of RNA chemistry of the Institute of Chemical Biology and Fundamental Chemistry of the Siberian Branch of the Russian Academy of Sciences. We used the following siRNAs: senScr 5'-CAA GUC UCG UAU GUA GUG GUU-3', antiScr 5'-CCA CUA UAU ACG AGA CUU GUU-3', senEGFR 5'-GUC CGC AAG UGU AAG AAG UTT-3', antiEGFR 5'-ACU UCU UACU ACU UGC GGA CTT-3'. The average concentration of ribooligonucleotides in the solution was calculated to be 0.203 mM.

siRNA hybridization

Equimolar amounts of sen- and anti-sen siRNAs were mixed with 5-fold siRNA hybridization buffer (100 mM $C2H_3NaO_2$, 30 mM HEPES-KOH, 2 mM $Mg(CH_3COO)_2$, pH 7.4) in the ratio 2 : 2 : 1. The samples were heated in a water bath for 2 min at 90°C and cooled to room temperature. Two volumes of 1× siRNA hybridization buffer were added to the resulting mixture. The final concentration of siRNA duplexes was 27 μM.

siRNA cell transfection

The siRNA transfection was performed using Lipofectamine 3000 reagent (Invitrogen, USA) according to the manufacturer's protocol. The cells were plated 24 h before the experiment, treated with 100 nM siRNA, and incubated for 4 h at 37°C. Then, the medium was replaced with a complete medium suitable for the cell culture and the cultivation was continued.

Cell survival assay

The cell viability was determined 72 h after treatment with the drug using the MTT test as described in [12]. The IC50 values were calculated using the CompuSyn version 1.0 software. The initial solution

(5 mg/ml) of cetuximab Erbitux® (Merck Healthcare, Germany) was stored at +4°C. For cell culture experiments, cetuximab was diluted in a complete IMDM medium. The stock solution (31.7 mM) of AG1478 (Sigma-Aldrich, USA) in DMSO:MeOH (1 : 1) was stored at -20°C. For cell culture experiments, AG1478 was diluted in a complete IMDM medium so that the DMSO concentration in the wells was 0.5%.

FDA staining

An initial solution (1 mg/ml) of fluorescein diacetate, FDA (Sigma-Aldrich, USA), diluted in DMSO was stored at -20°C. The solution was added to the culture medium until the final concentration of 10 μg/ml. The spheroids were incubated in a complete IMDM medium with dissolved FDA for 30 min, followed by harvesting with centrifugation and washing with PBS. A fluorescence microscope (Eclipse Ti, Japan) and flow cytometry were used to analyze the cell viability and cytotoxicity.

Flow cytometry

Following the treatment, the spheroids were dissociated with Stempro™ Accutase™ reagent, washed in PBS, and incubated with antibodies to EGFR to determine EGFR levels. The cells were incubated with propidium iodide (PI) or FDA according to the manufacturer's protocol for viability assay. We used the following antibodies: mouse IgG monoclonal antibodies to the EGFR protein (Invitrogen, USA), secondary antibodies conjugated with the Alexa Fluor 647 fluorescent tag (Abcam, UK). All the assays were performed using a FACSCantoII flow cytometer (BD Biosciences, USA). The data were analyzed using the FACSDiva software (BD Biosciences, USA). The cell populations were isolated using forward and side light scattering to exclude small particles. At least 10,000 events were collected in each experiment.

Western blot analysis

Western blot analysis was performed according to the protocol described in [14]. The cells were lysed, the protein concentration was measured, and then the samples (15 μg) were separated using 10% SDS-PAGE and transferred to a PVDF membrane. The membrane was blocked with a 5% milk powder solution and incubated sequentially with primary and secondary antibodies conjugated with horseradish peroxidase. We used the following antibodies: primary IgG antibodies to actin (Sigma-Aldrich, USA), EGFR (Santa Cruz Biotechnology, USA), SNAIL + SLUG (Abcam), N-cadherin (Invitrogen, USA), E-cadherin (Abcam), and horseradish peroxidase conjugates of secondary antibodies to rabbit (Thermo Fisher, USA) and mouse antigens (Thermo Fisher). The chemiluminescent signal was recorded using the Novex ECL HRP reagent kit (Invitrogen) and the GE Amersham Imager 600 (GE, USA). Densitometric analysis of Western blots was performed using the GelAnalyser version 2010a image analysis software.

Statistical analysis

The results are presented as the arithmetic mean ± SD for the sample. Statistical analysis was performed using Student's *t*-criterion. The differences were considered statistically significant at $p < 0.05$.

RESULTS AND DISCUSSION

Effect of anti-EGFR siRNA on MCF7-EGFR spheroids

We evaluated the effect of EGFR downregulation on MCF7-EGFR spheroid formation by anti-EGFR siRNA. An international database of NCBI Nucleotides was used to determine the complementarity of the selected anti-EGFR siRNA to the sequence of exon 8 of the human EGFR gene. This exon encodes a fragment of EGFR subdomain III responsible for receptor-ligand binding [15].

The MCF7-EGFR spheroids were dissociated into individual cells and then seeded into plates with 100 nM anti-EGFR siRNA. Lipofectamine 3000 (LF) was used as a transfection agent. Scrambled siRNA was used as a negative control, and cells treated only with LF were used as a control for the cytotoxic activity of LF. The dynamics of growth and sphere formation after siRNA treatment and in the control samples were evaluated by automatic and direct sphere counting. Treatment of the cells with anti-EGFR siRNA resulted in a reduction in the number of spheroids compared to the control cells and the cells treated with Scramble siRNA (*Fig. 1A,B*).

The level of total cellular EGFR in MCF7-EGFR cells was found to be almost 10-fold higher than that in the MCF7wt cells (*Fig. 2B,D*). The EGFR knockdown caused by anti-EGFR siRNA was assessed by flow cytometry and Western blotting using antibodies to the surface and internal domains of the protein, respectively. The decrease in the level of surface EGFR on the second day after treatment of the MCF7-EGFR spheroids with siRNA was estimated to be 20–25% (*Fig. 2*). The Western blotting data are consistent with the results of a measuring of the surface EGFR levels in the cells treated with siRNA.

The influence of anti-EGFR siRNA on the formed structures was detected by placing the MCF7-EGFR spheroids in a non-adhesive plate and following incubation with siRNA. Anti-EGFR siRNA was found

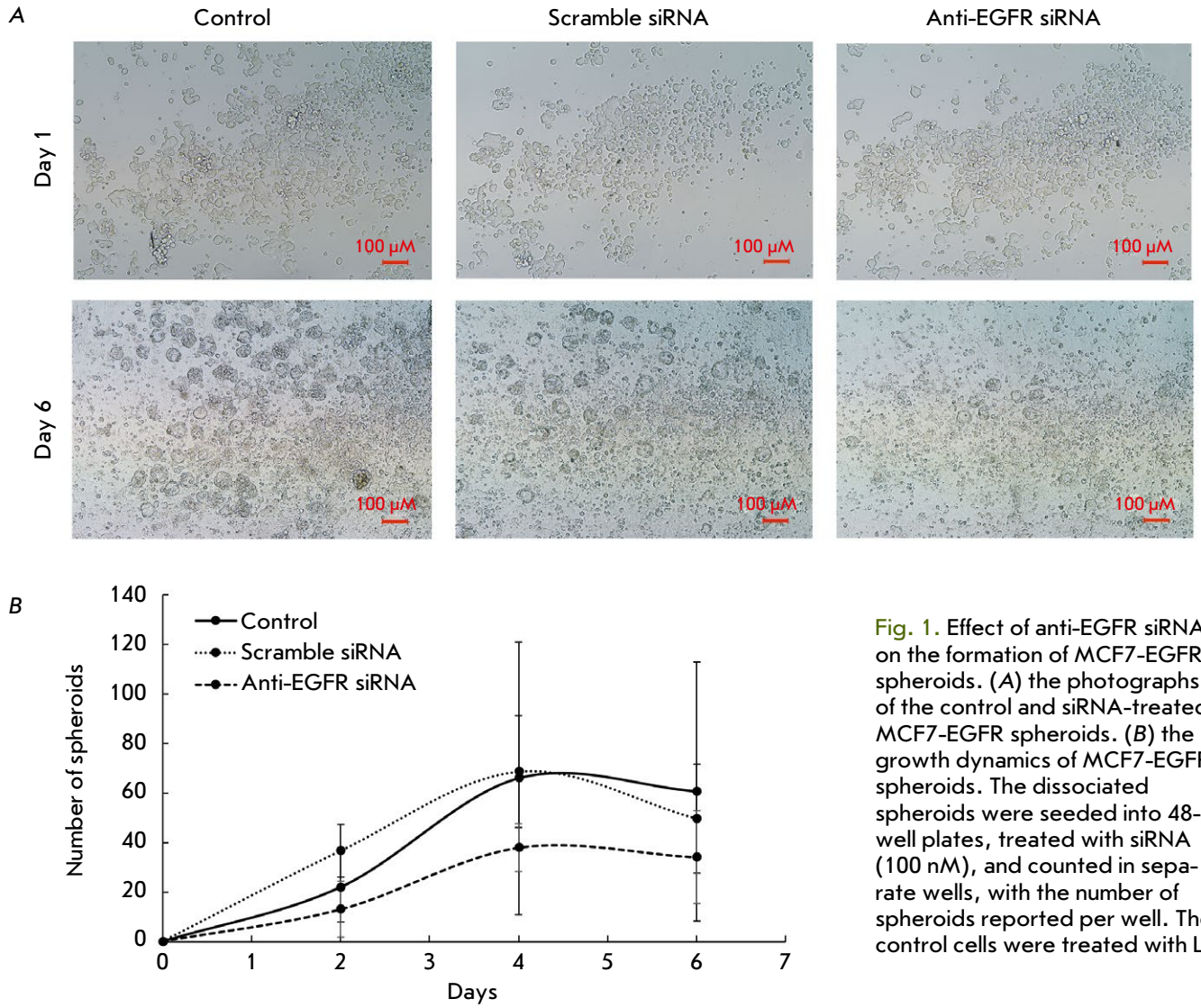

Fig. 1. Effect of anti-EGFR siRNA on the formation of MCF7-EGFR spheroids. (*A*) the photographs of the control and siRNA-treated MCF7-EGFR spheroids. (*B*) the growth dynamics of MCF7-EGFR spheroids. The dissociated spheroids were seeded into 48-well plates, treated with siRNA (100 nM), and counted in separate wells, with the number of spheroids reported per well. The control cells were treated with LF

to have no effect on the spheroid structure (*Fig. 3*). siRNAs at a concentration of 20–200 nM are commonly used to effectively inhibit target protein expression [16–18]. However, the siRNA penetration into the spheroids may proceed worse than in the cells growing in a monolayer. Therefore, higher concentrations of siRNA are often used in experiments with spheroids or transfection when performed in a serum-supplemented medium [19, 20]. It is noteworthy that, in our study, increasing the concentration of anti-EGFR siRNA to 200 nM did not lead to a further decrease in EGFR levels. The transfection in the serum medium did not increase the efficiency of EGFR suppression in the MCF7-EGFR spheroids (data not shown). We believe further optimization of MCF7-EGFR spheroid transfection with siRNA to be highly relevant.

The data obtained suggest that suppression of EGFR by specific siRNAs at the spheroid assembly stage leads to a decrease in the rate of spheroid formation in a MCF7-EGFR culture. At the same time, suppressing EGFR in mature spheroids does not lead to their destruction.

Effect of cetuximab on MCF7wt cells and mature MCF7-EGFR spheroids

Given that cetuximab binding to the target causes cell death, this drug is used in the immunotherapy of EGFR-positive malignancies [21]. We evaluated the cytotoxic activity of cetuximab against MCF7-EGFR spheroids: the drug (25–200 μg/ml) was added to the spheroids as they were left to continue to cultivate under standard conditions for 72 h. The cells

A

	Average MFI
Control	$1.8 \times 10^4 \pm 0.2 \times 10^4$
Scramble siRNA	$1.8 \times 10^4 \pm 0.02 \times 10^4$
Anti-EGFR siRNA	$1.2 \times 10^4 \pm 0.1 \times 10^4$

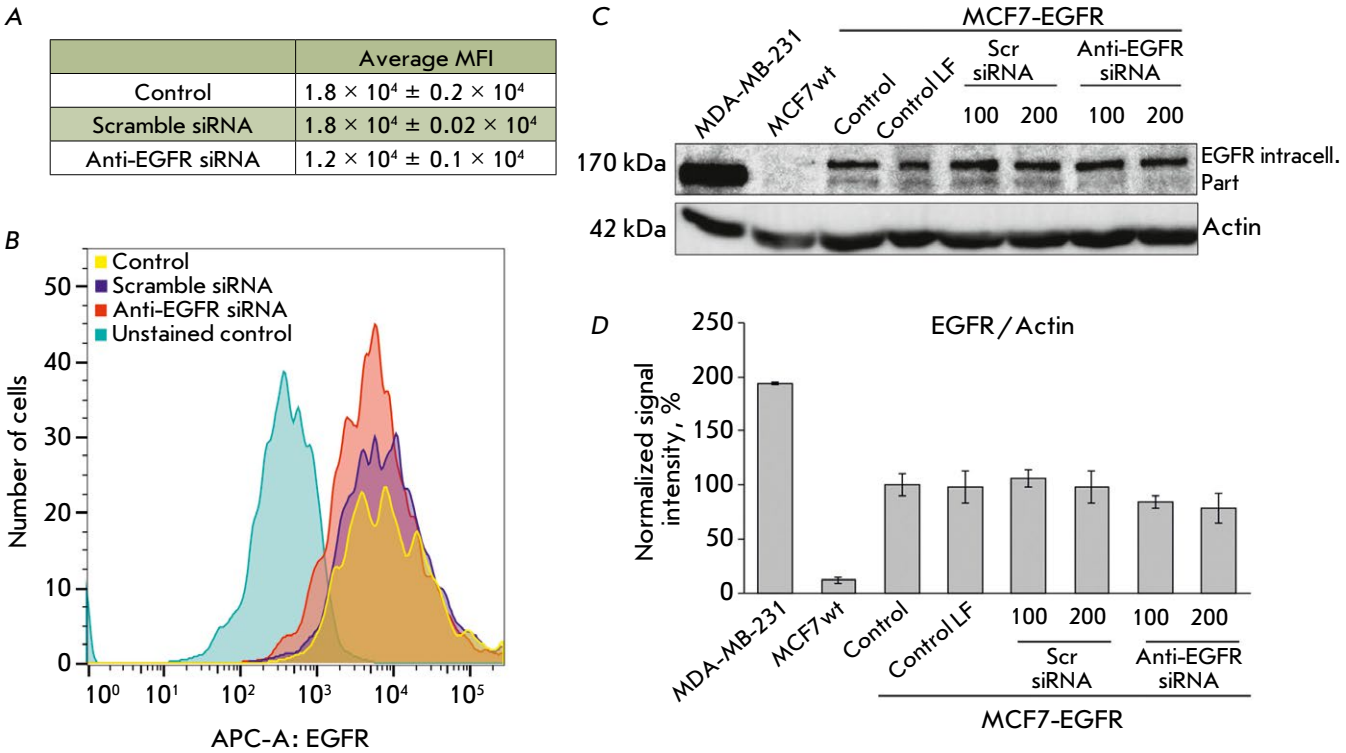

Fig. 2. Evaluation of EGFR reduction in MCF7-EGFR cells under the action of anti-EGFR siRNA. (*A*) the quantification of the $EGFR^+$ cell population. The data are presented as the mean fluorescence intensity (MFI) of $EGFR^+$ cells relative to the control cells ± SD from two independent experiments. (*B*) the representative image of the cytometric analysis. (*C*, *D*) the changes in EGFR levels after anti-EGFR siRNA treatment. MDA-MB-231, MCF7wt were used as control cell lines. The MCF7-EGFR spheroids were dissociated and treated with Scramble siRNA, anti-EGFR siRNA (100–200 nM) for 48 h. (*C*) the representative images of the Western blot analysis. (*D*) the Western blot analysis of EGFR/actin in the cells

were then stained with propidium iodide (PI), and the percentage of PI-negative cells was determined by flow cytometry, corresponding to the population of living cells (*Fig. 4A*). The IC50 value of cetuximab was 136 μg/mL for the MCF7-EGFR spheroids and 304 μg/mL for the MCF7wt parental cell line, which was 2.5-fold higher than that for the MCF7-EGFR spheroid cells, indicating cell resistance to the drug (*Fig. 4B*). By comparing the experimental IC50 values with published data for other EGFR-positive tumor cells, such as lung cancer A549 (IC50 = 146 μg/ml) [22], the MCF7-EGFR cell line can be characterized as cetuximab-sensitive. Thus, MCF7-EGFR spheroid cells cultured under standard conditions can be treated with cetuximab.

Since the study aimed to assess the non-cytotoxic effects of cetuximab on spheroids, cetuximab concentrations lower than the IC25 value were further used. Fluorescein diacetate (FDA), an esterase substrate capable of penetrating the cell, was used to visualize the living cells. FDA can be used as a viability assay tool that measures both enzymatic activity and cell membrane integrity [23]. The MCF7-EGFR spheroids

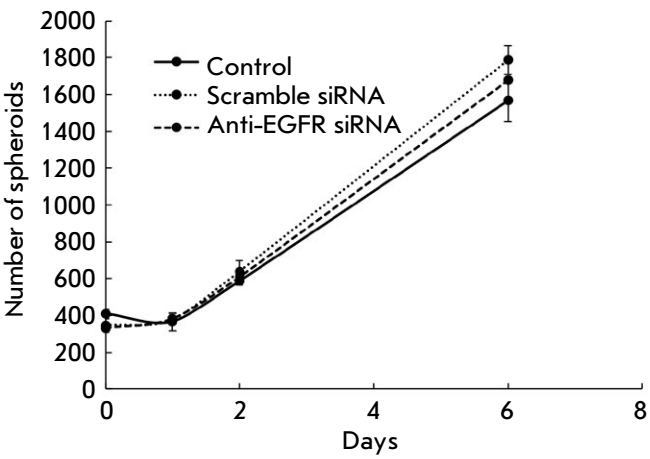

Fig. 3. Analysis of the effect of anti-EGFR siRNA on the structure of MCF7-EGFR spheroids. The growth kinetics of MCF7-EGFR spheroids. The spheroids were seeded, treated with siRNA (100 nM), and counted in separate wells of 24-well plates with the number of spheroids per well. The control spheroids were treated with LF. The data are presented as the mean ± SD of three independent experiments

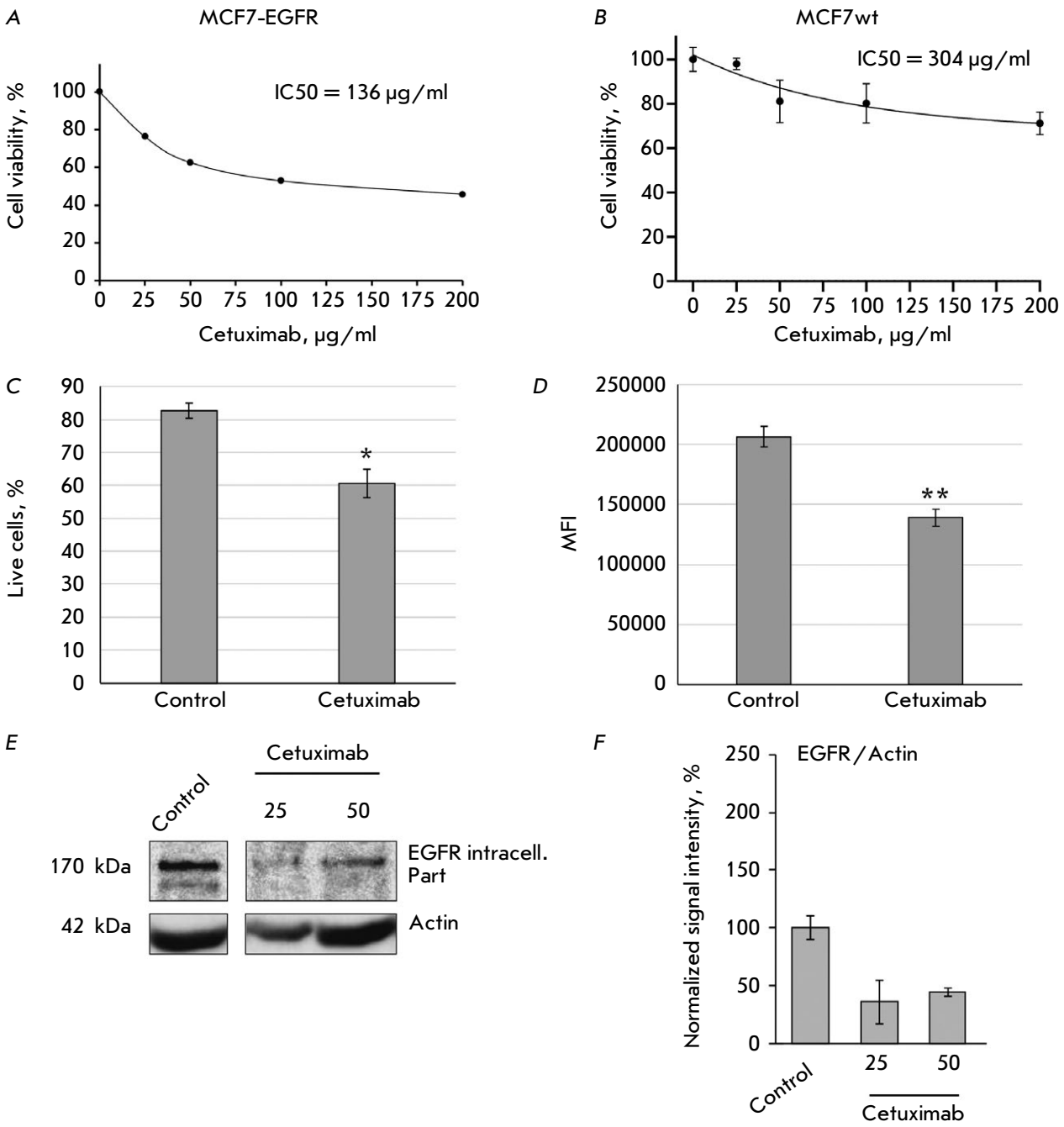

Fig. 4. The cytotoxic activity of cetuximab against MCF7-EGFR spheroids (*A*) and wild-type MCF7 cells (*B*). The IC50 values were determined by the MTT assay. (*C*, *D*) – the estimation of the proportion of live MCF7-EGFR spheroid cells after cetuximab treatment by flow cytometry. The MCF7-EGFR cells were incubated with cetuximab (50 μg/ml) for 72 h and stained with FDA. (*C*) the mean % of live cells ± SD of two independent experiments. (*D*) MFI, the mean fluorescence intensity of live cells. The differences were significant at $^{*}p < 0.05$, $^{**}p < 0.01$. (*E*, *F*) the changes in the EGFR levels after cetuximab treatment. MCF7-EGFR spheroids were dissociated and treated with cetuximab (25–50 μg/mL) for 48 h. (*E*) the representative images of the Western blot analysis. (*G*) the Western blot analysis of EGFR/actin in the cells

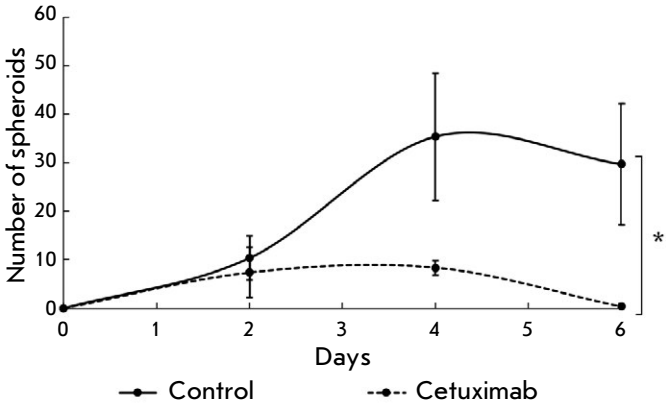

Fig. 5. Analysis of the cetuximab effect on MCF7-EGFR spheroid formation. The spheroids were dissociated, seeded in a 48-well nonadhesive plate, treated with cetuximab (50 μg/ml), and counted in individual wells. The data are presented as the mean ± SD of three independent experiments; $^{*}p < 0.05$

were treated with cetuximab (50 μg/ml) for 72 h and stained with FDA. Flow cytometry of the cells treated with cetuximab revealed a decrease in the population of live cells by up to 20% of the values in the control group (*Fig. 4B,D*). The samples of spheroids not treated with the cytotoxic agent also had dead cells, the presence of which can be explained by the formation of necrotic spheroid nuclei caused by the lack of oxygen and nutrient transport, as we described earlier [10]. Cetuximab was found to decrease the EGFR level more considerably than anti-EGFR siRNA: up to 60% relative to untreated MCF7-EGFR cells (*Fig. 4D,E*).

Adding cetuximab at the stage of dissociated spheroid cells reduces MCF7-EGFR spheroid formation

The dynamics of spheroid formation was assessed after treatment with cetuximab to confirm the ability of cetuximab to inhibit the formation of MCF7-EGFR spheroids. MCF7-EGFR spheroids were dissociated and cultured under standard conditions in the presence of cetuximab (50 μg/ml). The cetuximab treatment resulted in complete suppression of sphere formation on the sixth day of cultivation (*Fig. 5*).

In addition, we evaluated the effect of cetuximab on the spheroids formed. The MCF7-EGFR spheroids were seeded on a non-adhesion culture plate in a cetuximab-added medium (50 μg/ml) for 72 h. The cetuximab treatment resulted in a decrease in the number of spheroids, indicating that MCF7-EGFR spheroid degradation was stimulated when EGFR was inhibited (*Fig. 6A,B*). The spheroids treated with cetuximab and stained with FDA were analyzed by fluorescence microscopy. Multiple individual cells appeared in the presence of cetuximab, with the number of large and structured spheroids decreasing compared with the control (*Fig. 6B*).

Following the exposure to the cetuximab inhibitor, the number of spheroids decreased compared to untreated samples, with this effect shown for both dissociated spheroids and already-formed spheroids. We believe cetuximab to have a predominantly persistent antiproliferative effect on both new and existing spheroids. In contrast to siRNA, the efficacy of cetuximab delivery to the cells of the inner layer of the spheroid is not in doubt since the effects of cetuximab have been confirmed at the organismal level [5].

Effect of AG1478 on the MCF7-EGFR cell spheroid formation

We analyzed how the MCF7-EGFR cells were affected by the EGFR inhibitor tyrphostin (AG1478, or AG), known to inhibit the binding of ATP molecules to the intracellular domain of the receptor. The IC50 value of AG1478 for wild-type MCF7 cells was determined to be almost twice as high as that for MCF7-EGFR cells (*Fig. 7A,B*). Thus, we have demonstrated a change in the sensitivity of MCF7-EGFR cells to EGFR-inhibitory agents compared to MCF7wt cells.

To analyze the effect of AG1478 on spheroid formation, we dissociated MCF7-EGFR spheroids, seeded them onto plates, and added AG1478 (10 μM) to the cells after 24 h of cultivation. The AG1478 treatment significantly reduced the number of spheroids compared to the control cells (*Fig. 7B*).

Effect of siRNA and cetuximab on the levels of adhesion proteins and epithelial-mesenchymal transition regulatory proteins

Rao et al. have demonstrated that EGFR regulates the integrin activation and the spatial organization of focal adhesions [24]. Therefore, it is worth studying the relationship between EGFR levels and spheroid formation when not only horizontal, but also vertical interactions are formed between cells and significant changes in the adhesion properties occur. Cell adhesion is considered to be an important component controlling the interactions between cells and their environment. EGFR has been shown to destabilize E-cadherin-mediated adhesion by enhancing E-cadherin endocytosis, modifying its interaction with the cytoskeleton, and reducing its expression, thereby promoting oncogenesis [25]. To compare the effects of anti-EGFR agents on the levels of certain proteins in MCF7-EGFR spheroids treated with siRNA or cetux-

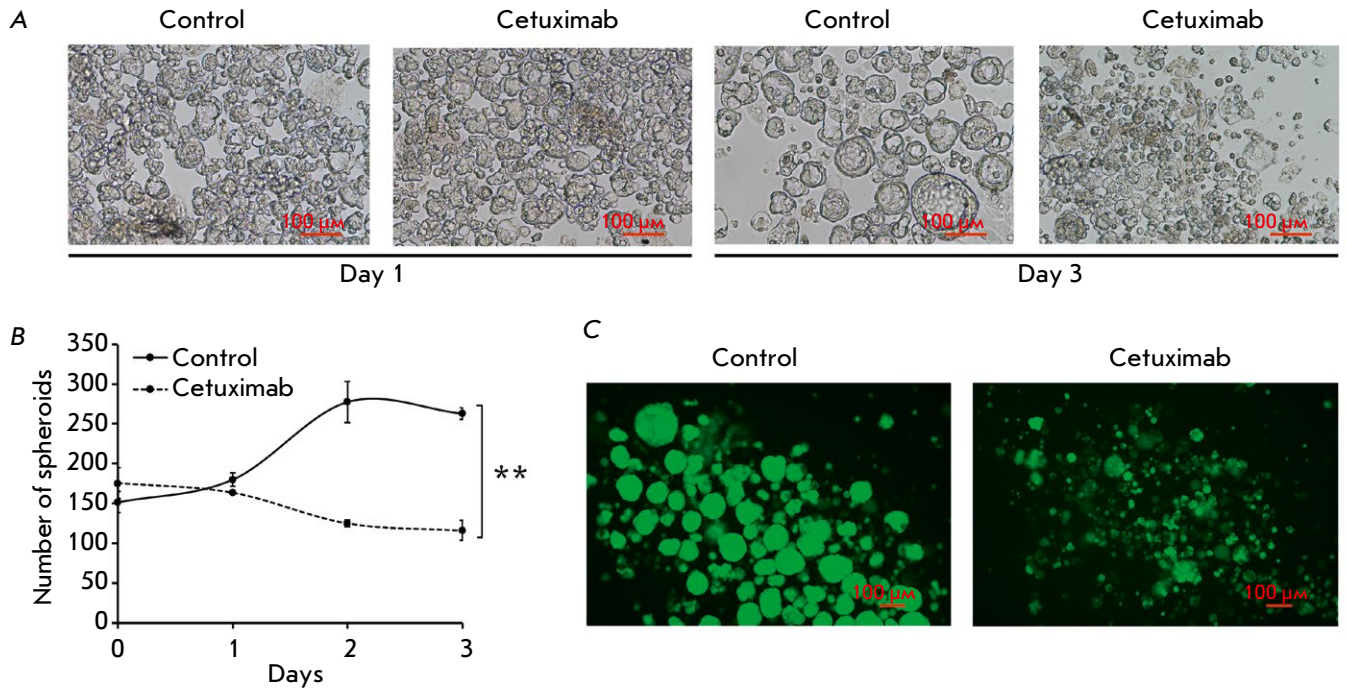

Fig. 6. Analysis of the cetuximab effect on the structure of the MCF7-EGFR spheroids. (*A*) the photographs of the control and cetuximab-treated MCF7-EGFR spheroids. (*B*) the growth kinetics of the MCF7-EGFR spheroids cultured in a medium with and without cetuximab. The spheroids were seeded, treated with cetuximab (50 μg/ml), and counted in the individual wells of 48-well plates, and the number of spheroids per well was indicated. The data are presented as the mean value ± SD of three independent experiments; $^{**}p < 0.01$. (*C*) The microscopic analysis of MCF7-EGFR spheroids treated with cetuximab for 72h and stained with FDA

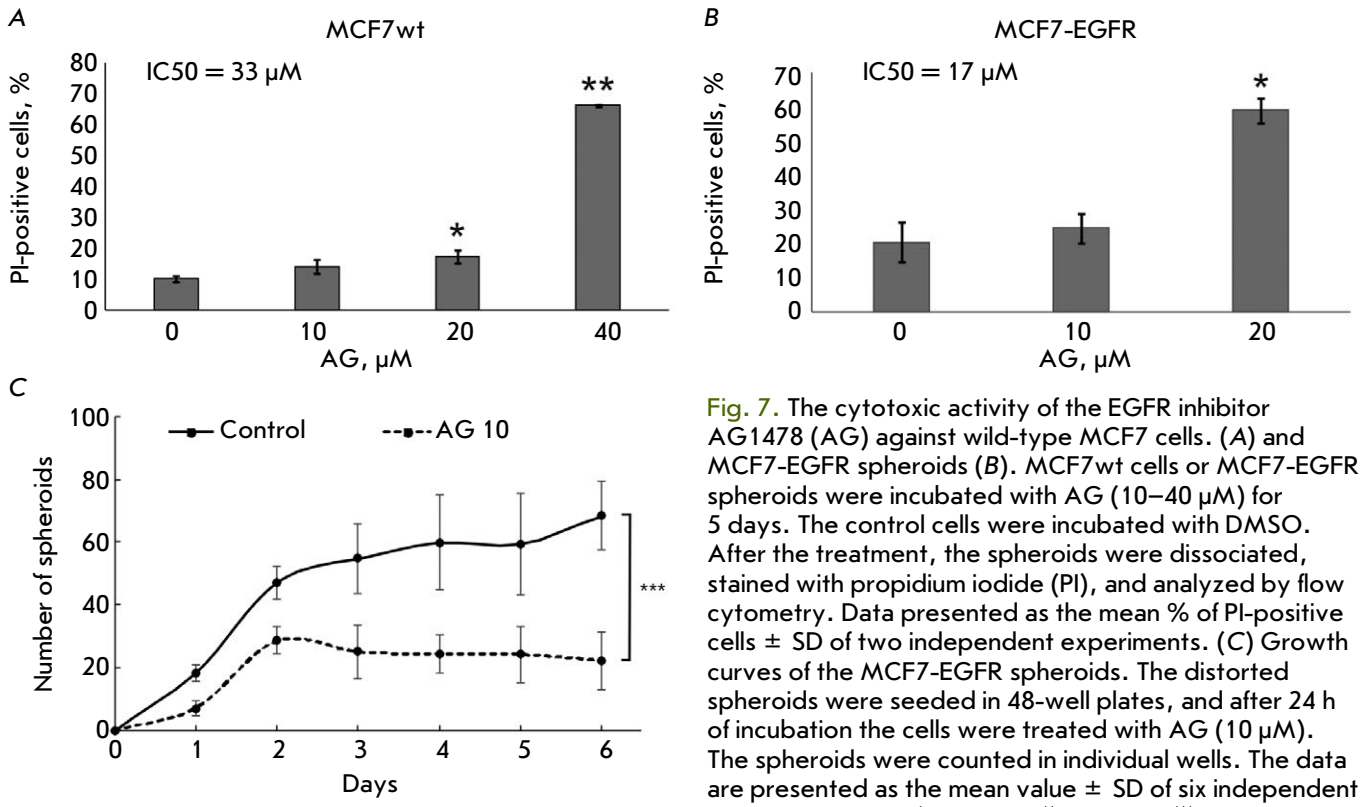

Fig. 7. The cytotoxic activity of the EGFR inhibitor AG1478 (AG) against wild-type MCF7 cells. (*A*) and MCF7-EGFR spheroids (*B*). MCF7wt cells or MCF7-EGFR spheroids were incubated with AG (10–40 μM) for 5 days. The control cells were incubated with DMSO. After the treatment, the spheroids were dissociated, stained with propidium iodide (PI), and analyzed by flow cytometry. Data presented as the mean % of PI-positive cells ± SD of two independent experiments. (*C*) Growth curves of the MCF7-EGFR spheroids. The distorted spheroids were seeded in 48-well plates, and after 24 h of incubation the cells were treated with AG (10 μM). The spheroids were counted in individual wells. The data are presented as the mean value ± SD of six independent experiments, with $^{*}p < 0.05$, $^{**}p < 0.01$, $^{***}p < 0.001$

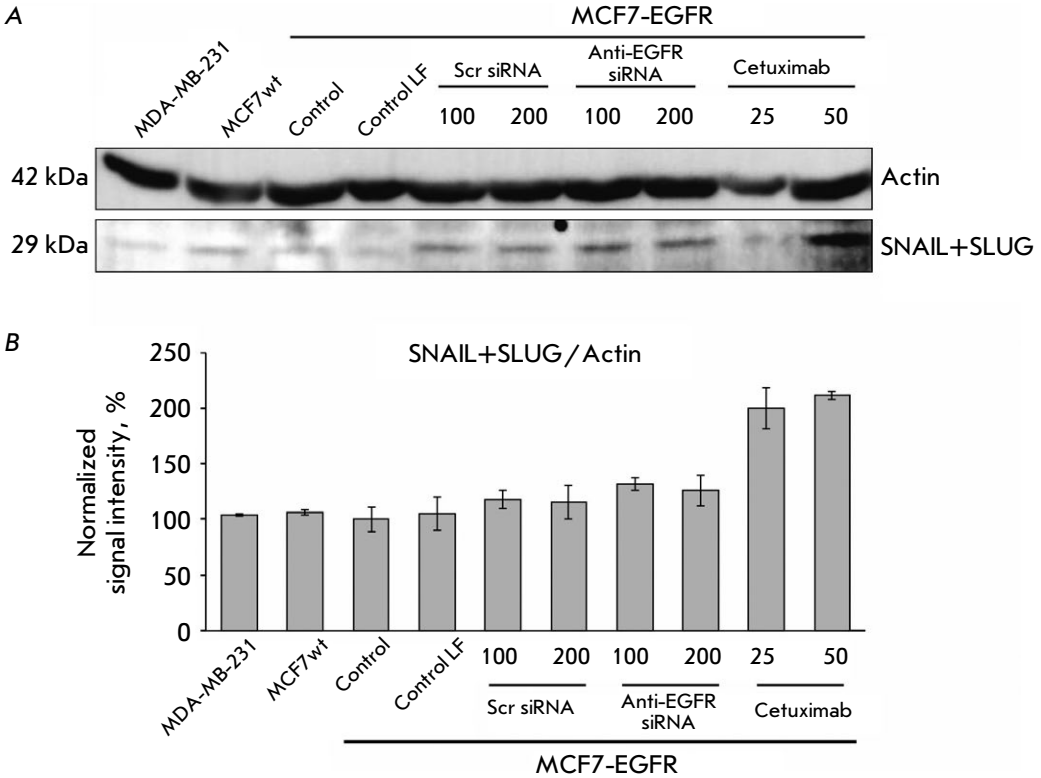

Fig. 8. The changes in cellular proteins after the anti-EGFR siRNA and cetuximab treatment. MDA-MB-231, MCF7wt were used as control cell lines. The MCF7-EGFR spheroids were dissociated and treated with Scramble siRNA, anti-EGFR siRNA (100–200 nM), or cetuximab (25–50 μg/ml) for 48 h. (*A*) the representative pictures of the Western blots analysis. (*B*) the Western blots analysis of SNAIL+SLUG/Actin in the cells

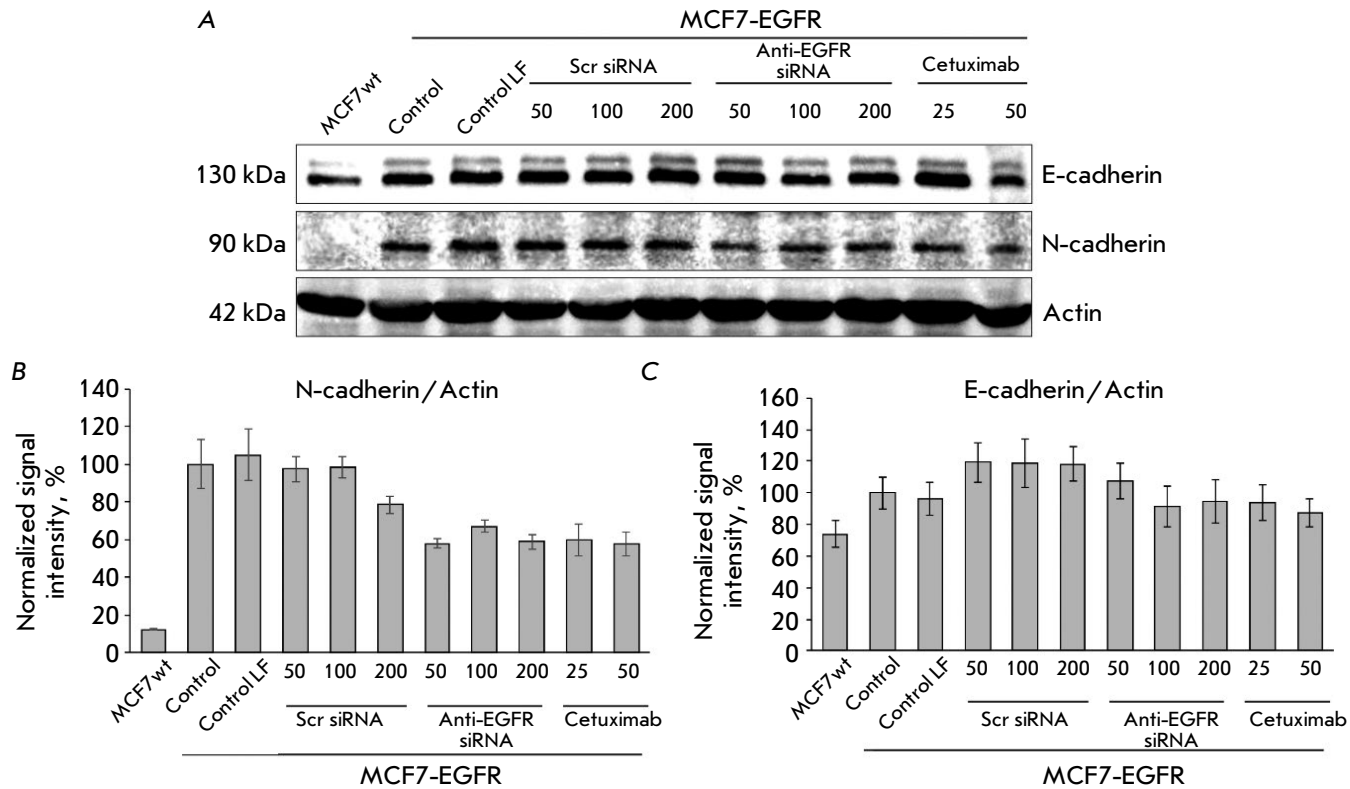

Fig. 9. The changes in cellular proteins after anti-EGFR siRNA and cetuximab treatment. MDA-MB-231, MCF7wt were used as control cell lines. The MCF7-EGFR spheroids were dissociated with accutase and treated with Scramble siRNA (scr siRNA), anti-EGFR siRNA (50–200 nM), or cetuximab (25–50 μg/ml) for 48 h. (*A*) The representative pictures of the Western blots analysis. (*B*, *C*) the Western blots analysis of N-cadherin/Actin (*B*) and E-cadherin/Actin (*C*)

imab and in parental MCF7wt cells, we analyzed the levels of SNAIL/SLUG, N-cadherin, and E-cadherin by Western blotting.

The transcription factors SNAIL and SLUG were reported to be involved in the regulation of epithelial-mesenchymal transition, an important factor in three-dimensional models [26]. We found no differences in the basal level of SNAIL/SLUG proteins between the MCF7wt and MCF7-EGFR cell lines. Although the incubation with siRNA had no effect on the SNAIL/SLUG levels, cetuximab treatment resulted in a twofold increase in the SNAIL/SLUG levels in the MCF7-EGFR cells (*Fig. 8A,B*).

The N-cadherin to E-cadherin ratio in the cell is considered to be an important factor determining intercellular adhesion and spheroid formation [27]. We have found the baseline level of N-cadherin in the MCF7-EGFR cell line to be more than 5-fold higher than that in the original MCF7wt cell line. The anti-EGFR agent treatment led to a decrease in the level of N-cadherin in MCF7-EGFR spheroids (*Fig. 9A,B*). The baseline level of E-cadherin in MCF7-EGFR cells did not differ statistically significantly from that in the MCF7-EGFR spheroids. Moreover, the level of E-cadherin in the MCF7-EGFR spheroids was not affected by the addition of anti-EGFR siRNA or cetuximab (*Fig. 9A,C*).

CONCLUSION

We have revealed the tyrosine kinase receptor EGFR to be involved in the maintenance of MCF7-EGFR cell sphere formation. The importance of EGFR in spheroid formation was confirmed in experiments with EGFR inhibitors. The suppression of EGFR at the stage of individual cells has been demonstrated to reduce spheroid formation, whereas the treatment of already-formed spheroids showed no such effect. We suggest the EGFR expression to be significant, at least at the stage of spheroid formation. For a significant knockdown effect of the EGFR gene using siRNA on large spheroids, the efficiency of the transfection system should be increased. In addition, we have demonstrated the transition of MCF7-EGFR cells into three-dimensional structures to be associated with a significant increase in the expression of the N-cadherin protein. Our findings led us to assume that sphere formation by MCF7-EGFR cells could be partially related to the cellular pathways regulating the epithelial-mesenchymal transition. The results obtained in this study appear to owe in part to the properties of MCF7 cells, with high-EGFR MDA-MB-231 cells not forming spheroids without the addition of growth factors and matrices. Nevertheless, developing such a cell model with abnormal N-cadherin activation is essential for identifying potential molecular targets of tumor progression. Moreover, MCF7-EGFR spheroids are considered to be a model for testing the therapeutic effects of the combination of EGFR and N-cadherin inhibitors. ●

This research was supported by the Russian Science Foundation grant No. 20-74-10039 (cultivation of cancer cells and spheroids), Novosibirsk Government grant No. 7 (Gr-7) (experiments with siRNA,) and the budget funding project No. 121030200173-6 (experiments with cetuximab).

REFERENCES

1. Sporn M.B., Roberts A.B. // Nature. 1985. V. 313. № 6005. P. 745–747.
2. Normanno N. // Front. Biosci. 2001. V. 6. № 1. P. d685.
3. Foley J., Nickerson N.K., Nam S., Allen K.T., Gilmore J.L., Nephew K.P., Riese D.J. // Semin. Cell Dev. Biol. 2010. V. 21. № 9. P. 951–960.
4. Hynes N.E., Lane H.A. // Nat. Rev. Cancer. 2005. V. 5. № 5. P. 341–354.
5. Chidharla A., Parsi M., Kasi A. StatPearls. Treasure Island (FL): StatPearls Publ., 2022.
6. Kirkpatrick P., Graham J., Muhsin M. // Nat. Rev. Drug Discov. 2004. V. 3. № 7. P. 549–550.
7. Brand T.M., Iida M., Wheeler D.L. // Cancer Biol. Therapy. 2011. V. 11. № 9. P. 777–792.
8. Setten R.L., Rossi J.J., Han S. // Nat. Rev. Drug Discov. 2019. V. 18. № 6. P. 421–446.
9. Hu B., Zhong L., Weng Y., Peng L., Huang Y., Zhao Y., Liang X.-J. // Sig. Transduct. Target Ther. 2020. V. 5. № 1. P. 101.
10. Troitskaya O., Novak D., Nushtaeva A., Savinkova M., Varlamov M., Ermakov M., Richter V., Koval O. // IJMS. 2021. V. 22. № 23. P. 12937.
11. Patrakova E.A., Biryukov M.M., Troitskaya O.S., Novak D.D., Milahina E.V., Gugin P.P., Zakrevskiy D.E., Schweigert I.V., Koval O.A. // Cytology. 2023. V. 65. No. 1. P. 398–53.
12. Koval O., Kochneva G., Tkachenko A., Troitskaya O., Sivolobova G., Grazhdantseva A., Nushtaeva A., Kuligina E., Richter V. // BioMed. Res. Internat. 2017. V. 2017. P. 1–14.
13. Zhang C., Yuan W., Wu Y., Wan X., Gong Y. // Life Sci. 2021. V. 266. P. 118886.
14. Nushtaeva A., Ermakov M., Abdurakhmanova M., Troitskaya O., Belovezhets T., Varlamov M., Gayner T., Richter V., Koval O. // IJMS. 2023. V. 24. № 3. P. 2494.
15. Saxon M.L., Lee D.C. // J. Biol. Chem. 1999. V. 274. № 40. P. 28356–28362.
16. Zhao M., Yang H., Jiang X., Zhou W., Zhu B., Zeng Y., Yao K., Ren C. // Mol. Biotechnol. 2008. V. 40. № 1. P. 19–26.

17. Hou K.K., Pan H., Ratner L., Schlesinger P.H., Wickline S.A. // ACS Nano. 2013. V. 7. № 10. P. 8605–8615.
18. Kilroy G., Burk D.H., Floyd Z.E. // PLoS One. 2009. V. 4. № 9. P. e6940.
19. Al-Husaini K., Elkamel E., Han X., Chen P. // Can. J. Chem. Eng. 2020. V. 98. № 6. P. 1240–1254.
20. Morgan R.G., Chambers A.C., Legge D.N., Coles S.J., Greenhough A., Williams A.C. // Sci. Rep. 2018. V. 8. № 1. P. 7952.
21. Baselga J. // Eur. J. Cancer. 2001. V. 37. P. 16–22.
22. Wang M., Chang A.Y.-C. // Oncotarget. 2018. V. 9. № 23. P. 16533–16546.
23. Szabó P., Jordan G., Kocsis T., Posta K., Kardos L., Šajn R., Alijagić J. // Environ. Monit. Assess. 2022. V. 194. № 9. P. 632.
24. Rao T.C., Pui-Yan Ma V., Blanchard A., Urner T.M., Grandhi S., Salaita K., Mattheyses A.L. // J. Cell Sci. 2020. P. jcs.238840.
25. Ramírez Moreno M., Bulgakova N.A. // Front. Cell Dev. Biol. 2022. V. 9. P. 828673.
26. Mikami S., Katsube K.-I., Oya M., Ishida M., Kosaka T., Mizuno R., Mukai M., Okada Y. // Lab. Invest. 2011. V. 91. № 10. P. 1443–1458.
27. Wang M., Ren D., Guo W., Huang S., Wang Z., Li Q., Du H., Song L., Peng X. // Internat. J. Oncol. 2016. V. 48. № 2. P. 595–606.

CRISPR/Cas9 Essential Gene Editing in Drosophila

I. S. Osadchiy, S. O. Kamalyan, K. Y. Tumashova, P. G. Georgiev, O. G. Maksimenko*
Institute of Gene Biology, Russian Academy of Sciences, Moscow, 119334 Russian Federation
*E-mail: maksog@mail.ru
Received: December 08, 2022; in final form, April 04, 2023
DOI: 10.32607/actanaturae.11874

ABSTRACT **Since the addition of the CRISPR/Cas9 technology to the genetic engineering toolbox, the problems of low efficiency and off-target effects hamper its widespread use in all fields of life sciences. Furthermore, essential gene knockout usually results in failure and it is often not obvious whether the gene of interest is an essential one. Here, we report on a new strategy to improve the CRISPR/Cas9 genome editing, which is based on the idea that editing efficiency is tightly linked to how essential the gene to be modified is. The more essential the gene, the less the efficiency of the editing and the larger the number of off-targets, due to the survivorship bias. Considering this, we generated deletions of three essential genes in *Drosophila*: *trf2*, *top2*, and *mep-1*, using fly strains with previous target gene overexpression ("pre-rescued" genetic background).**

KEYWORDS **CRISPR/Cas9, genome editing, essential gene editing, housekeeping genes.**
ABBREVIATIONS **gRNA – guide RNA; chr – chromosome; kb – kilobase; TRF2 – TBP-related factor 2; Top2 – type II topoisomerase; MEP-1 – MOG interacting and ectopic P-granules protein 1.**

INTRODUCTION

Recent advances in the use of CRISPR/Cas9 as a programmable tool for the introduction of DNA double-strand breaks significantly expanded possibilities in deciphering the functions of genes and genomic regulatory elements. The CRISPR/Cas9 system is the most suitable for knocking out a gene of interest (GOI) by generating shifts in the reading frame of the target gene. However, if the GOI is an essential one, attempts to generate a knock-out can be ineffective due to lethality in successfully edited embryos, biological plasticity that rescues the induced frameshift or deletion by translation reinitiation, defective exon skipping, etc. [1]. Here, we report on a case of CRISPR/Cas9 use, in combination with target gene overexpression, that allowed us to quite effectively knock out three essential genes in *Drosophila*. A similar approach has recently been validated in human HEK293T cells [2]. By using this approach, we deleted a relatively long region of the GOI coding sequence and replaced it with a landing platform, which allows for fast and effective insertion of modified gene constructs.

EXPERIMENTAL

The strategy presented here is an addition to the methods described in [3–5] and suitable for ubiquitously expressed essential genes. Our method consists of three steps (*Fig. 1*):

1. Insertion of the GOI copy (lacking CRISPR/Cas9 target sequences) and reporter gene 1 into a "safe harbor" knock-in site located on a different chromosome. This step results in the generation of the rescue line with homologous expression of the GOI copy. For this, we have created rescue constructs carrying protein-coding sequences of either TRF2, Top2, or MEP-1 under the control of the *Ubi-p63E* promoter and the *yellow* gene as reporter 1. Previously obtained knockouts of these genes were embryonic lethal. The constructs were inserted into either 86Fb (TRF2/Top2) or 38D (MEP-1) chromosomal loci via φC31-mediated site-specific integration.

2. Replacement of the GOI with the *attP* site by injection of three plasmids: carrying Cas9 and gRNAs for extensive deletion of the GOI protein-coding sequence and a template plasmid for homology-directed repair (HDR) containing the *attP* site for the φC31 integrase and reporter gene 2 (*mCherry*), flanked by *loxP* sites. This step results in the generation of the GOI knockout line with a GOI copy overexpression background.

In this work, the following CRISPR/Cas9 *Drosophila* strains obtained from The Bloomington *Drosophila* Stock Center at Indiana University were used: BL54591 (*Cas9* under the control of the *nanos* promoter) and BL58492 (*Cas9* under the control of the *Actin5C* promoter). Alternatively, the Addgene

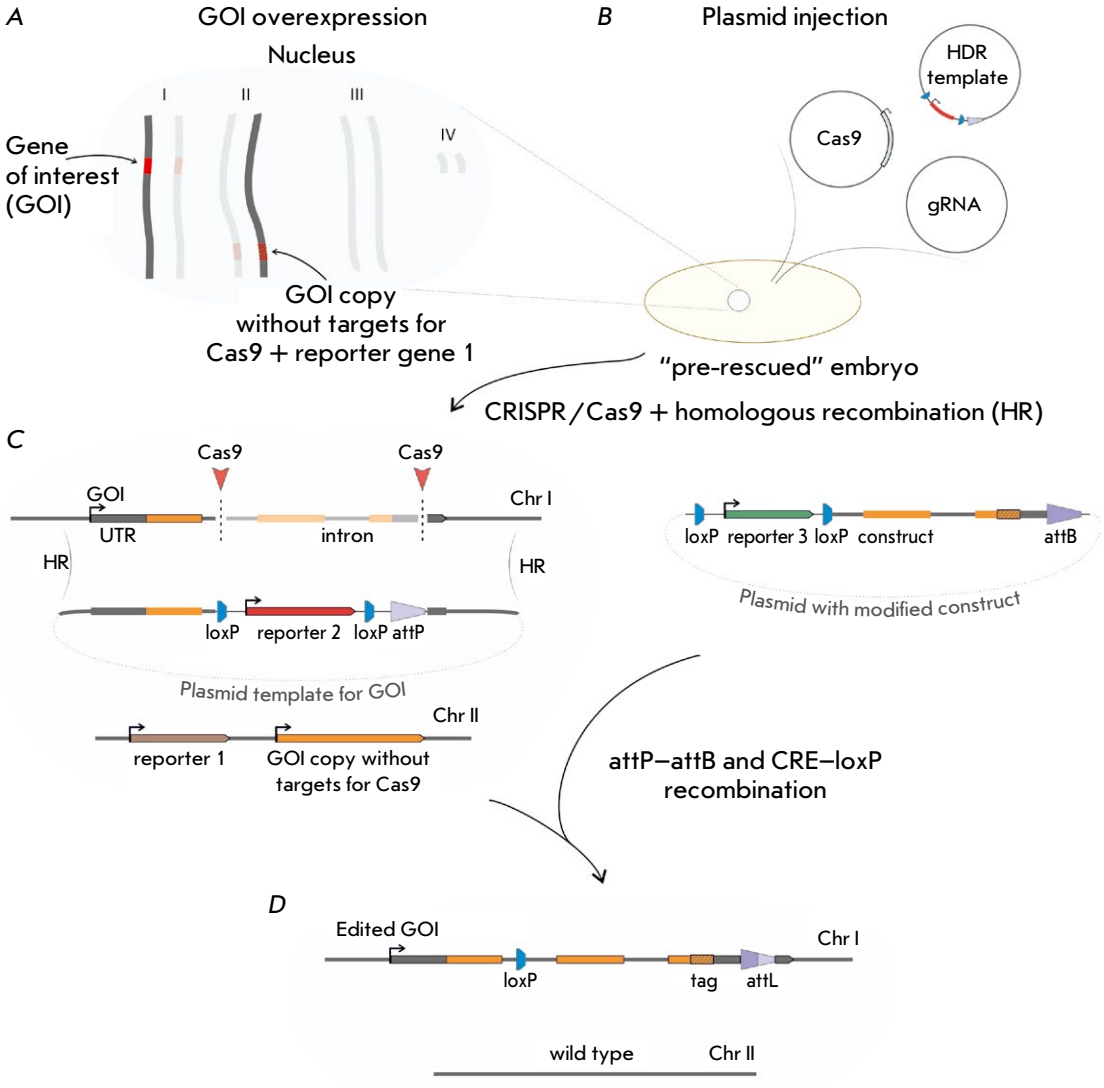

Fig. 1. The strategy for essential gene replacement. (*A*) Insertion of a gene copy lacking targets for Cas9 and reporter gene 1 (*yellow*) into a "safe harbor" knock-in site on a different chromosome via site-specific recombinase-mediated integration (SSRMI). (*B*) Microinjection of an HDR template and plasmids expressing Cas9 and gRNAs into "pre-rescued" embryos. (*C*) CRISPR/Cas9-mediated DNA double-strand breaks and homologous recombination (HR) with the plasmid template carrying *loxP*-flanked reporter gene 2 (*mCherry*) and an *attP* site. (*D*) The result of subsequent SSRMI of the modified gene of interest (GOI) sequence followed by CRE-mediated reporter gene 2 (*mCherry*) and 3 (*white*) excision and removal of the GOI copy

#62209 helper plasmid was added to the injection mixture as a source of Cas9. CRISPR targets were designed using the Optimal Target Finder software (University of Wisconsin) [4] and cloned into the vector based on pCFD4-U6:1_U6:3tandemgRNAs (Addgene #49411). The following gRNAs were used for *trf2* deletion: gRNA1 (tcttcgtgcatactcttagc), gRNA2 (tgcttttcgcttcggtgtcc), and gRNA3 (accaagtagctagagactta); the gRNA1/gRNA2 pair leads to deletion of a 6.7 kb genomic fragment; gRNA1/gRNA3 causes deletion of a 1.1 kb fragment. For *mep-1*, the following gRNAs were used: gRNA1m (acgaacagcagggcgcgcgc), gRNA2m (cagcaagtgacgctggcttg), and gRNA3m (aggggatcttcggcctcgca). They produce 5.6 (gRNA1m/ gRNA2m) and 2 kb (gRNA1m/ gRNA3m) deletions. For *top2* deletion, gRNA1t (gttcccagtacagtagcacc) and gRNA2t (tctacggcgtgttcccgctt) producing a 2 kb deletion were used.

The flies obtained after injection (F0) were individually mated with y^1w^{1118} flies; potential genome editing events in the progeny (F1) were detected by mCherry fluorescence. The insertion of the landing

platform (attP-mCherry) into the genome was confirmed by PCR with primers annealing outside the homology regions used for HDR.

3. Insertion of a modified GOI variant labelled with loxP-flanked reporter gene 3 (*white* gene) via site-specific recombination. Flies were injected with a mixture containing two plasmids: a plasmid with a modified gene variant and the attB site, and the φC31 integrase helper plasmid (Addgene #26290). After integration of the modified variant, reporter genes 2 and 3 were removed by crossing with a Cre recombinase-expressing line.

RESULTS AND DISCUSSION

The TRF2 protein is a paralog of the basal transcription factor TBP; its inactivation is associated with embryonic lethality [6, 7].

Previously, we failed to replace the *trf2* gene with a landing platform for site-specific integration of modified gene variants despite the use of two different Cas9 sources (Cas9-expressing fly lines and the Cas9-expressing plasmid injected into embryos) and two gRNA combinations [8]. The whole *trf2* gene spans approximately 25 kb, while its protein-coding region is roughly 7 kb. The chosen gRNA combinations produced two DNA double-strand breaks at distances of 6.7 and 1.1 kb for deletion and concomitant replacement by the landing platform of the whole protein-coding region or only the start codon-containing region, respectively (*Fig. 2A*).

The results obtained for the different editing schemes used for *trf2* gene replacement are summarized in *Table 1*.

The F0 embryos without background *trf2* overexpression were characterized by a low survival rate. In the developing larvae, *mCherry* reporter fluorescence was observed in tissues in the vicinity of the injection site and throughout the whole embryo. The larvae with the most spread and intense fluorescence died later during development. As a result of mating the surviving F0 flies with the wild-type line, only one fly line with insertion of the landing platform into the intron corresponding to the 5` double-strand break without the deletion of the *trf2* coding region was obtained.

In order to overcome the high lethality rate due to *trf2* deletion, we generated a fly line with *trf2* overexpression by site-specific integration of the *trf2* short isoform using a line with the attP at locus 86Fb.

The *trf2*-overexpressing embryos injected with the gene editing mix had normal viability. As a result, we obtained five fly lines with insertion of the *mCherry* reporter gene for each of the gRNA combinations, producing 6.6 and 1.1 kb deletions, respectively.

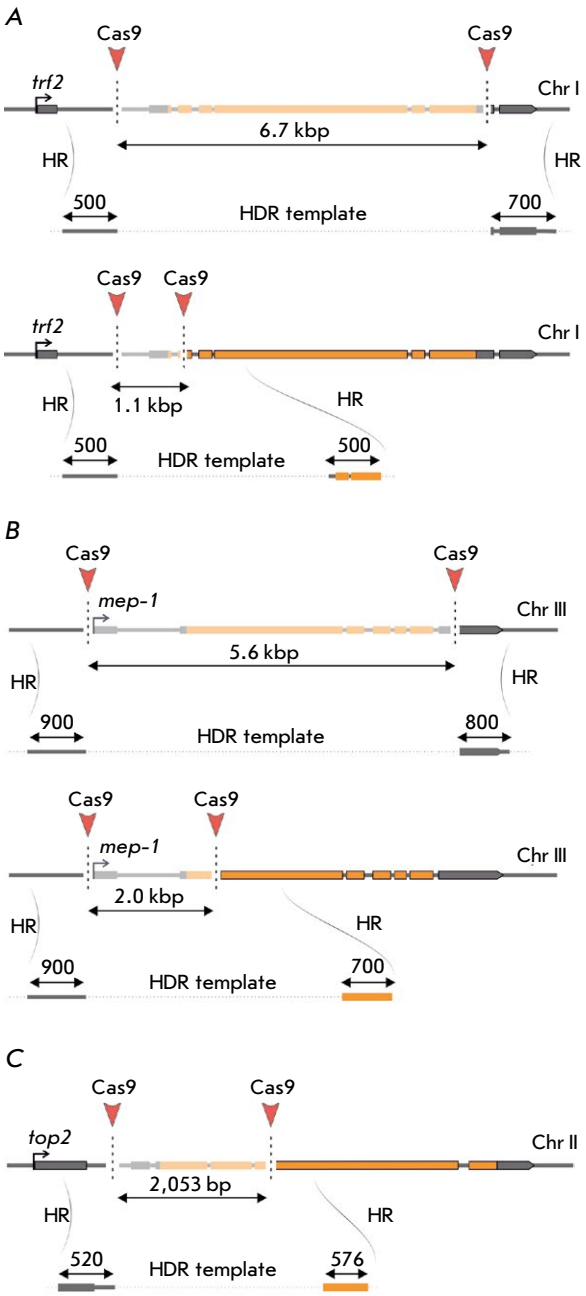

Fig. 2. CRISPR/Cas9- and HDR-mediated gene replacement with the *attP* site and reporter gene *mCherry*. The genes *trf2* (*A*), *mep-1* (*B*), and *top2* (*C*) and homologous recombination templates for either full-length or partial deletions are presented

We additionally validated this approach on other genes: *mep-1* and *top2*.

MEP-1 is a protein that facilitates the recruitment of the nucleosome remodeling and histone deacetylation (dNuRD) complex to many gene promoters [9, 10]. It is an important regulator of early development

Table 1. Results of plasmid microinjections for the replacement of the *trf2*, *mep-1*, and *top2* genomic regions with a landing platform

	Fly line	Cas9 source	Deletion, bp	Embryos injected	Flies eclosed, F0	mCherry+ F1 lines	Off-targets
TRF2	y^1w^{1118}	Cas9-expressing plasmid	6700	200	100	–	–
	54591	Cas9 under *nanos* promoter	6700	250	140	**1**	+
	58492	Cas9 under *Actin5C* promoter	6700	200	80	–	–
			1100	250	120	–	–
	y^1w^{1118} + TRF2 overexpression	Cas9-expressing plasmid	6700	100	80	**5**	2
			1100	100	80	**5**	2
MEP-1	y^1w^{1118}	Cas9-expressing plasmid	2000	300	160	–	–
			5600	150	90	**1**	–
	y^1w^{1118} + MEP-1 overexpression		5600	240	175	**4**	–
TOP2	y^1w^{1118}	Cas9-expressing plasmid	2053	150	100	–	–
	y^1w^{1118} + Top2 overexpression		2053	150	80	**3**	–

in *Drosophila*; *mep-1* gene inactivation leads to embryonic lethality.

As in the case of *trf2*, the selected gRNA combinations resulted in two DNA double-strand breaks spaced 5.6 or 2 kb apart for the full-length and start codon region deletions, respectively (*Fig. 2B*). The results obtained for the different editing schemes used for *mep-1* gene replacement are summarized in *Table 1*.

Embryos injected with the mixture for *mep-1* gene replacement without *mep-1* overexpression background had moderate lethality during development. Mating of F0 flies resulted in only one fly line, which had a long gene deletion. Meanwhile, injection of the embryos with background *mep-1* overexpression led to the generation of four fly lines with the landing platform. Thus, *mep-1* deletion is not completely lethal; however, its overexpression increases the viability of injected embryos and, as a consequence, gene editing effectiveness.

Topoisomerase 2 (Top2) is an enzyme that releases topological tension in the DNA molecule; it contributes to genome stability and participates in key cell processes such as replication, transcription, and recombination [11].

For the replacement of the *top2* gene with the landing platform, we designed a pair of gRNAs targeting Cas9 to the loci 2 kb apart from each other located in 5`UTR and exon 3 of *top2*. The editing plasmid mixture for gene replacement was injected into y^1w^{1118} fly embryos. There were no cases of platform insertion in the progeny of individual matings of F0 with wild type flies. However, editing upon insertion of the Top2 coding sequence in the 86Fb chromosomal locus resulted in three knockout fly lines (*Table 1*).

The use of Cas9 for genome editing is frequently accompanied by additional unspecified mutations throughout the genome. Since mutations usually manifest themselves through phenotype and/or a change in the survival rate, GOI overexpression on a different chromosome allows one to probe the mutations on the GOI chromosome in a line homozygous for GOI deletion. Therefore, it is possible to select only lines without severe mutations.

The generated fly lines homozygous for Δ*trf2*, Δ*mep-1,* or Δ*top2* deletion were lethal without the additional rescuing copy. This corroborated the essentiality of the edited genes and provided initial evidence of successful gene replacement with the *attP*-platform. Site-specific integration of a restoring construct (coding for the wild-type gene variant) into the corresponding landing platform line and subsequent removal of the reporter genes led to the recovery of gene function and normal viability of homozygous flies lacking the rescuing copy. Thus, overexpression induced prior to gene editing allowed us to obtain landing platforms for a detailed study of three *Drosophila* proteins: TRF2, Top2, and Mep-1. ●

This work was supported by the Russian Science Foundation (grant No. 19-74-30026).

REFERENCES

1. Smits A.H., Ziebell F., Joberty G., Zinn N., Mueller W.F., Clauder-Münster S., Eberhard D., Fälth Savitski M., Grandi P., Jakob P., et al. // Nat. Methods. 2019. V. 16. № 11. P. 1087–1093.
2. Wang B., Wang Z., Wang D., Zhang B., Ong S.G., Li M., Yu W., Wang Y. // J. Biol. Eng. BioMed Central. 2019. V. 13. № 1. P. 35.
3. Gratz S.J., Ukken F.P., Rubinstein C.D., Thiede G., Donohue L.K., Cummings A.M., O'Connor-Giles K.M. // Genetics. 2014. V. 196. № 4. P. 961–971.
4. Zolotarev N., Georgiev P., Maksimenko O. // Biotechniques. Future Science. 2019. V. 66. № 4. P. 198–201.
5. Bischof J., Maeda R.K., Hediger M., Karch F., Basler K. // Proc. Natl. Acad. Sci. USA. 2007. V. 104. № 9. P. 3312–3317.
6. Kedmi A., Zehavi Y., Glick Y., Orenstein Y., Ideses D., Wachtel C., Doniger T., Waldman Ben-Asher H., Muster N., Thompson J., et al. // Genes Dev. 2014. V. 28. № 19. P. 2163–2174.
7. Duttke S.H.C. // Trends Biochem. Sci. 2015. V. 40. № 3. P. 127–129.
8. Osadchiy I.S., Georgiev P.G., Maksimenko O.G. // Dokl. Biochem. Biophys. 2019. V. 486. № 1. P. 224–228.
9. Reddy B.A., Bajpe P.K., Bassett A., Moshkin Y.M., Kozhevnikova E., Bezstarosti K., Demmers J.A., Travers A.A., Verrijzer C.P. // Mol. Cell. Biol. Am. Soc. Microbiol. 2010. V. 30. № 21. P. 5234–5244.
10. Kunert N., Wagner E., Murawska M., Klinker H., Kremmer E., Brehm A. // EMBO J. 2009. V. 28. № 5. P. 533–544.
11. Sutormin D.A., Galivondzhyan A.K., Polkhovskiy A.V., Kamalyan S.O., Severinov K.V., Dubiley S.A. // Acta Naturae. 2021. V. 13. № 1. P. 59–75.

Cell Therapy: A New Technology for Cerebral Circulation Restoration after Ischemia/Reperfusion

I. B. Sokolova*, O. P. Gorshkova
Pavlov Institute of Physiology, Russian Academy of Sciences, St. Petersburg, 199034 Russian Federation
*Email: SokolovaIB@infran.ru
Received: February 07, 2023; in final form, April 07, 2023
DOI: 10.32607/actanaturae.14338

ABSTRACT **Cell therapy with mesenchymal stem cells (MSCs) may be a promising technique for cerebral blood flow restoration after transient ischemia. Before a practical application of the cell material, 7–9 days are required for its cultivation. We studied the efficacy of human MSC (hMSC) transplantation performed 7 days after cerebral ischemia/reperfusion (I/R) to help recover cerebral circulation. The intravital micrograph technique was used to comparatively evaluate the vasculature density in the pia mater and the reactivity of the pial arteries in response to acetylcholine (ACh) in rats after I/R (clamping of both carotid arteries and a simultaneous decrease in and strict maintenance of the mean BP at 45 ± 2 mm Hg for 12 min) and with/without hMSC transplantation. Perfusion (P) in the sensorimotor cortex was assessed using laser dopplerography. After 14 and 21 days, the vasculature density in I/R-affected rats was 1.2- to 1.4-fold and 1.2- to 1.3-fold lower, respectively, than that in the controls. The number of ACh-dilated arteries decreased 1.6- to 1.9-fold and 1.2- to 1.7-fold 14 and 21 days after I/R, respectively. After 21 days, the P level decreased 1.6-fold, on average. Administration of hMSCs on day 7 after I/R resulted in complete recovery of the vasculature density by day 14. ACh-mediated dilatation fully recovered only in arteries of less than 40 μm in diameter within 21 days. After 21 days, the P level was 1.2-fold lower than that in the controls but significantly higher than that in rats after I/R without hMSCs. Delayed administration of MSCs after a transient cerebral ischemic attack affords the time for the procedures required to prepare cell material for transplantation and provides a good therapeutic response in the pial microvasculature.**
KEYWORDS **ischemia/reperfusion, brain, intravenous transplantation, mesenchymal stem cells, microvascular density, reactivity, perfusion.**
ABBREVIATIONS **BP – blood pressure; I/R – ischemia/reperfusion; SOR – sham-operated rat; MSCs – mesenchymal stem cells; hMSCs – human mesenchymal stem cells; P – perfusion; ED – endothelial dysfunction; ACh – acetylcholine.**

INTRODUCTION

Today the concept of a neurovascular unit (NVU) is widely used in the study of ischemic brain pathologies [1]. NVU is a structural and functional unit that comprises neurons, glial cells, astrocytes, pericytes, and vessels that provide gas and metabolic exchange [2]. NVU is involved in the regulation of the blood flow through the contractility of pericytes in the capillary bed [3] and smooth muscle cells (SMCs) in the arterial walls [4]. The key factor in NVU recovery after transient ischemia is the reactivity of NVU arteries [5]. Cell therapy using mesenchymal stem cells (MSCs) may be one of the most promising modern techniques to restore the structure and ability to function of the brain vasculature after transient ischemia [6]. However, practical application of cell material requires time to culture MSCs. If the patient's MSCs are isolated in advance and stored in a cryobank, it would take 7–9 days to produce the required amount of cell material [7].

The aim of this study was to elucidate the effect of intravenous hMSC transplantation, which was performed 7 days after ischemia/reperfusion, on the vasculature density, pial artery reactivity, and tissue perfusion in the cerebral cortex 14 and 21 days after ischemia.

MATERIALS AND METHODS

The study was performed in animals received from the Center for Collective Use "Biocollection of the Pavlov Institute of Physiology of the Russian Academy of Sciences for the Investigation of the Integrative Mechanisms of Nervous and Visceral System Activity" (Saint-Petersburg). The study was conducted in accordance with the regulations of the Ministry of Health and Social Development of the Russian Federation No. 708n of August 23, 2010 "Rules for Laboratory Practice", Directive 2010/63/EU of the European Parliament and the Council of the European Union on the protection of animals used for scientific purposes, and the requirements of the Commission for Control over the maintenance and use of laboratory animals at the Pavlov Institute of Physiology of the Russian Academy of Sciences (protocol No. 09/05 of 05.09.2022).

Animals

The experiments were performed on male Wistar rats (n = 68). The animals were housed under standard vivarium conditions with natural light and free access to water and food.

Ischemia/reperfusion

Ischemia was induced in chloral hydrate-anesthetized rats (intraperitoneally, 43 mg/100 g of body weight) by 12-minute occlusion of both carotid arteries and simultaneous controlled hypotension (reduction and strict maintenance of blood pressure (BP) at 45 ± 2 mm Hg by drawing/reinfusion of blood into a heparinized syringe). BP was directly measured through a femoral artery catheter connected to a DTX Plus™ transducer (Argon Critical Care Systems, Singapore) attached to a computer running original BP monitoring software developed in our laboratory. After the ischemia period, the withdrawn blood was completely reinfused. After suturing the surgical wounds and anesthesia recovery (on heated tables), the animals were returned to their standard cages.

MSCs and their transplantation

hMSCs derived from a single donor were used for intravenous transplantation. MSC isolation from the bone marrow, culturing, and phenotyping were performed at Trans-Technologies LLC according to minimally modified standard procedures [8, 9]. In particular, hMSCs were cultured using α-MEM nutrient medium (Hyclone, New Zealand) supplemented with 20% fetal bovine serum (Gibco, USA) and 100 μg/mL penicillin/streptomycin (Gibco, USA). hMSCs were phenotyped using flow cytometry on a FACSscan flow cytometer (Becton Dickinson, USA). hMSCs were stained with anti-positive CD90, CD105, CD44, and CD73 and negative CD45, CD34, CD14, CD11b, HLA-DR, and 7AAD marker antibodies (Becton Dickinson, USA). MSCs at passage 2 or 3 were used for the transplantation. Intravenous transplantation was performed in separate groups of rats on day 7 after cerebral I/R. Each animal was injected with 5 million hMSCs in 30 μL of the culture medium.

All subsequent surgical and experimental procedures were performed on anesthetized (Zoletil, 20 mg/kg, ip, Virbac, France) rats; euthanasia was performed by administration of an increased Zoletil dose.

Animal groups

1. Control group: sham-operated (SO) Wistar rats that underwent surgery without I/R. The vasculature density, pial artery reactivity, and perfusion in the sensorimotor cortex in this and all subsequent groups in separate animal subgroups (acute experiments) were studied 14 and 21 days after surgery. Rat weight and BP were 303 ± 12.7 g and 133 ± 5 mm Hg, respectively, on day 14 (n = 10) and 330 ± 12.2 g and 135 ± 2 mm Hg, respectively, on day 21 (n = 9).

2. Wistar rats that underwent brain I/R. Weight and BP were 256 ± 5 g and 133 ± 5 mm Hg, respectively, on day 14 (n = 8) and 318 ± 4 g and 124 ± 4 mm Hg, respectively, on day 21 (n = 9).

3. Wistar rats that underwent brain I/R and were intravenously injected with hMSCs on day 7. Weight and BP were 340 ± 4.5 g and 128 ± 4 mm Hg, respectively, on day 14 (n = 10) and 336.7 ± 8.4 g and 132 ± 3.1 mm Hg, respectively, on day 21 (n = 10).

Imaging and monitoring of the microvasculature

A hole (S ≈ 1 cm^2) was drilled in the parietal area of the animal's skull to intravitally monitor pial artery response. The dura mater within the hole was removed, thereby opening the area for further study. The brain surface was continuously irrigated with a Krebs solution (pH 7.4) at 37°C. The mean BP was monitored and maintained at an approximately constant level throughout the experiment. The body temperature of the animals was maintained at 38°C throughout the experiment. Perfusion (P) in the cerebral cortex tissue was measured using a multifunctional laser diagnostic complex LAKK-M (LAZMA, Russia). A sensor of the device was placed at 3 points over the sensorimotor cortex with approximate coordinates AP = 1, 2, and 3 mm from the bregma; SD = 1.0 mm lateral to the sagittal suture. The LAKK-M complex software automatically calculated the mean microcirculation P.

The pial arteries were visualized in the same experimental animals using an original setup that included an MC-2ZOOM stereoscopic microscope (Micromed, Russia), a DCM-510 SCOPE digital camera for a microscope (Scopetek, China), and a personal computer. The number of arteries and the total number of vessels in a certain area were evaluated in static images using the PhotoM cytophotometry software (developed by A. Chernigovsky, http://www.t_lambda.chat.ru). The vasculature density was calculated as the vessel number to area ratio (units/μm^2). Then, pial artery diameters were measured. During the experiment, 40 to 120 pial arteries were examined in each animal. The diameter of the arteries was measured under standard conditions under continuous irrigation of the brain surface with the Krebs solution and an acetylcholine (ACh) solution (10^{-7} M) (Sigma-Aldrich, USA). All examined pial arteries were divided into groups according to their diameters: 60–80 μm, 40–60 μm, 20–40 μm, and less than 20 μm. The effect of ACh was assessed based on the number of dilated arterial vessels and their degree of dilatation. A change in the number of ACh-dilated vessels was expressed as a percentage of the total number of examined vessels in a group. The degree of dilatation ΔD was assessed as the difference in diameters after (D2) and before (D1) exposure to ACh divided by the vessel diameter D1 before exposure, %:

$$\Delta D = (D2 - D1)/D1 \times 100.$$

If a diameter change was less than 5.0 ± 0.5%, it was considered as a lack of response. As we had previously found, this value was detected at rest in the lack of any exposure. Data for each group of vessels from different animals were averaged for a separate experimental group of rats and used for statistical comparisons.

Statistical evaluation of data

Mathematical data processing was performed using the Microsoft Excel 2003 statistical package and InStat 3.02 software (GraphPad Software Inc., USA). The data are presented as the arithmetic mean and its error. Testing of experimental data for normal distribution was carried out using the Kolmogorov–Smirnov test. The means of independent samples with a normal distribution were compared using the analysis of variance, followed by pairwise comparison of the groups using the Tukey's test. If the sample distribution was not normal, the groups were compared using the Kruskal–Wallis test, followed by pairwise comparison using the Mann–Whitney U-test. Differences were considered significant at a confidence level of more than 95% ($p < 0.05$).

RESULTS

Flow cytometry analysis revealed that the hMSC culture was comprised of 99.7% $CD90^+$, $CD73^+$, $CD105^+$, and $CD44^+$ cells (true MSCs); 0.3% of $CD45^+$ and $CD34^+$ cells (hematopoietic cells); and 0.5% of $CD14^+$, $CD11b^+$, and $HLA\text{-}DR^+$ cells. The $7AAD^+$ (non-viable) cells accounted for less than 0.9–1%.

The microvasculature density in the pia mater of the sensorimotor cortex in the SO and I/R rats is shown in *Fig. 1*. The microvasculature density and the arterial vessel density in the I/R group were lower, 1.4-fold and 1.2-fold, respectively, than those in the SO group 14 days after I/R and 1.2-fold and 1.3-fold, respectively, 21 days after I/R. The microvasculature density in the pia mater of I/R group animals subjected to intravenous hMSC transplantation was the same as that in the SO rats both on days 14 and 21 after I/R.

In the I/R group (the animals not treated with cell therapy), application of Ach to the brain surface significantly deteriorated the pial artery reactivity (*Fig. 2*). In the rats from group 2, the number of Ach-dilated arterial vessels (an increase in the diameter) was 1.8-fold and 1.3- to 2.1-fold, on average, less than that in the SO rats after 14 and 21 days, respectively.

In the group of animals injected with hMSCs on day 7 after I/R, the dilatation response of large pial arteries (> 40 μm in diameter) was 1.3- to 2-fold, on average, lower than that in the SO rats; i.e., approximately the same as in the animals of the 2nd group 14 days after I/R (7 days after hMSC injection). The number of ACh-dilated arteries with a diameter of 20–40 μm was lower (1.3-fold, on average) than that in the SO rats and higher than that in group 2 (1.4-fold, on average). In the smallest arteries (< 20 μm in diameter), the dilatation response to ACh fully recovered to the level of that in the SO rats. The reactivity of the largest arteries (60–80 μm in diameter) had not recovered by day 21 after I/R (14 days after hMSC injection). The number of ACh-dilated arteries with a diameter of 20–60 μm was almost identical to that in the SO rats; this indicator for the vessels with a diameter of less than 20 μm was statistically significantly higher than that in the SO group. There were no differences between the groups in the degree of diameter changes (data not shown).

After 14 days, the P level in the sensorimotor cortex tissue in all I/R animals was still approximately identical to that in the SO rats (*Fig. 3*). On day 21, a significant decrease in P (1.6-fold, on average) was observed in group 2. In the animals from the cell

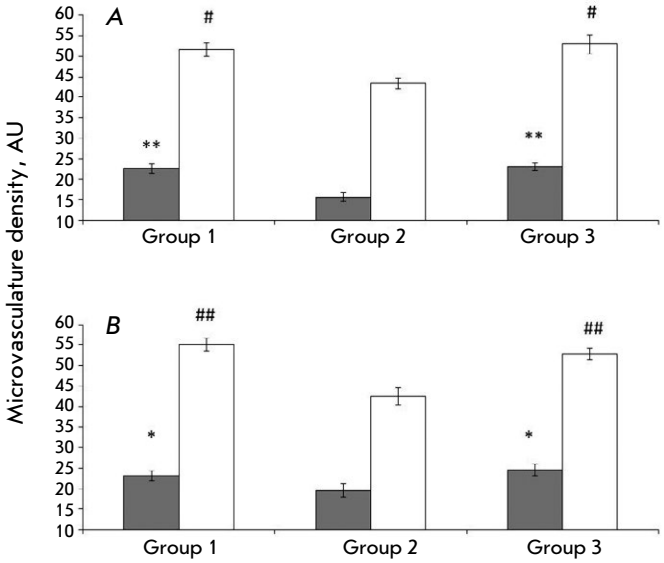

Fig. 1. Indicator of the vascular bed density of the sensorimotor cortex pial membrane in the experimental animals. (*A*) – 14 days after I/R, (*B*) – 21 days after I/R. *Dark columns* – the artery density; *light columns* – the density of the all-vascular network.
Horisontally – experimental animals groups; *vertically* – indicator of the microvascular bed density (number of vessels / unit area).
* – changes in the arterial density are significant compared to the corresponding values in the animals after I/R;
# – changes in the density of the all-vascular network are significant compared to the corresponding values in the animals after I/R (*,# $p < 0.05$, **,## $p < 0.01$, Tukey test)

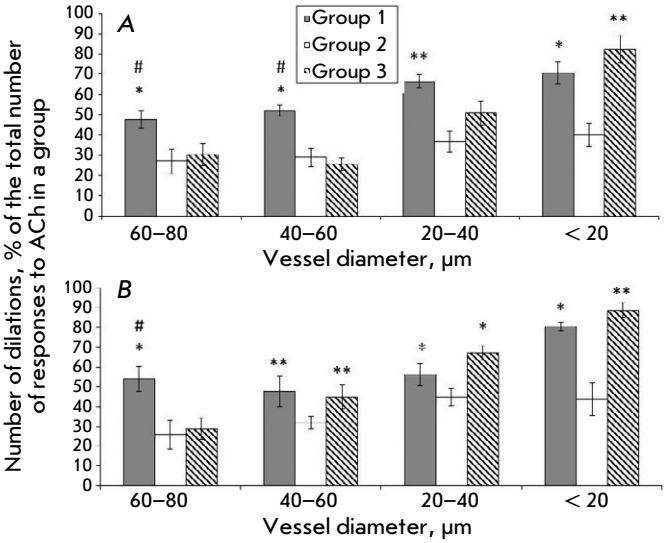

Fig. 2. The number of pial arteries that responded with dilation to the effects of ACh. (*A*) – 14 days after I/R, (*B*) – 21 days after I/R. *Dark columns* – sham-operated rats, *light columns* – rats after I/R, *oblique hatching* – rats after I/R, with intravenous transplantation of MSCc 7 days after I/R. *Horizontally* – vessels diameter, *vertically* – number of vessels dilated in response to ACh, % of the total number of reactions to ACh in the group.
* – significant changes in comparison with the corresponding values in the rats after I/R; # – significant changes in comparison with the corresponding values in the rats after I/R, with intravenous transplantation of MSCc 7 days after I/R (*,#$p < 0.05$, **$p < 0.01$, Tukey test)

therapy groups, a decrease in P, but less significant (1.2-fold, on average), was also detected on day 21 after ischemia.

DISCUSSION

The introduction of cellular technologies in medical practice requires that we develop techniques for the transplantation of MSCs that are quite remote from the site of the transient ischemia, ischemic stroke, brain injury, etc. However, treating these brain pathologies with MSCs requires accounting for the permeability of the blood–brain barrier for these cells. There is data in the literature indicating that there is an increase in the permeability of the blood–brain barrier during the first 7 days after I/R [10], which enables venously transplanted MSCs to migrate to the brain. MSCs, administered intravenously 24 h after occlusion of the middle cerebral artery, have been experimentally shown to migrate into the damaged brain tissue and appear in the walls of penumbra vessels [11]. Increased levels of the vascular endothelial growth factor (VEGF) and hypoxia-induced factor (HIF-1α) have been observed in the same area. MSCs secrete factors that promote tissue neovascularization: fibroblast growth factor 2 (FGF-2), VEGF, transforming growth factor (TGFβ), interleukins IL-6 and IL-8, angiogenin, hepatocyte growth factor (HGF), and platelet-derived growth factor (PDGF BB) [12]. In addition to angiogenesis activation, MSCs can protect cerebral vascular cells after an ischemic stroke [13, 14].

In this study, we were able to show that the vasculature density in the pia mater of rats transplanted with hMSCs on day 7 after I/R was approximately identical to that in the SO animals (*Fig. 1*) on days 14 and 21 after ischemia. I/R is known to be followed by the formation of ischemic areas in brain tissue [15, 16, 6]. Tissue ischemia stimulates the proliferation of hMSCs and enhances their paracrine function [17]. MSCs cultured under hypoxic conditions increase the production of the vascular endothelial growth factor (VEGF) and hypoxia-induced factor (HIF-1α) [18]. We contend that the recovery of the vasculature structure, following hMSC transplantation on day 7 after I/R in our experiments, occurred due to hMSC-acti-

vated angiogenesis. This insight is also confirmed by the ACh-induced reactivity of the pial arteries. We showed that ACh-mediated dilatation of large arteries (> 60 μm in diameter) did not recover after 14 or 21 days (*Fig. 2*). The dilatation response of arteries with a diameter of 20–40 μm was lower than that in the animals in the control group on day 14. Probably, damaged endothelial cells in the large vessels failed to recover due to the administration of hMSCs 7 days after I/R. In the smallest arteries (< 20 μm in diameter), the reactivity was the same as that in the control group as early as on day 14 (i.e., 7 days after administration of hMSCs). On day 21, the number of ACh-induced dilatations was statistically greater than that in the control group and the group of cell therapy performed on the day of the I/R. This confirms the activation of angiogenesis in ischemic brain tissue after hMSC transplantation on day 7 after I/R. In this case, there was also a paracrine therapeutic effect on the vascular wall. This is seen in arteries with a diameter of 20–60 μm, in which reactivity had not recovered to its control level by day 14 after I/R and was identical to that in the SO group by day 21 (14 days after administration of hMSCs) (*Fig. 2*). Probably, the ability to function of the endothelial cells in these vessels was damaged by I/R, but the cells survived and were able to recover thanks to MSC-secreted trophic factors [19, 20]. For example, increased production of HIF-1α may be considered as a therapeutic effect after I/R. In ischemic tissue, HIF-1α stimulates enhanced expression of the genes that provide cell adaptation to hypoxia and regulate vascular tone, cell proliferation, and apoptosis [21].

Restoration of the structure and functionality of the vasculature after I/R is very important for maintaining the physiological level of a cerebral blood flow rate. After a brief ischemic attack, when the cerebral blood flow rate abruptly falls, reperfusion leads to hyperemia. After 7–14 days, the blood flow rate usually drops to its initial level, but not always. This requires normalization of the blood gas composition (pO_2 and pCO_2) and acid-base balance (pH), activation of secondary angiogenesis, and restoration of a balanced production of vasoconstrictors and vasodilators by endothelial cells [22]. However, in a real-world situation, there may be a decrease in the microvasculature density, endothelial dysfunction (as in this study), compression of the vessel lumen by swollen processes of astrocytes, and intravascular accumulation of erythrocytes, platelets, and leukocytes in the brain by day 21 after I/R [23]. These developments worsen cerebral circulation. The use of hMSCs on day 7 after I/R maintained tissue perfusion (an integral indicator of blood circulation) at a higher level than that in the non-treated rats (*Fig. 3*).

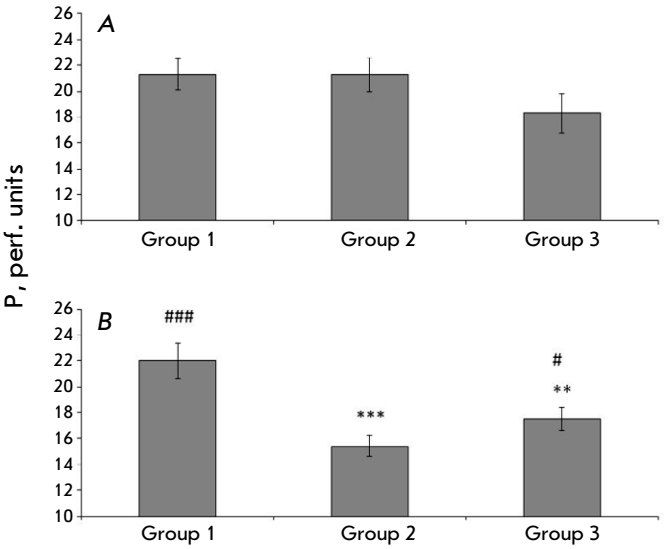

Fig. 3. Changes in the perfusion index in the sham-operated and ischemic rats. (*A*) – 14 days after I/R, (*B*) – 21 days after I\R. *Horizontally* – groups of experimental animals; *vertically* – perfusion (perf. units). ** – significant changes in comparison with the corresponding values in the sham-operated rats of this group; # – significant changes in comparison with the corresponding values in the rats after I/R ($^{\#}p < 0.05$, $^{**}p < 0.01$, $^{***,\#\#\#}p < 0.001$, Mann-Whitney U-test)

CONCLUSION

We found that intravenous transplantation of hMSCs on day 7 after I/R led to good therapeutic results: the animals retained/recovered the vasculature structure in the pia mater. Delayed administration of MSCs 7 days after a transient ischemic attack buys time for the procedures required for the production of cell material for transplantation and completely restores arterial reactivity in the microcirculatory region of the pial vasculature. ●

The authors are very grateful to Trans-Technologies LLC and personally to the General Director, Mr. D.G. Polyntsev, for providing cell material for the study.
There is no conflict of interest.
This study was supported by State Program 47 GP "Scientific and technological development of the Russian Federation" (2019–2030), topic 0134-2019-0001.

REFERENCES

1. Sato Y., Falcone-Juengert J., Tominaga T., Su H., Liu J. // Nat. Rev. Neurol. 2022. V. 11. № 18. P. 2823.
2. Schaeffer S., Iadecola C. // Nat. Neurosci. 2021. V. 24. № 9. P. 1198–1209.
3. Iadecola C. // Nat. Rev. Neurosci. 2004. V. 5. P. 347–360.
4. Jaminon A., Reesink K., Kroon A., Schurgers L. // Int. J. Mol. Sci. 2019. V. 20. № 22. P. 5694.
5. Tiedt S., Buchan A., Dichgans M., Lizasoain I., Moro M., Lo E. // Nat. Rev. Neurol. 2022. V. 18. № 10. P. 597–612.
6. Sokolova I.B., Gorshkova O.P., Pavlichenko N.N. // Cell Tissue Biol. 2022. V. 16. № 1. P. 32–37.
7. Lin Q., Tang X., Lin S., Chen B., Chen F. // Neural Regen. Res. 2020. V. 15. № 2. P. 324–331.
8. Mushahary D., Spittler A., Kasper C., Weber V., Charwat V. // Cytometry A. 2018. V. 93. № 1. P. 19–31.
9. Li X., Xie X., Yu Z., Chen Y., Qu G., Yu H., Luo B., Yifeng Lei Y., Li Y. // J. Cell. Physiol. 2019. V. 234. № 10. P. 18906–18916.
10. Kangussu L.M., Almeida-Santos A.F., Fernandes L., Alenina N., Bader M., Santos R., Massensini A., Campagnole-Santos J. // Brain Res. Bull. 2023. № 192. P. 184–191.
11. Sheikh A., Yano S., Mitaki S., Haque Md.A., Yamaguchi S., Nagai A. // Exp. Neurol. 2019. № 311. P. 182.
12. Han Y., Yang J., Fang J., Zhou Y., Candi E., Wang J., Hua D., Shao C., Shi Y. // Signal Transduct. Target Ther. 2022. V. 7. № 1. P. 92.
13. Afra S., Matin M. // Cell Tissue Res. 2020. V. 380. № 1. P. 1–13.
14. Liu K., Guo L., Zhou Z., Pan M., Yan C. // Microvasc. Res. 2019. № 123. P. 74.
15. Vrselja Z., Daniele S.G., Silbereis J., Talpo F., Morozov Y.M., Sousa A.M., Tanaka B.S., Skarica M., Pletikos M., Navjot Kaur N., et al. // Nature. 2019. V. 568. № 7752. P. 336–343.
16. Cao L., Miao M., Qiao J., Bai M., Li R. // Saudi J. Biol. Sci. 2018. V. 25. № 6. P. 1170–1177.
17. Yu H., Xu Z., Qu G., Wang H., Lin L., Li X., Xie X., Lei Y., He X., Chen Y., Li Y. // Cell Mol. Neurobiol. 2021. V. 41. № 3. P. 505–524.
18. Xu W., Xu R., Li Z., Wang Y., Hu R. // J. Cell. Mol. Med. 2019. V. 23. № 3. P. 1899–1907.
19. Gao Y., Chen H., Cang X., Chen H., Di Y., Qi J., Cai H., Luo K., Jin S. // Front. Cell Dev. Biol. 2022. № 10. P. 1016597.
20. Liu Y., Zhao Y., Yu Min Y., Guo K., Chen Y., Huang Z., Long C. // Int. J. Stem. Cells. 2022. V. 15. № 2. P. 217–226.
21. Han Y., Yang J., Fang J., Zhou Y., Candi E., Wang J., Hua D., Shao C., Yufang Shi Y. // Signal Transduct. Target Ther. 2022. V. 7. № 1. P. 92.
22. Kang P., Ying C., Chen Y., Ford A. L., An H., Lee J. // Stroke. 2022. V. 53. № 5. P. 1570–1579.
23. Bai J., Lyden P.D. // Int. J. Stroke. 2015. № 10. P. 143.

Search for Inhibitors of *Mycobacterium tuberculosis* Transketolase in a Series of Sulfo-Substituted Compounds

I. V. Gushchina[1≠], D. K. Nilov[2≠], T. A. Shcherbakova[2], S. M. Baldin[2], V. K. Švedas[1,2*]
[1]Lomonosov Moscow State University, Faculty of Bioengineering and Bioinformatics, Moscow, 119234 Russian Federation
[2]Lomonosov Moscow State University, Belozersky Institute of Physicochemical Biology, Moscow, 119234 Russian Federation
[≠]Authors who contributed equally to this work.
[*]E-mail: vytas@belozersky.msu.ru
Received: February 18, 2023; in final form, May 12, 2023
DOI: 10.32607/actanaturae.15709

ABSTRACT **As a result of the computer screening of a library of sulfo-substituted compounds, molecules capable of binding to the active site of transketolase from *Mycobacterium tuberculosis* were identified. An experimental verification of the inhibitory activity of the most promising compound, STK045765, against a highly purified recombinant enzyme preparation was carried out. It was shown that the STK045765 molecule competes for the binding site of the pyrophosphate group of the thiamine diphosphate cofactor and, at micromolar concentrations, is able to suppress the activity of mycobacterial transketolase. The discovered furan-sulfonate scaffold may serve as the basis for the creation of anti-tuberculosis drugs.**
KEYWORDS **sulfonates, sulfo group, inhibitors, thiamine diphosphate, transketolase, mycobacteria.**
ABBREVIATIONS **mbTK – mycobacterial transketolase.**

INTRODUCTION

Tuberculosis treatment is based on long-term multicomponent chemotherapy and is often accompanied by the development of drug resistance in *Mycobacterium tuberculosis*. Because of this, the search for new molecular targets and the development of drugs that can selectively suppress the growth of mycobacteria are of utmost importance. An analysis of the genome of the H37Rv strain of *M. tuberculosis* made it possible to establish metabolic pathways the suppression of which can provide the basis for the development of new drugs. In particular, the pentose phosphate pathway and the associated enzyme transketolase (mbTK) are crucial [1, 2]. mbTK catalyzes the reversible transfer of a two-carbon fragment from a donor substrate (ketose) to an acceptor substrate (aldose). One of the mbTK substrates, ribose 5-phosphate, is used for the synthesis of the mycobacteria cell wall [3, 4]. In this work, we carried out a computer screening for the ability of sulfo-substituted compounds to bind in the mbTK active center and experimental verification of the inhibitory properties of the selected, most promising candidate.

EXPERIMENTAL

The molecular model of mbTK for docking was obtained based on the 3rim crystal structure [4]. Hydrogen atoms were added taking into account the ionization of amino acid residues with the AmberTools 1.2 software, then their coordinates were optimized with the Amber 12 package [5], using the steepest descent and conjugate gradient algorithms. A library of sulfo-substituted compounds for screening was constructed based on the Vitas-M commercial set of low-molecular-weight compounds (https://vitasmlab.biz) using a substructure search for the sulfo group in ACD/SpectrusDB (https://www.acdlabs.com). The compounds were docked into the active site of the mbTK model using Lead Finder 1.1.16 [6]. The search region included the binding site of the thiamine diphosphate cofactor and the substrate [7]. Then, compounds capable of forming an electrostatic interaction with the Mg^{2+} ion, as well as other favorable contacts, were selected using a Perl script for structural filtration.

The recombinant mbTK protein was obtained using the pET-19b plasmid carrying the *Rv1449c* gene and the *Escherichia coli* strain BL21(DE3). Protein

isolation and purification were performed as described previously [8, 9]. The activity of mbTK was measured by the coupled NAD^+ reduction reaction, catalyzed by glyceraldehyde 3-phosphate dehydrogenase from rabbit muscles [10]. The reaction mixture contained glycylglycine (50 mM), dithiothreitol (3.2 mM), sodium arsenate (10 mM), magnesium chloride (2.5 mM), thiamine diphosphate (5 μM), xylulose 5-phosphate (140 μM), ribose 5-phosphate (560 μM), NAD^+ (370 μM), glyceraldehyde 3-phosphate dehydrogenase (3 U), and the STK045765 inhibitor at various concentrations (0–1000 μM). The reaction was started by adding a solution of the mbTK apo form to the reaction mixture incubated in a thermostated cell at pH 7.6 and 25°C. The reaction rate was monitored as an increase in the optical density of the solution at 340 nm using a Shimadzu UV-1800 spectrophotometer.

RESULTS AND DISCUSSION

The mbTK active site contains the cofactor thiamine diphosphate, as well as the Mg^{2+} ion [4]. The interaction of the pyrophosphate group with Mg^{2+} makes a significant contribution to the binding energy of thiamine diphosphate and is important for the design of mbTK inhibitors that were not reported prior to our study.

The sulfo group was chosen as a possible structural mimic of the pyrophosphate group capable of forming an electrostatic interaction with metal ions. From the library of commercially available low-molecular-weight compounds, 320 molecules with a terminal (negatively charged) sulfo group and 563 molecules with an esterified sulfo group were retrieved. As a result of docking, the positions of compounds of this class in the mbTK active site were determined. The docking poses were further subjected to structural filtration by taking into account direct electrostatic interactions of the sulfo group with Mg^{2+}. An expert analysis of the positions of the selected compounds identified five compounds with a terminal sulfo group (*Fig. 1*) that effectively interacted with Mg^{2+} and the surrounding residues of the mbTK active site. Less effective interactions of esterified sulfonates indicate that a negatively charged group is required for the inhibitor binding in the mbTK active site.

For experimental testing of inhibitory properties, the STK045765 molecule was selected, which forms the most favorable bonds and contacts when modeling enzyme-inhibitor complexes. In this molecule, the furansulfonate and naphthalene fragments are connected by a hydrazide linker. The negatively charged sulfo group of STK045765 is able to interact with the Mg^{2+} ion and His85 side chain (*Fig. 2*) in a similar

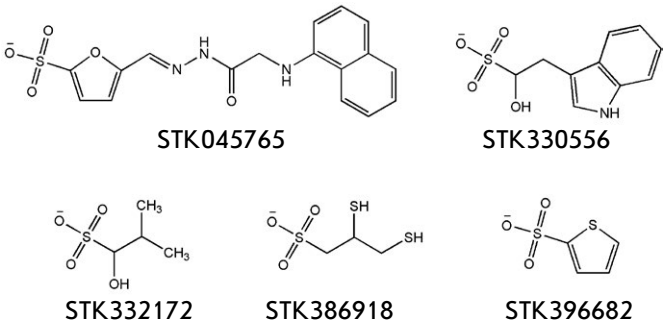

Fig. 1. Chemical structures of potential mbTK inhibitors selected by computer screening

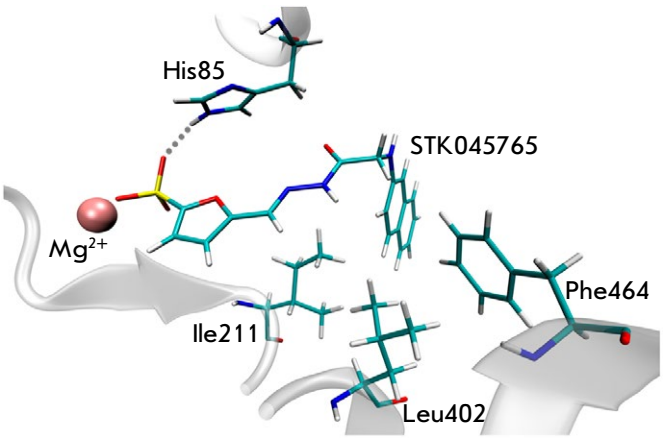

Fig. 2. Model of the enzyme-inhibitor complex of mbTK and STK045765. The sulfo group is able to interact with the Mg^{2+} ion and form a hydrogen bond with the His85 residue; the hydrophobic bicyclic structural fragment is complementary to the site formed by the Ile211, Leu402, and Phe464 residues. The figure was prepared using VMD 1.9.2 [11]

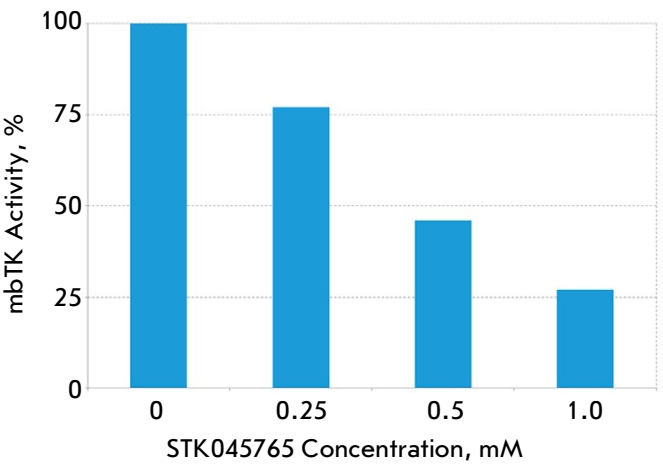

Fig. 3. Effect of the STK045765 inhibitor on the catalytic activity of mbTK

manner to the pyrophosphate group of the cofactor. Along with this, favorable hydrophobic contacts of the bicyclic structural fragment of STK045765 with the side chains of Ile211, Leu402, and Phe464 take place. Experimental verification confirmed the findings of molecular modeling. When an inhibitor was added to the reaction mixture, mbTK activity was suppressed: thus, in the presence of STK045765 at a concentration of 1 mM, the residual activity was 27% (*Fig. 3*).

CONCLUSIONS

Virtual screening of a library of sulfo-substituted compounds made it possible to identify potential inhibitors capable of binding to the mbTK active site and competing with the cofactor thiamine diphosphate. Experimental testing of one of the candidates (STK045765 containing a furansulfonate group) against a highly purified mbTK preparation confirmed that compounds of this class are capable of inhibiting enzymatic activity. As a result of the study, the first-in-class inhibitor of mbTK was discovered, the structure of which can become the basis for the development of more effective inhibitors – prototypes of anti-tuberculosis drugs. ●

This work was supported by the Russian Science Foundation (grant No. 15-14-00069-P).

REFERENCES

1. Cole S.T., Brosch R., Parkhill J., Garnier T., Churcher C., Harris D., Gordon S.V., Eiglmeier K., Gas S., Barry C.E. 3rd, et al. // Nature. 1998. V. 393. P. 537–544.
2. Kolly G.S., Sala C., Vocat A., Cole S.T. // FEMS Microbiol. Lett. 2014. V. 358. P. 30–35.
3. Wolucka B.A. // FEBS J. 2008. V. 275. P. 2691–2711.
4. Fullam E., Pojer F., Bergfors T., Jones T.A., Cole S.T. // Open Biol. 2012. V. 2. P. 110026.
5. Case D.A., Darden T.A., Cheatham T.E., 3rd, Simmerling C.L., Wang J., Duke R.E., Luo R., Walker R.C., Zhang W., Merz K.M., et al. AMBER 12. San Francisco: University of California, 2012.
6. Stroganov O.V., Novikov F.N., Stroylov V.S., Kulkov V., Chilov G.G. // J. Chem. Inf. Model. 2008. V. 48. P. 2371–2385.
7. Lüdtke S., Neumann P., Erixon K.M., Leeper F., Kluger R., Ficner R., Tittmann K. // Nat. Chem. 2013. V. 5. P. 762–767.
8. Shcherbakova T.A., Baldin S.M., Shumkov M.S., Gushchina I.V., Nilov D.K., Švedas V.K. // Acta Naturae. 2022. V. 14. № 2. P. 93–97.
9. Meshalkina L.E., Solovjeva O.N., Khodak Y.A., Drutsa V.L., Kochetov G.A. // Biochemistry (Moscow). 2010. V. 75. P. 873–880.
10. Kochetov G.A. // Methods Enzymol. 1982. V. 90. P. 209–223.
11. Humphrey W., Dalke A., Schulten K. // J. Mol. Graph. 1996. V. 14. P. 33–38.

GENERAL RULES

Acta Naturae publishes experimental articles and reviews, as well as articles on topical issues, short reviews, and reports on the subjects of basic and applied life sciences and biotechnology.

The journal *Acta Naturae* is on the list of the leading periodicals of the Higher Attestation Commission of the Russian Ministry of Education and Science. The journal Acta Naturae is indexed in PubMed, Web of Science, Scopus and RCSI databases.

The editors of *Acta Naturae* ask of the authors that they follow certain guidelines listed below. Articles which fail to conform to these guidelines will be rejected without review. The editors will not consider articles whose results have already been published or are being considered by other publications.

The maximum length of a review, together with tables and references, cannot exceed 50,000 characters with spaces (approximately 30 pages, A4 format, 1.5 spacing, Times New Roman font, size 12) and cannot contain more than 16 figures.

Experimental articles should not exceed 30,000 symbols (approximately 15 pages in A4 format, including tables and references). They should contain no more than ten figures.

A short report must include the study's rationale, experimental material, and conclusions. A short report should not exceed 12,000 symbols (5–6 pages in A4 format including no more than 12 references). It should contain no more than three figures.

The manuscript and all necessary files should be uploaded to www.actanaturae.ru:

1) text in Word 2003 for Windows format;
2) the figures in TIFF format;
3) the text of the article and figures in one pdf file;
4) the article's title, the names and initials of the authors, the full name of the organizations, the abstract, keywords, abbreviations, figure captions, and Russian references should be translated to English;
5) the cover letter stating that the submitted manuscript has not been published elsewhere and is not under consideration for publication;
6) the license agreement (the agreement form can be downloaded from the website www.actanaturae.ru).

MANUSCRIPT FORMATTING

The manuscript should be formatted in the following manner:

- Article title. Bold font. The title should not be too long or too short and must be informative. The title should not exceed 100 characters. It should reflect the major result, the essence, and uniqueness of the work, names and initials of the authors.
- The corresponding author, who will also be working with the proofs, should be marked with a footnote *.
- Full name of the scientific organization and its departmental affiliation. If there are two or more scientific organizations involved, they should be linked by digital superscripts with the authors' names. Abstract. The structure of the abstract should be very clear and must reflect the following: it should introduce the reader to the main issue and describe the experimental approach, the possibility of practical use, and the possibility of further research in the field. The average length of an abstract is 20 lines (1,500 characters).
- Keywords (3 – 6). These should include the field of research, methods, experimental subject, and the specifics of the work. List of abbreviations.
- INTRODUCTION
- EXPERIMENTAL PROCEDURES
- RESULTS AND DISCUSSION
- CONCLUSION

  The organizations that funded the work should be listed at the end of this section with grant numbers in parenthesis.
- REFERENCES

  The in-text references should be in brackets, such as [1].

RECOMMENDATIONS ON THE TYPING AND FORMATTING OF THE TEXT

- We recommend the use of Microsoft Word 2003 for Windows text editing software.
- The Times New Roman font should be used. Standard font size is 12.
- The space between the lines is 1.5.
- Using more than one whole space between words is not recommended.
- We do not accept articles with automatic referencing; automatic word hyphenation; or automatic prohibition of hyphenation, listing, automatic indentation, etc.
- We recommend that tables be created using Word software options (Table → Insert Table) or MS Excel. Tables that were created manually (using lots of spaces without boxes) cannot be accepted.
- Initials and last names should always be separated by a whole space; for example, A. A. Ivanov.
- Throughout the text, all dates should appear in the "day.month.year" format, for example 02.05.1991, 26.12.1874, etc.
- There should be no periods after the title of the article, the authors' names, headings and subheadings, figure captions, units (s – second, g – gram, min – minute, h – hour, d – day, deg – degree).
- Periods should be used after footnotes (including those in tables), table comments, abstracts, and abbreviations (mon. – months, y. – years, m. temp. – melting temperature); however, they should not be used in subscripted indexes (T_m – melting temperature; $T_{p.t}$ – temperature of phase transition). One exception is mln – million, which should be used without a period.
- Decimal numbers should always contain a period and not a comma (0.25 and not 0,25).
- The hyphen ("-") is surrounded by two whole spaces, while the "minus," "interval," or "chemical bond" symbols do not require a space.
- The only symbol used for multiplication is "×"; the "×" symbol can only be used if it has a number to its

right. The "·" symbol is used for denoting complex compounds in chemical formulas and also noncovalent complexes (such as DNA·RNA, etc.).
- Formulas must use the letter of the Latin and Greek alphabets.
- Latin genera and species' names should be in italics, while the taxa of higher orders should be in regular font.
- Gene names (except for yeast genes) should be italicized, while names of proteins should be in regular font.
- Names of nucleotides (A, T, G, C, U), amino acids (Arg, Ile, Val, etc.), and phosphonucleotides (ATP, AMP, etc.) should be written with Latin letters in regular font.
- Numeration of bases in nucleic acids and amino acid residues should not be hyphenated (T34, Ala89).
- When choosing units of measurement, SI units are to be used.
- Molecular mass should be in Daltons (Da, KDa, MDa).
- The number of nucleotide pairs should be abbreviated (bp, kbp).
- The number of amino acids should be abbreviated to aa.
- Biochemical terms, such as the names of enzymes, should conform to IUPAC standards.
- The number of term and name abbreviations in the text should be kept to a minimum.
- Repeating the same data in the text, tables, and graphs is not allowed.

GUIDENESS FOR ILLUSTRATIONS

- Figures should be supplied in separate files. Only TIFF is accepted.
- Figures should have a resolution of no less than 300 dpi for color and half-tone images and no less than 600 dpi.
- Files should not have any additional layers.

REVIEW AND PREPARATION OF THE MANUSCRIPT FOR PRINT AND PUBLICATION

Articles are published on a first-come, first-served basis. The members of the editorial board have the right to recommend the expedited publishing of articles which are deemed to be a priority and have received good reviews.

Articles which have been received by the editorial board are assessed by the board members and then sent for external review, if needed. The choice of reviewers is up to the editorial board. The manuscript is sent on to reviewers who are experts in this field of research, and the editorial board makes its decisions based on the reviews of these experts. The article may be accepted as is, sent back for improvements, or rejected.

The editorial board can decide to reject an article if it does not conform to the guidelines set above.

The return of an article to the authors for improvement does not mean that the article has been accepted for publication. After the revised text has been received, a decision is made by the editorial board. The author must return the improved text, together with the responses to all comments. The date of acceptance is the day on which the final version of the article was received by the publisher.

A revised manuscript must be sent back to the publisher a week after the authors have received the comments; if not, the article is considered a resubmission.

E-mail is used at all the stages of communication between the author, editors, publishers, and reviewers, so it is of vital importance that the authors monitor the address that they list in the article and inform the publisher of any changes in due time.

After the layout for the relevant issue of the journal is ready, the publisher sends out PDF files to the authors for a final review.

Changes other than simple corrections in the text, figures, or tables are not allowed at the final review stage. If this is necessary, the issue is resolved by the editorial board.

FORMAT OF REFERENCES

The journal uses a numeric reference system, which means that references are denoted as numbers in the text (in brackets) which refer to the number in the reference list.

For books: the last name and initials of the author, full title of the book, location of publisher, publisher, year in which the work was published, and the volume or issue and the number of pages in the book.

For periodicals: the last name and initials of the author, title of the journal, year in which the work was published, volume, issue, first and last page of the article. Must specify the name of the first 10 authors. Ross M.T., Grafham D.V., Coffey A.J., Scherer S., McLay K., Muzny D., Platzer M., Howell G.R., Burrows C., Bird C.P., et al. // Nature. 2005. V. 434. № 7031. P. 325–337.

References to books which have Russian translations should be accompanied with references to the original material listing the required data.

References to doctoral thesis abstracts must include the last name and initials of the author, the title of the thesis, the location in which the work was performed, and the year of completion.

References to patents must include the last names and initials of the authors, the type of the patent document (the author's rights or patent), the patent number, the name of the country that issued the document, the international invention classification index, and the year of patent issue.

The list of references should be on a separate page. The tables should be on a separate page, and figure captions should also be on a separate page.

The following e-mail addresses can be used to contact the editorial staff: actanaturae@gmail.com, tel.: (495) 727-38-60.